

Multiscale Phase-field Model for Phase Transformation and Fracture

Submitted in partial fulfillment of the requirements

for the degree of

Doctor of Philosophy

in

Civil and Environmental Engineering

Vaibhav Agrawal

B.Tech., Civil Engineering, Indian Institute of Technology Kanpur

M.S., Civil and Environmental Engineering, Carnegie Mellon University

Carnegie Mellon University

Pittsburgh, PA

August 9, 2016

Acknowledgments

I thank my advisor and committee chair Prof. Kaushik Dayal for his advise, encouragement and having patience with me throughout the past four years. He spent a lot of time to discuss research and answer my questions.

I would like to thank my current and previous group members Hossein, Jason, Mahnoush, Prashant, Arnab, Soumya, Amin and Abraham for being available to discuss my doubts and technical difficulties almost everyday. Through the group paper reading sessions, I have learned about research areas other than my own and that was one of the most exciting things during my stay at CMU and I would like to thank my advisor and group members for spending time and effort for the same. It has given me hope and confidence to attempt important problems outside my area of familiarity. Also, I would like to acknowledge Jason and Mahnoush for being very cooperative when we shared the teaching assistant responsibilities.

I am thankful to Prof. Anthony. D. Rollett, Prof. M. Ravishankar, Prof. Jacobo Bielak, Prof. Noel J. Walkington for taking the time to review my work and serving on my thesis committee.

I would like to acknowledge my friends, Arka Roy, Prathamesh Desai, Argha Namhata, Sudhanshu Nahata, Ankit Jain, Tejas Wanjari and Pradeep Karuturi for their presence which made these past four years very enjoyable and exciting.

I would also like to thank Maxine Leffard, the administrative staff of the Civil and Environmental Engineering department and the Office of International Education for being very cooperative with the administrative work.

I thank National Science Foundation (1349458) and Army Research Office (W911NF-10-1-0140) for financial support. I also thank Carnegie Mellon University College of Engineering for financial support

through the Bertucci Graduate Fellowship.

Finally, I thank my parents and brother for their continuous support and encouragement.

Abstract

We address two problems in this thesis. First, a phase-field model for structural phase transformations in solids and second, a model for dynamic fracture. The existing approaches for both phase transformations and fracture can be grouped into two categories. Sharp-interface models, where interfaces are singular surfaces; and regularized-interface models, such as phase-field models, where interfaces are smeared out. The former are challenging for numerical solutions because the interfaces or crack needs to be explicitly tracked, but have the advantage that the kinetics of existing interfaces or cracks and the nucleation of new interfaces can be transparently and precisely prescribed. The diffused interface models such as phase-field models do not require explicit tracking of interfaces and makes them computationally attractive. However, the specification of kinetics and nucleation is both restrictive and extremely opaque in such models. This prevents straightforward calibration of phase-field models to experiment and/or molecular simulations, and breaks the multiscale hierarchy of passing information from atomic to continuum. Consequently, phase-field models cannot be confidently used in dynamic settings.

We present a model which has all the advantages of existing phase-field models but also allows us to prescribe kinetics and nucleation criteria. We present a number of examples to characterize and demonstrate the features of the model. We also extend it to the case of multiple phases where preserving kinetics of each kind of interface is more complex.

We use the phase transformation model with certain changes to model dynamic fracture. We achieve the advantage of prescribing nucleation and kinetics independent of each other. We demonstrate examples of anisotropic crack propagation and crack propagation on an interface in a composite material.

We also report some limitations of phase-field models for fracture which have not been mentioned in the existing literature. These limitations include dependence of effective crack width and hence the effective

surface energy on the crack speed, lack of a reasonable approximation for the mechanical response of cracked region and inability to model large deformations.

Contents

Acknowledgments	i
Abstract	iii
1 Introduction	1
2 Formulation and one-dimensional characterization	7
2.1 Introduction	7
2.1.1 Organization	13
2.1.2 Notation and Definitions	14
2.2 Formulation	16
2.2.1 Energetics	16
2.2.2 Evolution Law	19
2.2.3 Thermodynamics and Dissipation	24
2.2.4 Formal Sharp-Interface Limit	26
2.3 Traveling Waves in One Dimension	27
2.4 Dynamics of Interfaces in One Dimension	30
2.5 Effect of the Small Parameter l	33
2.6 Competition Between Inertia and Dissipation	34
2.7 Discussion	39

2.A	Connection to Noether's Theorem	41
2.B	Non-existence of Supersonic Interfaces in Standard Phase-field Models	43
3	Two-dimensional characterization and boundary kinetics	45
3.1	Introduction	45
3.1.1	Organization	47
3.2	Summary of the Proposed Phase-Field Model	48
3.3	Formulation of a Two-Dimensional Energy for Twinning	49
3.4	Non-Monotone Kinetic Laws	50
3.4.1	1D Non-Monotone Kinetics	51
3.4.2	2D Non-Monotone Kinetics	52
3.5	Anisotropic Kinetics in Two Dimensions	52
3.6	Stick-slip Twinning Kinetics	55
3.7	Rate-Dependent and Asymmetric Nucleation	56
3.7.1	Rate-Dependent and Asymmetric Nucleation in One Dimension	57
3.7.2	Rate-Dependent and Asymmetric Nucleation in Twinning	58
3.8	Imposing Principal Normal Stress- and Shear Stress- Dependent Nucleation for Twinning	60
3.9	Competition Between Nucleation and Kinetics in Twinning	61
3.10	Boundary Kinetics	62
3.10.1	Formulation of Boundary Kinetics	64
3.10.2	Faceting of a Flat Stressed Interface	66
3.10.3	Competition Between Bulk and Boundary Kinetics	68
3.10.4	A Singularity In Boundary Kinetics	69
3.11	Discussion	70
4	Analysis of lamellar twins	73

4.1	Introduction	73
4.2	Formulation	74
4.3	Twinning under plane-strain	75
4.4	Twinning calculations in antiplane formulation	78
4.4.1	Isotropic and anisotropic kinetics	79
4.4.2	Curvature dependent kinetics	81
4.5	Twin crossing grain boundary	83
5	Extension of the model for n-phases	87
5.1	Introduction	87
5.2	Formulation for more than two phases: Energy and Balance law	89
5.2.1	Balance law	89
5.2.2	Energetics	91
5.2.3	Kinetic constraint	93
5.3	An example	94
5.4	Discussion	96
6	Fracture	97
6.1	Introduction	97
6.2	Formulation	99
6.3	Mode-I calculations	101
6.4	Anisotropic Kinetics	104
6.4.1	Anisotropy + Elastostatics	104
6.4.2	Anisotropy + Elastodynamics	105
6.5	Modifying energy to account for crack-face compression	107
6.5.1	Modifying energy by resolving strain into normal and shear components	108

6.6	Width of the phase-field crack	115
6.6.1	Approximation of surface energy as a volume integral	116
6.6.2	Calculations	117
6.7	Crack nucleation on a bi-material interface	118
6.8	A comment on mass density for cracked phase	121
6.9	Supersonic mode-II crack	121
6.9.1	Isotropic kinetics	122
6.9.2	Anisotropic kinetics: subsonic crack growth	123
6.9.3	Anisotropic kinetics: supersonic crack growth	123
7	Conclusions	127
	Bibliography	131

List of Figures

1.1	Schematic of energy landscape as a function of configuration space. Configuration is intact when the material behaves elastically and is cracked when the bonds are broken.	2
2.1	Contour and surface plots of the energy $\dot{W}(\mathbf{E}, \phi)$ assuming 1D with only a single strain component, using $l = 0.1$ (above) and $l = 0.01$ in the function H_l used in the definition of the energy.	18
2.2	Left: a field ϕ with a number of interfaces. Right: $\nabla\phi$ provides a measure of (signed) interface density per unit length.	20
2.3	Left: A schematic representation of a curve threading an interface. Right: The flux of interfaces at one end of the curve. $\hat{\mathbf{t}}$ is the tangent to the end of the curve, and v_n^ϕ is the interfacial normal velocity field. The relative velocity of the interface with respect to the direction $\hat{\mathbf{t}}$ is $\frac{v_n^\phi}{ \hat{\mathbf{n}} \cdot \hat{\mathbf{t}} }$, and is defined as the distance along the direction $\hat{\mathbf{t}}$ traversed by the threading interface in unit time.	21
2.4	Plots of Φ , $H_l(\Phi - 0.5)$, U' respectively for traveling wave solutions with different values of M using linear kinetics.	29
2.5	M vs. classical driving force for linear kinetics and quadratic kinetics, derived from the traveling wave solutions. The classical driving force is $f = \llbracket U \rrbracket - \langle \sigma \rangle \llbracket u_x \rrbracket$, and is evaluated using the values of fields at the edges of the domain.	30
2.6	u_x (left) and $H_l(\phi(x) - 0.5)$ at different times after the elastic wave hits the phase interface, showing the steady state evolution of the interface.	32

2.7	Left: Driving force in the vicinity of the interface, showing that it constant. The interface is moving towards the left. Right: Interface velocity vs. classical driving force for different kinetic laws.	32
2.8	Comparison of linear and quadratic kinetics from dynamic simulations and traveling wave solutions. The chosen kinetic relations have different coefficients for the dynamics and traveling wave cases.	33
2.9	Left: Interface velocity vs. classical driving force with linear kinetics computed using traveling waves for different values of l . Right: Interface velocity vs. classical driving force with stick-slip kinetics computed using dynamic calculations for different values of l . Below: Interface velocity vs. applied end load for the same dynamic calculations. . . .	35
2.10	The stress-strain curve showing phases 1 and 3. The chords link the states on either side of the phase interface. The upper chord is a supersonic interface, and the lower chord is subsonic. The slope of a chord gives the interface velocity, and the slope of a stress-strain branch gives the sonic speed for that branch.	36
2.11	Top: A stationary interface as a compressive elastic wave approaches from the right. Left: The evolution of $H_l(\phi - 0.5)$ shows the phase interface in ϕ . Right: The evolution of u_x shows the phase interface in u_x . The key point is that the evolution of phase interfaces in ϕ and u_x are decoupled.	39
3.1	Evolution of $H_l(\phi(x) - 0.5)$ (left) and u_x (right) with a non-monotone kinetic response.	51
3.2	The left column is the evolution with linear kinetics, and the right column is the evolution with non-monotone kinetics, with snapshots of the $F_{11} - 1$ field taken at the same time for both processes. The phases are not stress-free compatible. The top row, at small times, is fairly similar. As evolution progresses, there are quantitative but not qualitative differences.	53
3.3	The top figure shows the initial configuration, the lower left figure shows the configuration after some time using linear kinetics, and the lower right figure shows the configuration after some time using non-monotone kinetics. All plots are of the $F_{11} - 1$ field. As in the incompatible case, there are quantitative but no obvious qualitative differences. . .	54

3.4 The $F_{11} - 1$ field at different times for an anisotropic kinetic response. Nucleation takes place within a circle of radius 0.1 at the center of the domain. The interface velocity is anisotropic, and the effect can clearly be seen because everything else in the problem maintains circular symmetry. It can be seen that regions where the interface normal is perpendicular to \mathbf{d}_m do not show any motion / growth after the initial nucleation stage. 55

3.5 The $F_{11} - 1$ field at a given time for varying applied load levels. In the first case, well below the critical load, there is no evolution; in the second case, just above the critical load, there is very slow evolution; in the third case, well above the critical load, there is rapid evolution. 56

3.6 Left: Hysteresis curve for two loading rates demonstrating effect of rate-dependent nucleation. Right: Hysteresis curve demonstrating asymmetric nucleation, i.e., forward and reverse nucleation criteria are independently prescribed without changing the energy \dot{W} . The bold horizontal line marks the stress around which the energy \dot{W} is symmetric. 58

3.7 A hysteresis loop for twinning demonstrating the ability to apply rate-dependent and asymmetric nucleation criteria in 2D. 59

3.8 The $F_{11} - 1$ field before the elastic waves interact with the stress field around the circular inclusion (left), and after (right). Complex nucleation patterns can be seen, with the elastic stresses driving the interfaces – through the driving force in the kinetic response – to incline at $\pm\pi/4$. The lighter regions indicate the nucleated phase. Elastic waves that are created during the process of nucleation are also seen. 62

3.9 The $F_{11} - 1$ field as the elastic waves interact with the stress field around the circular inclusion, causing nucleation and growth. The lighter regions indicate the nucleated phase. The left column is the evolution with small nucleation rate ($A_{0\rightarrow 1} = 2$), and the right column is the evolution with large nucleation rate ($A_{0\rightarrow 1} = 20$). The plots show snapshots taken at the same time for both processes. 63

3.10 The same bulk interface velocity field v_n^ϕ can lead to very different overall evolution depending on the kinetic response v_e^ϕ of the interface-boundary junction line. Adapted with permission from [SB98]. 64

3.11 The top figure shows the initial condition. The left column shows the final state with linear kinetics on the boundary (the entire sample and zoomed-in at the boundary). The right column is the same with the interface pinned on the boundary. All plots are of the $F_{11} - 1$ field. 67

3.12 The first figure shows the initial configuration with a stress-free compatible interface. The other figures show the evolution under applied load after some time for (i) slower, (ii) equal, and (iii) faster, boundary kinetics compared to bulk kinetics. All plots are of the $F_{11} - 1$ field. 68

3.13 Left: the initial configuration with an interface normal to a traction-free boundary. Right: the evolution of the interface. There is no shear traction on the plane parallel to the interface at the surface, thereby not providing a driving force for the interface-boundary junction to evolve. 70

4.1 $(\nabla u)_{11}$ at different times (t=1,3,5,7,9). The compatible directions are e_2 77

4.2 u_2 at different times (t=1,5,10). The compatible direction is e_2 . Left column corresponds to isotropic kinetics, right column corresponds to anisotropic kinetics: $\hat{v} = \kappa|f|(0.1 + |\nabla\phi \cdot e_1|/|\nabla\phi|)$ 80

4.3 Schematic showing a twin interface, its normal n , and the tangent to the interface t , at a point. Near the tip the normal changes rapidly from pointing towards e_2 to $-e_2$ 81

4.4 $\hat{v} = \kappa f \left(0.1 + \frac{|\nabla n^t \cdot t}{50.0}\right)$. Figure showing u_2 at two different times during the evolution of twin. This form of curvature dependence does give needle like structure but the phase interface is "wiggly". 82

4.5 Same as the second picture in Fig.4.4 but with contour plots highlighting the wiggly interface. 83

4.6 Left and right half of the plate represent two grains. Right half of the plate ($x > 0.5$) is rotated by $\Pi/4$ w.r.t. to the left. Left column: nucleation site on left, evolution at t=1,4,8,12. Right column: nucleation site on right edge, evolution at t=1,6,12,18,24. 86

5.1 3-phase toy problem. The images are $t=5,13,14,15,16$. In the first figure, the bright region on the left half is phase 3, the gray region on right half is phase 2, black is phase 1. Phase 2 grows towards both left and right edge and merges with phase 3 at $t=14$. Finally phase-1 between phase-2 and phase-3 (near center of the plate) disappears. It is clear that the phase parameters do not get stuck at any intermediate value during the whole process. 95

6.1 Isotropic kinetics: ϕ at different times 102

6.2 Isotropic kinetics: $|\sigma_{11}|$ at different times 103

6.3 Waves approaching crack-tip from top interfere with crack growth. The head of the tip is subjected to the waves sooner than the sloped parts of the tip. This may result in a Y-shape formation around the tip which eventually can lead to two separate crack branches. 103

6.4 Elastostatics. Crack evolution at $t = 7$ and $t = 19$ 105

6.5 Damped elastodynamics. Crack evolution at $t = 15$ and $t = 35$ 106

6.6 The first row of figures is corresponding to a 0-stiffness material. The second row is the response of model described above. Both the figures on the left correspond to tensile boundary conditions and the figures on right correspond to compressive boundary conditions. 114

6.7 Results from solving (6.6.2). Every parameter is same for the two calculations except magnitude of tensile load applied on the left and right edges. Crack width is higher for the second case in which applied load is higher. 118

6.8 ε_{11} for mode-I crack through a bimaterial interface without any nucleation. The circular inclusion is situated at $(0.5, 0.5)$ and is stressed. 119

6.9 ε_{11} for mode-I crack through a bimaterial interface. Nucleation is defined on the bimaterial interface. The circular inclusion is situated at $(0.5, 0.5)$ and is stressed. 120

6.10 ε_{12} for a mode-II crack at different times (for $t = 0$ to $t = 6$). Shear loading is applied on the right edge, left edge is fixed. As expected, the crack curves. 122

6.11 ε_{12} for a mode-II crack with anisotropic kinetics at different times (for $t = 1$ to $t = 14$). Shear loading ($\tau = 0.1$) is applied on the right edge, left edge is fixed. Crack evolution is subsonic w.r.t shear waves speed and crack still curves. The plots look very similar to 6.10 123

6.12 ε_{12} for a mode-II crack at different times (for $t = 0$ to $t = 4$). Shear loading ($\tau = 0.1$) is applied on the right edge, left edge is fixed. Linear kinetics ($\hat{v} = \kappa.(\hat{\nabla}\phi \cdot e_2)sign(f)|f|$). Mach cones formed by shear waves can be seen. Unlike calculation in Fig.6.11 for mode-II cracks, in this calculation the crack did not bend. Also, the crack was slightly thicker than earlier cases 124

6.13 Poynting vector for supersonic and subsonic mode-II crack 126

Chapter 1

Introduction

There are many kinds of defects in crystalline solids which govern the mechanical properties such as dislocations which are line defects, grain boundaries which are interface defects, voids, precipitates, etc. Structural phase transformation is a diffusion less transformation of one crystal structure to another. The transformation leads to phase interfaces which are also planar defects. Fracture or cracks can also be seen as defect in which the bonds between certain atoms have broken resulting in new free surface.

Both these processes are important for a variety of reasons. Twinning, a special case of phase transformation in which the two phases are variants of the same parent, is an important factor in forming of metals with hexagonal crystal structures (HCP) and manufacturing of transformation induced plasticity (TRIP) steel. In certain metal alloys, phase interfaces or twin boundaries prohibit the movement of dislocations leading to higher strength. Apart from use in understanding and enhancing mechanical properties, phase transformation also leads to the shape memory effect which can have application in microactuators and MEMS devices.

Cracks are important because it is a common form of failure of solids. Once a crack forms, it leads to stress concentration near the crack tips which makes the material even more susceptible to failure. Some of the everyday examples are cracks in civil engineering structures such as concrete and steel, cracks in solder joints in microelectronic components, shattering of glasses of cell phone screens and wind-shields of vehicles. Another area of study related to cracks is earthquakes. High stresses build up at the tectonic faults, where two tectonic plates join. One way to release the stress is by relative shearing of plates which results in earthquakes.

Nucleation and evolution of any defect requires use of multiscale methods. The sharp interface theories for phase interfaces have highlighted that just the elastodynamics does not completely determine the system and more constitutive information is necessary. Similarly the continuum level theories (by Griffith, Rice, etc) which address the conditions for crack growth assume rules apart from stress equilibrium such as principal of local symmetry or maximum energy dissipation and related ideas to determine the direction of crack propagation. Even these criteria do not address the nucleation condition for a new crack. Figure 1 shows a schematic of energy vs configuration-space plot for a material which can crack. The propagation and nucleation of new cracks depends upon whether the system can cross this barrier. This information is not contained in the continuum level models if they only use elastic properties such as stiffness, strain energy and surface energy because they only capture the near-equilibrium response of the material (for both a material undergoing fracture or phase change). On the other hand, atomistic models contain the necessary information, i.e., the energy barrier, but they are computationally expensive and can only be done for small systems of size of few thousand atoms. Therefore, there is need for a continuum level model which can take the essential information from the smaller scales as input. There are some

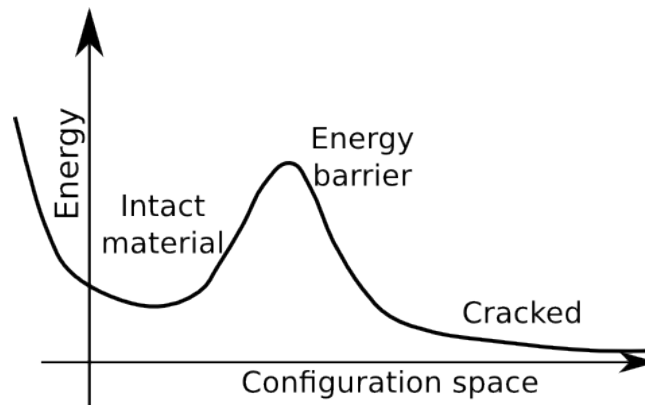


Figure 1.1: Schematic of energy landscape as a function of configuration space. Configuration is intact when the material behaves elastically and is cracked when the bonds are broken.

existing continuum approaches for both fracture and phase transformation. For e.g. [AK90, AK91b] developed a model which treats phase interfaces as sharp interface across which deformation gradient is discontinuous. It allows for prescription of a kinetic relation which can be derived from either atomistic calculations or measured from experiments. There is also a class of models which treat the interface as diffused over a region rather than a discontinuity of displacement gradient such as [AK91a]. Phase-field models also are a type of diffused interface model and they have been used in the context of phase

transformation, for e.g. see [LL07, YEC09]. Apart from the sharp interface model, none other available in the literature, to the best of my knowledge, allows one to prescribe both nucleation criteria and kinetic law for interfaces in a transparent manner. Of course, there are parameters in the model which can be fitted to atomistic simulations and/or experiments, however they put severe restrictions on the choice of kinetics and nucleation criteria, thus, breaking the multiscale hierarchy of the approach.

Similar issues exist in the modelling of dynamic fracture. Some of the continuum level methods are extended finite elements, cohesive zone methods, see [CO96, BGV09, SP03]. They require tracking of the crack in some or the other way and make the computational algorithm complex and expensive. Phase-field models have also been used for dynamic fracture, see for e.g. [KKL01, BVS⁺12, BLR11, HM12]. In essence, the displacement is governed by linear momentum balance and for evolution of the phase-field either minimization w.r.t phase-field or the Ginzburg-Landau type of evolution is assumed. These approaches simplify the computation and implementation, especially in case of complex loading conditions when multiple cracks can interact and crack branching can happen.

In this thesis we develop a phase-field model which has which has all the features of the existing phase-field models, i.e., ease of implementation and computation, but also allows us to prescribe kinetic law and nucleation criteria as well. First, we develop the model for phase transformation involving just two phases. We achieve the aforementioned features by using an evolution for phase field which comes from a geometric balance law of interface defect density and has separate terms for kinetics of existing interfaces and nucleation of new interfaces. The energy is constructed such that it has a coupling between strain and phase field just enough that phase field driving force governs the kinetics of existing interfaces but does not affect nucleation. We characterize and demonstrate various features of the model including existence of travelling wave solutions, prescribable complex kinetic laws and nucleation criteria, kinetics at boundaries of the domain. We analyse supersonic interfaces in trilinear material and show that our model does not capture it and neither does any of the existing phase field models.

Twinning is a special case of phase transformation and twins often form needle like structures, see for e.g. figure 2 and 3 in [CMZ⁺06]. [HRL99] model and explain formation of such structures using level-set method. We perform the same calculation using our phase-field model as an example.

The issue of prescribing kinetic law and nucleation criteria also persists and is more complex in the situation when there are multiple phases, i.e., when there are more than two phases material can transform

into. For n possible phases, there can be ${}^n C_2$ possible interfaces and each of the interfaces, ideally, should have its own kinetics independent of other phases. Some of the existing work on this problem are [SPN⁺96, SP99] and [LR15]. The former describes model for n -phase which allows to prescribe kinetics for each kind of interface but I do not know of any work presenting numerics of the model coupled with elasticity. The latter highlights and addresses the issue of appearance of unwanted and unphysical phase configurations such as three phase parameters being non-zero at one material point. They resolve the problem by introducing energy penalty which prohibits formation of unwanted phase configurations.

We extend our model to the multiple phase setting. The initial part of representing an $i - j$ interface between i -th and j -th phase in our extension is similar to the work in [SP99]. We address the issue of formation of unwanted phase configurations using kinetic constraints. Although, it is possible to use energy penalty to resolve the issue we refrain from using the approach since modifying the energy density will affect the driving force for each interface which may lead to coupling of kinetics of different kinds of interfaces.

The second problem we address in this thesis is a phase-field model for fracture. Crack in the phase-field context can also be understood as a phase transformation problem with one phase being the intact, undamaged material and the second phase being the cracked material. The cracked material is modelled as a negligible stiffness material with a constant surface energy density. We use the same evolution law for phase-field which was derived for phase interfaces; in this context crack faces represent the evolving interface.

Using the evolution law is energetically different from what other phase-field [BVS⁺12, BLR11] models use, which is minimization of energy w.r.t. phase field. The physical interpretation of minimization is that crack propagation is much faster than elastodynamics and equilibrates immediately. This condition also implies the Griffith's criteria for crack propagation, i.e., energy release rate is equal to energy spent to generate the new surface. Hence, there is no dissipation and energy of the system (including the surface energy of crack) is conserved as crack propagates. Use of evolution law endows a notion of rate to crack propagation and results in a dissipative system. However, that is a necessary aspect of modelling kinetics and nucleation for the crack.

Anisotropy in crack growth is important. One approach to model anisotropy in crack growth in phase-field models is to specify the surface energy of the crack as anisotropic as in [LPM⁺15] however some of

the limitations of the approach are possible forms of anisotropy are restricted and require smoother shape functions for numerical implementation. We suggest a way to model anisotropy in the crack propagation via kinetic anisotropy rather than energetic one which addresses these issues.

The initial motivation for the modelling fracture was same as that for phase transformation problem, i.e., to achieve prescribable kinetic law and nucleation criteria for cracks. However we found some severe problems associated with existing phase field models for fracture which we have not been mentioned in the existing literature so we highlight those issues.

In the quasistatic phase model given by [BFM08], the crack width depends only upon the regularization parameter. The existing models for dynamic fracture, such as [BLR11, BVS⁺12], are essentially same as the quasistatic model except linear momentum balance with inertia is solved instead of stress equilibrium. We have found that in this situation crack width depends not only upon the regularization parameter but also on the crack speed. In quasistatics, energy is minimized with respect to both the displacement and phase-field, the energy cost of the cracked region keeps the crack just enough wide so that the intact material beside it can relax. While in elastodynamics, the elastic fields take time (proportional to wave speed) to equilibrate which leads to widening of cracks. The model we have developed also suffers from similar issues.

Another issue is response of the cracked region. Some existing work on phase field models for fracture (for e.g. [BLR11]) model the crack as a material of zero or negligible stiffness. This is a reasonable approximation if only antiplane or mode-III cracks are considered however for a general loading condition it is not suitable for e.g. it will result in incorrect behaviour for a crack under pure compression. [MWH10] suggested the response of the degraded material based on spectral decomposition of the strain tensor to resolve this issue. It resolves the issue of crack under compression however does not result in the correct stress state for arbitrary loadings and we construct an example in the relevant chapter to demonstrate this. It is important to take crack orientation into account for modelling the elastic response of the cracked region which we attempt by using crack face normal $\mathbf{n} = \nabla\phi/|\nabla\phi|$ where ϕ is the phase field. While we were able to reproduce a more physical response, there are still some unresolved issues such as behaviour near the crack tip where crack-face normal cannot be used to determine crack orientation.

Finally, we apply the developed model to a composite material. The interface between two materials can be either more or less susceptible to crack than either of the two materials. One approach to model

this behaviour is by modifying the fracture toughness \mathcal{G}_c of the interface. We propose and demonstrate another approach to capture this behaviour by using the nucleation term in our model. While the two approaches seem to capture the same macroscopic response, they represent different microscopic origins. The first one is an energetic consideration based on the energy required to create new surface, the second one can be seen as coming from an instability at the atomic scale.

Each chapter in this thesis is written to be read independently, therefore has its own, detailed introduction and formulation. Finally we conclude with some of the open problems and limitations of our work and insights for them.

Chapter 2

Formulation and one-dimensional characterization

2.1 Introduction

Twinning and structural phase transformations are important in areas as diverse as superelasticity and shape-memory in functional materials [Bha03a], forming of structural metals [BCR10], nanostructured metals with exceptional properties such as high strength and high ductility [HB14, KAF09, WTAF09], and the dynamic response of metals under extreme conditions [CSWRS09]. The typical microstructure in these settings consists of homogeneously deformed regions separated by interfaces across which the deformation varies extremely rapidly. Many important aspects of these phenomena are governed by the nucleation, motion, and response of the interfaces.

In the continuum setting, twinning and structural transformations are modeled using nonconvex strain energy density functions $W(\epsilon)$, an approach introduced in the seminal paper of Ericksen [Eri75] in 1D. The nonconvexity allows for the coexistence of different phases or twins for a given stress value $\sigma = \frac{dW}{d\epsilon}$. The different phases are separated by interfaces across which the strain is discontinuous. Since the standard continuum theory contains no lengthscale, these interfaces are “sharp”, i.e. singularly localized. Ericksen observed that the continuum balance of linear momentum is insufficient to identify a unique spatial location of the interfaces, even assuming the existence of a single interface. In the static setting without inertia, he used energy minimization as a selection criterion to obtain a unique solution.

Abeyaratne and Knowles [AK90, AK91b] examined nonconvex models in the dynamic setting with inertia. Again, balance of linear momentum does not provide a unique solution even in the simplest case of a single interface in 1D. Further, energy minimization is not applicable in dynamic problems and cannot be used to resolve this. Invoking thermodynamics, viz. positive dissipation, provides some weak restrictions on the motion of the interface, but still leaves a massively nonunique problem with essentially a 1-parameter family of solutions that is parametrized by the location of the interface. [AK90, AK91b], and related work in [Tru82], find that imposing additional closure relations makes the problem unique. Namely, the closure relations are (i) the kinetic relation that relates the velocity of the interface to the thermodynamic work conjugate driving force, and (ii) the nucleation criterion that provides for the formation of new interfaces. Physically, the closure relations can be thought of as a macroscopic remnant of the lattice-level atomic motion from one energy well to another that is lost in the continuum theory. However, a systematic derivation from a microscopic theory as well as experimental confirmation remain a topic of active research.

The closure relations – nucleation criterion and kinetic relation – have the advantage of clear and direct physical interpretations. In particular, they fit naturally into a multiscale modeling framework by allowing for precisely-defined constitutive input on the behavior of interfaces from either experiment or modeling (e.g., molecular dynamics). However, numerical computations with this approach are extremely challenging, because the sharp interfaces require complex and expensive tracking algorithms in a numerical discretization. This is an unfeasible challenge when one expects numerous interfaces that are evolving, interacting, and nucleating. Therefore, this *sharp-interface approach* has not been widely applied to larger problems.

In contrast to this, there is a large body of work on methods that regularize or smooth the interface by adding strain gradients, viscous dissipation, and similar effects to the stress response, e.g. [AK91a, Ros95, Tur97, Tru93, FM06]. In 1D, the stress in these models is typically given by:

$$\sigma = \frac{dW}{d\epsilon} + \nu \frac{\partial \epsilon}{\partial t} - \kappa \frac{\partial^2 \epsilon}{\partial x^2} \quad (2.1.1)$$

In these *regularized-interface approaches*, the evolution of interfaces is obtained simply by solving momentum balance $\text{div } \sigma = \rho \ddot{u}$. The solutions are typically unique but depend strongly on the regularization

parameters, viz. the viscosity ν and the capillarity κ . While the nonconvexity in W favors the formation of interfaces, the gradient regularization $\kappa \frac{\partial^2 \epsilon}{\partial x^2}$ penalizes the sharpness of interfaces and thereby prevents them from being singular. Because interfaces are not singular and hence do not need to be explicitly tracked, these approaches are relatively easy to apply to large problems. Further, nucleation of new interfaces and topology transitions occur naturally without additional computational effort or constitutive input.

In the closely-related phase-field approaches, the situation is similar. The phases are distinguished by a scalar field ϕ , and the energy is nonconvex in ϕ with a coupling to elasticity. A typical phase-field energy density [Che02, SL07, ZB05, AA12, YD10, SY08, LLSL10] has the form

$$w(\phi) + \frac{1}{2} (\boldsymbol{\epsilon} - \boldsymbol{\epsilon}_0(\phi)) : \mathbf{C} : (\boldsymbol{\epsilon} - \boldsymbol{\epsilon}_0(\phi)) + \kappa |\nabla \phi|^2 \quad (2.1.2)$$

$w(\phi)$ is a nonconvex energy and favors the formation of interfaces, while the gradient term $\kappa |\nabla \phi|^2$ regularizes them. These terms are coupled to linear elasticity through the elastic strain $(\boldsymbol{\epsilon} - \boldsymbol{\epsilon}_0(\phi))$, that is the difference between the total strain $\boldsymbol{\epsilon} \equiv \text{grad } \mathbf{u}$ and the stress-free strain $\boldsymbol{\epsilon}_0(\phi)$ that depends on the phase. The total energy E is obtained by integrating the energy density over the body and accounting for the boundary working. The evolution is governed by a gradient descent in ϕ , i.e. $\mu \dot{\phi} = \frac{\delta E}{\delta \phi}$, and linear momentum balance for the evolution of the displacement / strain field. Phase-field models share the key features of the strain-gradient models:

1. the evolution of interfaces is unique, and governed by μ , κ and other model parameters;
2. nucleation and topology transitions occur naturally without additional input, and like kinetics, are governed by μ , κ and other model parameters;
3. nucleation and kinetics are modeled together in a single equation; and
4. they are relatively easy to apply to large problems because interfaces are not singular.

Feature 4 of phase-field models is an important advantage of these approaches. However, Features 1, 2, and 3 are *not* advantages, but instead important shortcomings of these models. While it is certainly important to obtain unique solutions, the fact that the nucleation and kinetics of interfaces are governed by a small set of parameters implies that the range of behavior that can be modeled is highly restricted. In addition, the nucleation and kinetics of interfaces are physically distinct processes from the atomic

perspective, but in these models are governed through the same evolution equation.

Feature 1 greatly limits the ability to formulate a model that produces a desired kinetic response. For example, the kinetics of interfaces in strain-gradient models is analyzed by [AK91a], and they find that the range of kinetic responses that can be obtained by varying ν and κ is extremely constrained¹. For instance, an important feature that is widely observed is stick-slip behavior of interfaces, e.g. [FS11], but this cannot be readily modeled in strain-gradient or phase-field models. In general, it is difficult to prescribe a given kinetic response directly; making the parameter μ a function of various quantities *may* allow this, but the dependence on these quantities to obtain a desired kinetic response is opaque. Therefore, calibrating a desired kinetic response using this route can require much trial-and-error that is tedious, unsystematic, and very expensive.

The situation in Feature 2 is similar to that in Feature 1, except that it is *much* more difficult! Existing phase-field models are completely opaque, even in 1D, about the precise critical condition at which nucleation occurs [DB06]. The nucleation behavior in a three-dimensional setting, with a complex energy landscape and numerous local extrema, combined with both inertial and gradient descent dynamics, is even more complex. Consequently, the inverse problem is extremely hard: namely, how do we set up the energy and evolution to obtain a desired nucleation response? That is, given some critical conditions under which nucleation takes place – perhaps from experimental observation or molecular calculations – how do we tailor the various functions and parameters in the model to achieve this behavior? Modifying the energy barriers is an obvious starting point, but is difficult to do systematically; for instance, changing an energy barrier affects the nucleation behavior of both the forward and reverse transformations. In a situation with numerous possible transformations, modifying the barrier can have unintended effects on all the transformations. Another strategy is to use spatially-localized defects (or “soft spots”, e.g. [ZB05]), where the energy landscape is locally modified to have shallow barriers to aid nucleation. This approach is difficult to use in situations that have not already been well-characterized by other techniques. For instance, to obtain a desired nucleation stress, how should the soft spots be spatially arranged? should we have more soft spots with higher barriers, or a few soft spots with lower barriers? what shape should they be? and so on. The current approach is typically ad-hoc, and involves trying a given configuration of soft spots, and doing full-field calculations to test if the given configuration provides the desired nucle-

¹In generalized versions, e.g. [FG94, Ros95, GF97], a larger class of kinetics is possible, but the relation between the model parameters and the induced kinetics is often not transparent even for 1D.

ation behavior. Other strategies to induce nucleation, such as adding external driving noise, differ in the details, but have the same basic problem that modeling a desired nucleation behavior essentially requires solving an unwieldy inverse problem posed in a very large space in an unsystematic and expensive way, when the forward problem itself is not well-understood. In addition, this inverse problem can be highly geometry- and problem-specific; calibration for a specific geometry will likely not be transferable to other geometries. This difficult situation is vastly compounded when one begins to consider the realistic case that there is not simply one type of twinning interface, but rather various different ones for orientations, each with a different propensity to nucleate and move, with the entire problem posed in 3D. Further, it is likely that critical conditions for nucleation in real systems is not simply related to the energy conjugate driving force; rather, there is likely rate-dependence, possibly dependence on hydrostatic stress even in volume-preserving twinning transformations, and so on.

Feature 3 complicates the process of calibrating a model to an observed nucleation and kinetics because the separation between these processes in the model is largely absent.

The failings of existing phase-field models make them impossible to use in a hierarchical multiscale setting. Hierarchical multiscale approaches rely on the passage of information from fundamental models to larger-scale models. In the setting of structural transformations, atomic calculations (e.g., [DWW14, OSPM14, WBT10, BT10, BEKT12]) as well as experiments (e.g., [NRC06, EC93]) have provided important information on twin kinetics and nucleation. But almost none of this information can be used in the existing phase-field models, beyond some minor calibrations. This wastes the wealth of insights that have been gathered from atomistics and experiment, and breaks the multiscale link between the atomic level and the continuum.

The advantages and failings of the different approaches described above provide the motivation for our work. We present a regularized-interface model that has the advantage that computations are easy and efficient because we do not need to track interface evolution, nucleation, and topology transitions. However, our formulation is also designed to obtain the key advantage of the sharp interface formulation, namely that we can transparently, precisely, and readily specify complex nucleation and kinetics behavior. The technical strategy consists of 2 elements: (i) parametrization of the energy in a specific way, and (ii) evolution of ϕ through a geometric conservation law.

The first element is to re-parametrize the energy density so that it continues to reproduce the elastic

response of each phase away from energy barriers, but leads to a clear separation between kinetics and nucleation. Briefly, the re-parametrized energy density $\overset{\circ}{W}(\mathbf{F}, \phi)$ is independent of ϕ except when ϕ is in a narrow range that can be considered to be the transition between the phases; an example is shown in Fig. 2.1 and explained in detail below. Therefore, the work-conjugate driving force for ϕ vanishes when ϕ is away from the transition range, and consequently ϕ cannot evolve irrespective of the value of stress and other mechanical quantities. Hence, when a region of the body is in a single phase, i.e. ϕ is uniform in a region, then ϕ cannot evolve and a new phase cannot nucleate. The only region where ϕ can evolve is when it is in the transition range, which occurs near an interface. Therefore, the energy allows a material region to undergo a transformation only when an interface sweeps over it, and nucleation of a new phase away from an interface is completely prohibited. We will re-introduce nucleation through the balance law in a separate term from the kinetics; the advantage of this approach is that nucleation cannot occur through the kinetic law. Thereby, our approach makes a clear distinction between kinetics and nucleation as mechanisms for the evolution of ϕ : the kinetic law cannot cause nucleation, and the nucleation term does not affect kinetics. This is in sharp contrast to standard phase-field models where a uniform phase may nucleate a new phase if the driving force *for kinetics* is sufficiently large, even if the desired critical conditions for nucleation have not been met. There, the variational derivative of the energy with respect to ϕ governs both the kinetics of existing interfaces as well as the nucleation of new phases. Therefore, the process of nucleation is intimately and opaquely mixed in with the prescribed kinetics in these models, making it hard to prescribe precise nucleation criteria.

The second element is to use a geometrically-motivated conservation law to govern the evolution of ϕ . Briefly, we interpret $\nabla\phi$ as a geometric object that provides us with the linear density of interfaces. Then, for a material line element, we count the number of interfaces that are entering and leaving at each end of the element. The statement of the conservation law is that the increase in the number of interfaces threaded by the line element is equal to the net number of interfaces that are entering, plus the creation of interfaces through a source term. The motion of interfaces is described by an interface velocity field v_n^ϕ , distinct from the material velocity field. The value of v_n^ϕ at each point can have a complex functional dependence on *any* mechanical field, e.g. stress, stress rate, nonlocal quantities, and so on, and this provides a route to transparently specify extremely complex kinetic response. Similarly, the source term in the balance law provides transparent and precise control on the nucleation of new

interfaces, by activating the source only when the critical conditions for nucleation are realized. An important element is that the kinetic term is multiplied by $|\nabla\phi|$; therefore a uniform phase will not show any evolution of ϕ due to the kinetic term regardless of the stress level, and the only possible mechanism for the evolution of ϕ from a uniform state is by nucleation.

2.1.1 Organization

The paper is organized as follows.

- In Section 2.2, we describe the re-parametrization of the energy, the formulation of the interface balance principle, and the driving forces on interfaces obtained by enforcing positive dissipation. We also examine formally the sharp-interface limit of the dissipation in our model.
- In Section 2.3, we examine in 1D the behavior of steadily-moving interfaces in our model using a traveling-wave approach to show the relation between the prescribed kinetic response and the effective kinetics in terms of interface velocity and classical driving force.
- In Section 2.4, we perform 1D dynamic calculations to understand the evolution of interfaces. As in the section on traveling waves, we aim to find the effective kinetic relation induced by our model.
- In Section 2.5, we examine the effect of a small parameter that has been introduced in the re-parametrization of the energy.
- In Section 2.6, we examine the competition between thermodynamics and momentum balance in setting the kinetics of an interface. We point out the difficulty our model has in dealing with certain phase interfaces whose evolution is uniquely described by momentum balance and that therefore does not require an additional kinetic relation.
- In Section 3.11, we review our work.
- In Appendix 2.A, we examine briefly the connection to Noether's principle.
- In Appendix 2.B, we examine the possibility of supersonic phase interfaces in standard phase-field models.

2.1.2 Notation and Definitions

Boldface denotes vectors and tensors. We have used Einstein convention, i.e. repeated indices imply summation over those indices, except when noted.

ϕ	phase field
$\boldsymbol{\alpha} \equiv \nabla \phi$	gradient of phase field interpreted as the linear density of interfaces
$\hat{\mathbf{n}} \equiv \frac{\boldsymbol{\alpha}}{ \boldsymbol{\alpha} }$	unit normal vector to the interface between phases
$\hat{\mathbf{t}}$	unit tangent to a curve in space
\mathbf{x}_0	material particle in the reference configuration
\mathbf{x}	material particle in the deformed configuration
$\nabla \equiv \nabla_{\mathbf{x}}$ and $\nabla_{\mathbf{x}_0}$	gradient with respect to \mathbf{x} and \mathbf{x}_0 respectively; $\nabla_{\mathbf{x}} = \mathbf{F}^{-T} \nabla_{\mathbf{x}_0}$
Ω and Ω_0	the body in the current and reference configuration respectively
$\partial\Omega$ and $\partial\Omega_0$	the boundary of Ω and Ω_0 respectively
\mathbf{N} and \mathbf{N}_0	the outward normals to $\partial\Omega$ and $\partial\Omega_0$ respectively
$\mathbf{F} \equiv \nabla_{\mathbf{x}_0} \mathbf{x}$	deformation gradient
ρ_0	mass density in the reference configuration
$J \equiv \det \mathbf{F}$	Jacobian of the deformation
$\mathbf{C} \equiv \mathbf{F}^T \mathbf{F}$	Right Cauchy-Green deformation tensor
$\mathbf{E} \equiv \frac{1}{2}(\mathbf{C} - \mathbf{I})$	Green-Lagrangian strain tensor
$\boldsymbol{\epsilon} \equiv \frac{1}{2}(\mathbf{F} + \mathbf{F}^T) - \mathbf{I}$	linearized strain tensor
$W(\mathbf{F})$	classical elastic energy density
$\overset{\circ}{W}(\mathbf{F}, \phi)$	modified elastic energy density
$\boldsymbol{\sigma} = \frac{\partial W}{\partial \mathbf{F}}$ or $\frac{\partial \overset{\circ}{W}}{\partial \mathbf{F}}$	First Piola-Kirchhoff stress
\mathbf{v}	material velocity
v_n^ϕ	normal velocity field for interface motion
\hat{v}_n^ϕ	kinetic response function for interface normal velocity
G	nucleation/source term
f	driving force
f_{bulk}	bulk driving force
f_{edge}	edge driving force
$[[\cdot]]$	The jump in a quantity across an interface

For simplicity, we abuse notation and use interchangeably $W(\mathbf{F})$ and $W(\mathbf{E})$, and $\overset{\circ}{W}(\mathbf{F}, \phi)$ and $\overset{\circ}{W}(\mathbf{E}, \phi)$. For these quantities and σ , we use the same symbol both for the field and for the material response function.

$H_l(x)$ represents a function that resembles the Heaviside step function. It transitions rapidly but smoothly from 0 to 1 and is symmetric about $x = 0$, and l represents the scale over which the function transitions. It is assumed to be sufficiently smooth for all derivatives in the paper to be well-defined. The particular choice in this paper is $H_l(x) = \frac{1}{2}(1 + \tanh(x/l))$. The derivative of $H_l(x)$ is written $\delta_l(x)$, and is a smooth function that formally approximates the Dirac measure.

2.2 Formulation

Similar to the standard phase-field models, we use two primary fields, \mathbf{x} to describe the deformation, and ϕ to track the phase of the material. The evolution of \mathbf{x} is governed by balance of linear momentum, i.e. $\text{div}_{\mathbf{x}_0} \left(\frac{\partial \overset{\circ}{W}(\mathbf{F}, \phi)}{\partial \mathbf{F}} \right) = \rho_0 \ddot{\mathbf{x}}(\mathbf{x}_0, t)$. We assume that the elastic energy density $W(\mathbf{F})$ and the kinetic and nucleation relations for interfaces have been well-characterized and are available. We aim to formulate a regularized-interface model that has the same elastic response and kinetic and nucleation behavior for interfaces. We describe below how to set up $\overset{\circ}{W}(\mathbf{F}, \phi)$ given $W(\mathbf{F})$, the evolution equation for the kinetics and nucleation of ϕ , and the thermodynamics associated with our model.

2.2.1 Energetics

We start by assuming that the classical strain energy density $W(\mathbf{F})$ of the material is available, perhaps by calibrating to experiment or from lower-scale calculations. We wish to obtain the modified energy density $\overset{\circ}{W}(\mathbf{F}, \phi)$, which will have certain features that provide critical advantages for nucleation, yet stays largely faithful to $W(\mathbf{F})$. Therefore, we require the following of $\overset{\circ}{W}$: (i) away from energy barriers, $W(\mathbf{F}) = \overset{\circ}{W}(\mathbf{F}, \phi)$ for the value of ϕ that corresponds to the appropriate phase; and (ii) $\overset{\circ}{W}$ should be convex in the (linear or nonlinear) strain for a given value of ϕ , preventing transformations purely through the evolution of \mathbf{F} , and hence enables the dynamics of ϕ to govern the phase transformation.

We begin by considering two phases with characteristic strains given by \mathbf{E}_1 and \mathbf{E}_2 . We emphasize that

these strains need *not* correspond to stress-free states, but that the tangent modulus at those points is positive-definite. Then, define the functions for $A = 1, 2$:

$$\psi_A(\mathbf{E}) = W(\mathbf{E}_A) + \underbrace{\boldsymbol{\sigma}_T}_{\equiv \frac{\partial W}{\partial \mathbf{E}} \Big|_{\mathbf{E}_A}} : (\mathbf{E} - \mathbf{E}_A) + \frac{1}{2} (\mathbf{E} - \mathbf{E}_A) : \underbrace{\mathbf{C}_T}_{\equiv \frac{\partial^2 W}{\partial \mathbf{E} \partial \mathbf{E}} \Big|_{\mathbf{E}_A}} : (\mathbf{E} - \mathbf{E}_A) \quad (2.2.1)$$

ψ_A approximates the behavior of W near the states \mathbf{E}_1 and \mathbf{E}_2 , and ψ_A are convex in the arguments.

We now define the re-parametrized energy density $\mathring{W}(\mathbf{F}, \phi)$:

$$\mathring{W}(\mathbf{E}, \phi) = (1 - H_l(\phi - 0.5)) \psi_1(\mathbf{E}) + (H_l(\phi - 0.5)) \psi_2(\mathbf{E}) \quad (2.2.2)$$

where H_l is a smooth function that resembles the Heaviside (described in Section 2.1.2). Therefore, $\mathring{W}(\mathbf{E}, \phi \simeq 0) = \psi_1(\mathbf{E})$ and $\mathring{W}(\mathbf{E}, \phi \simeq 1) = \psi_2(\mathbf{E})$; further, $\mathring{W}(\mathbf{E}_1, 0) = W(\mathbf{E}_1)$ and $\mathring{W}(\mathbf{E}_2, 1) = W(\mathbf{E}_2)$.

Fig. 2.1 plots an example of \mathring{W} with a scalar strain measure to enable representation on paper. The low-strain phase corresponds roughly to $0.0 < \phi < 0.3$, and the high-strain phase corresponds roughly to $0.7 < \phi < 1.0$. The transition range is roughly $0.3 - 0.7$. In general, ϕ is in the transition range only in the vicinity of an interface. In a uniform phase region, ϕ will take on a value appropriate to that phase.

The key reason to re-formulate the energy is to achieve a clear separation between nucleation and kinetics. In standard phase-field models, the form of the energetic coupling between ϕ and strain can lead to the nucleation of a new phase in a single-phase region purely through the kinetic equation, making the separation between nucleation and kinetics impossible. Here, \mathring{W} is independent of ϕ if it is outside the transition range; consequently, there can be no driving force for kinetic evolution when ϕ is outside this range, irrespective of the level of stress or other fields. Consequently, away from an interface, ϕ will not evolve through the kinetic response irrespective of the local mechanical state. Hence, the kinetic response cannot cause nucleation of a new phase in a single-phase region. The kinetic equation can play a role only when ϕ is in the transition set in the vicinity of an interface, i.e., it can affect the behavior of an interface but not a uniform phase.

While our energy does not permit nucleation, the conservation law that we set up below for interfaces permits us to specify precisely the nature of nucleation. Further, the kinetic equation described there is

multiplied by $|\nabla\phi|$, which suppresses the kinetic evolution of ϕ when it is spatially-uniform away from an interface. Hence, away from an interface, the only way that ϕ can evolve is when the nucleation term – that can be a function of stress or any other field – in the interface conservation law is activated.

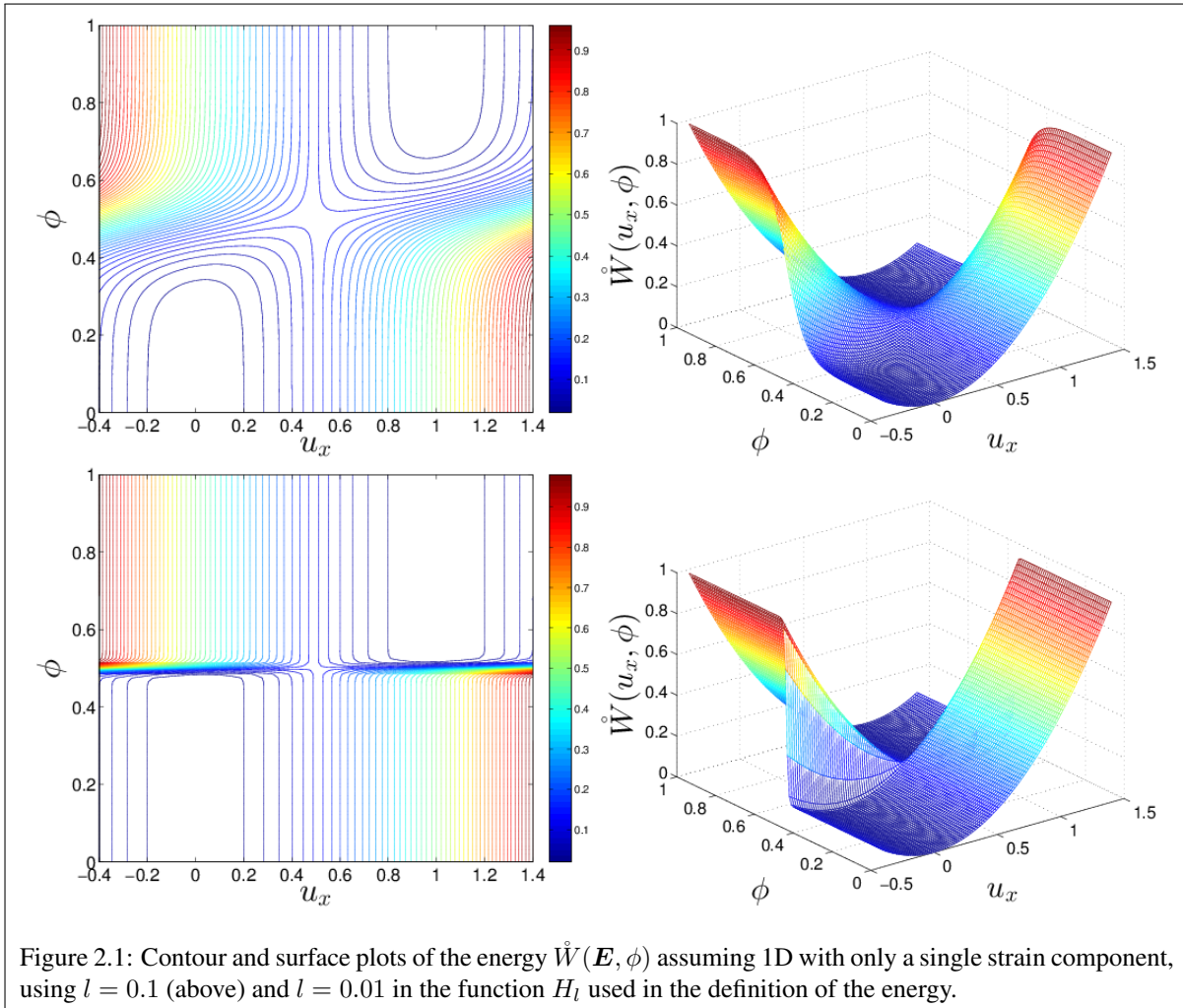


Figure 2.1: Contour and surface plots of the energy $\hat{W}(\mathbf{E}, \phi)$ assuming 1D with only a single strain component, using $l = 0.1$ (above) and $l = 0.01$ in the function H_l used in the definition of the energy.

We remark on some features of this energy:

1. Using σ_T , the tangent stress, allows us to position the characteristic strains $\mathbf{E}_1, \mathbf{E}_2$ at any point in strain-space where the tangent modulus is positive-definite. These do not need to correspond to stress-free strains, and this property is useful in modeling situations such as stress-induced martensite, where one phase is observed only under stress.
2. We have used only two terms in the Taylor expansion around the characteristic strains. Increased fidelity to W may be possible with use of additional terms, but this requires care to retain convexity in \mathbf{E} . Our reason to have convexity is loosely based on obtaining unique solutions, and preventing

- phase transformations that occur without the evolution of ϕ . It is possible that convexity can be too strong an assumption [Ant05]. However, this is a larger issue beyond the scope of our work here.
3. \mathring{W} is faithful to the original energy W near the characteristic strains, but less so further away. At the barriers, it is completely at odds with W , because \mathring{W} is convex for fixed ϕ . However, passage over the barrier is governed by nucleation and kinetics, hence we do not need to accurately model it through \mathring{W} . We further note that the driving force on an interface in sharp-interface classical elasticity is $f_{class} \equiv \llbracket W \rrbracket - \langle \boldsymbol{\sigma} \rangle : \llbracket \mathbf{F} \rrbracket = W(\mathbf{F}^+) - W(\mathbf{F}^-) - \frac{1}{2}(\boldsymbol{\sigma}(\mathbf{F}^+) + \boldsymbol{\sigma}(\mathbf{F}^-)) : (\mathbf{F}^+ - \mathbf{F}^-)$, where \mathbf{F}^\pm are the limiting deformation gradients on either side of the interface [AK06]. Therefore, f_{class} does not depend on the details of the barrier for given \mathbf{F}^\pm .
 4. Stresses and other applied fields can lead to the usual elastic deformations through the elastic response of each phase in any part of the domain, both near and away from interfaces.
 5. The energy density of the body includes a contribution $\frac{1}{2}\epsilon|\nabla\phi|^2$. As in standard phase-field models, this prevents the formation of singularly-localized interfaces. Therefore, the total energy written in the reference configuration is $\int_{\Omega_0} \left[\mathring{W}(\mathbf{F}, \phi) + \frac{1}{2}\epsilon|\mathbf{F}^{-T}\nabla_{\mathbf{x}_0}\phi_0|^2 \right] d\Omega_0$, up to boundary terms. For simplicity, we approximate the gradient contribution in the reference by $\int_{\Omega_0} \frac{1}{2}\epsilon|\nabla_{\mathbf{x}_0}\phi_0|^2 d\Omega_0$.
 6. Our energetic prescription shares some features of standard phase-field models. For instance, both models (typically) have convex energy density in the elastic strain for a *fixed* value of ϕ . The nonconvexity in ϕ in the energy density for standard phase-field models is observed when the strain is allowed to completely relax to the stress-free state for each value of ϕ . Our energy also has this nonconvexity, which can be seen in examining Fig. 2.1: if we increase ϕ while traversing a curve that minimizes the energy with respect to the strain, we see that it is nonconvex. While it is possible that one would not call them “wells”, because the energy remains constant when ϕ is outside the critical range, there is nonconvexity in our model; for example, the point (0.5, 0.5) in the strain- ϕ space is a barrier between the low-energy states.

2.2.2 Evolution Law

Our starting point in formulating the evolution of ϕ is to note that $\nabla\phi$ provides, roughly, a measure of the number or “strength” of the interfaces in the ϕ field per unit length, Fig. 2.2.

In general, given a field $\phi(\mathbf{x})$ with localized transitions between constant values, we can readily locate

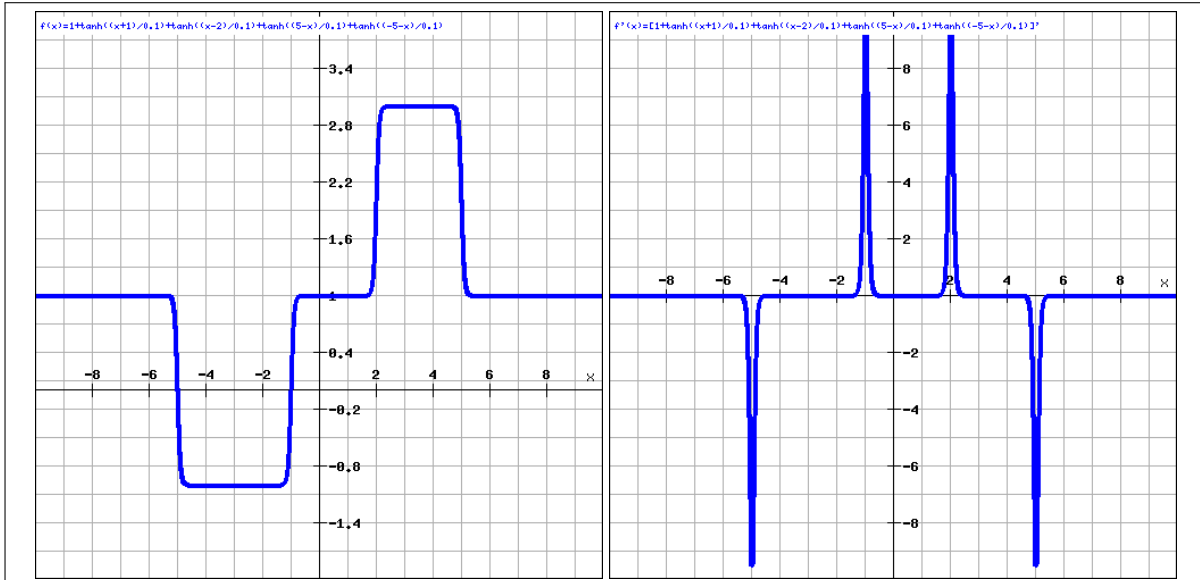


Figure 2.2: Left: a field ϕ with a number of interfaces. Right: $\nabla\phi$ provides a measure of (signed) interface density per unit length.

the interfaces in this field using $\nabla\phi$. Further, if we pick any curve and integrate $\nabla\phi$ along this curve, the value that we obtain provides a measure of the net number of interfaces that we have traversed, assuming that all interfaces have the same “strength”. If the interfaces have different strengths, we obtain a measure of the net interface strength that we have traversed. This physical picture provides the intuition behind what follows, but it also expresses the simple fact that if we have a single-valued field ϕ , then integrating the gradient is simply the difference between ϕ at either end of the curve.

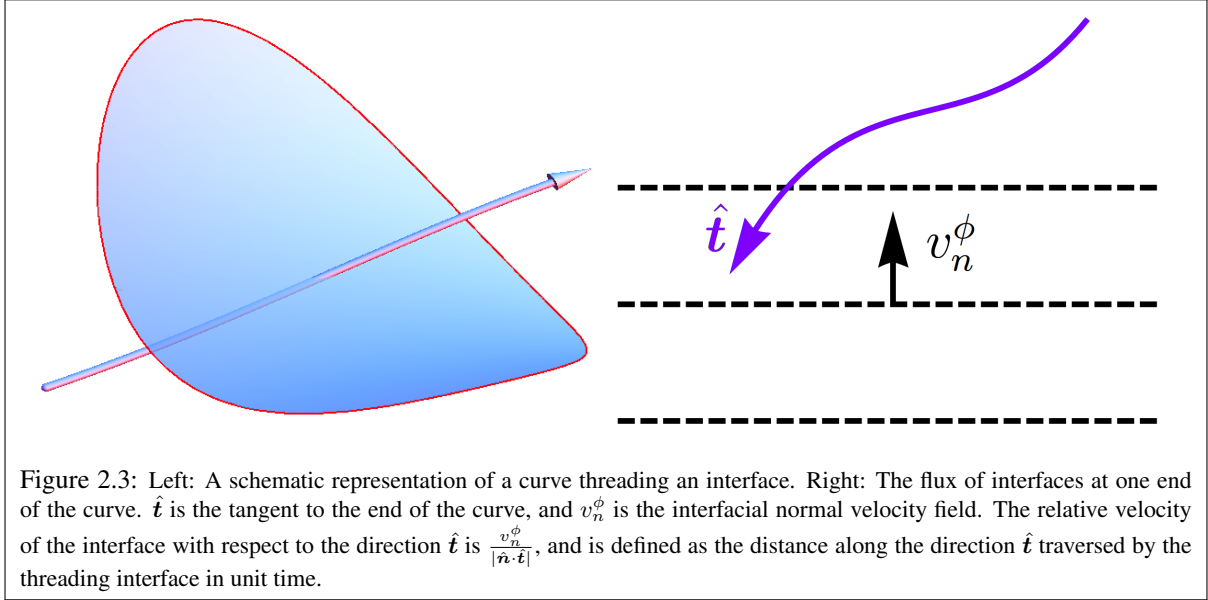
The geometric picture is roughly related to gradients of fields being so-called 1-forms, i.e., they are objects that are naturally integrated along curves [MH94]. Analogies of this are commonplace in elasticity: e.g., the divergence of a field is a 3-form and is naturally integrated over volumes, as is used in the conservation laws for mass, momentum, and energy. The curl of a field is a 2-form and is naturally integrated over surfaces, as is used in proving the single-valuedness of a deformation field corresponding to $\text{curl } \mathbf{F} = \mathbf{0}$, as well as in dislocation mechanics where $\text{curl } \mathbf{F}$ provides an areal density of dislocation line defects [Ach01].

Given this notion of the interface density field $\nabla\phi$, we then formulate a balance law (see Fig. 2.3). Let the interfaces have a normal velocity given by the field v_n^ϕ ; note that this velocity is distinct from the material velocity $\dot{\mathbf{u}}$. Now consider a curve $C(t)$ in space. This curve “threads” or passes through some number of interfaces. Further, interfaces are entering or exiting at both ends of the curve due to their motion

described by the field v_n^ϕ . The conservation principle is that the net increase in the number of interfaces that are threaded by $C(t)$ is a balance between interfaces entering, interfaces exiting, and interfaces being created and destroyed by sources and sinks.

$$\frac{d}{dt} \left\{ \begin{array}{c} \text{interfaces threaded} \\ \text{by the curve} \end{array} \right\} = \left\{ \begin{array}{c} \text{interfaces entering} \\ \text{the curve} \end{array} - \begin{array}{c} \text{interfaces leaving} \\ \text{the curve} \end{array} \right\} + \left\{ \begin{array}{c} \text{interface} \\ \text{creation} \end{array} \right\}$$

Using that this must hold for every curve $C(t)$ enables us to localize the balance law.



The flux of interfaces through the ends of the curve $C(t)$ can be computed by referring to Fig. 2.3. Let $\hat{\mathbf{t}}$ be the unit tangent to the end of the curve, and $\hat{\mathbf{n}} \equiv \frac{\nabla\phi}{|\nabla\phi|}$ the unit normal to the interface. Then the flux can be written

$$|\nabla\phi| \frac{\nabla\phi \cdot \hat{\mathbf{t}}}{|\nabla\phi \cdot \hat{\mathbf{t}}|} \frac{v_n^\phi}{|\hat{\mathbf{n}} \cdot \hat{\mathbf{t}}|} |\hat{\mathbf{t}} \cdot \hat{\mathbf{n}}| \quad (2.2.3)$$

The first term represents the strength of the interface; the second term is simply $+1$ if the interface enters and -1 if it leaves; the third term is the velocity of the interface projected onto the $\hat{\mathbf{t}}$ direction to obtain the velocity *relative* to the curve direction, i.e. the distance along the $\hat{\mathbf{t}}$ direction traversed by the interface in unit time; and the fourth term picks out only the portion of the flux that is threading the curve by moving along $\hat{\mathbf{t}}$.

An alternate picture is to note that $\nabla\phi \cdot \hat{\mathbf{t}}$ is the (signed) interface density along the direction $\hat{\mathbf{t}}$, and $\frac{v_n^\phi}{\hat{\mathbf{n}} \cdot \hat{\mathbf{t}}}$ is

the velocity of the interface relative to the direction $\hat{\mathbf{t}}$, so the flux is simply:

$$\nabla\phi \cdot \hat{\mathbf{t}} \frac{v_n^\phi}{\hat{\mathbf{n}} \cdot \hat{\mathbf{t}}} \quad (2.2.4)$$

Both expressions for the flux are identical, and simplify to $|\nabla\phi|v_n$ when we substitute $\hat{\mathbf{n}} \equiv \frac{\nabla\phi}{|\nabla\phi|}$ ².

Defining the interface density $\alpha := \nabla\phi$, we have:

$$\underbrace{|\alpha|v_n^\phi}_{\text{net flux of interfaces}} \Big|_{C^-}^{C^+} = \underbrace{\frac{d}{dt} \int_{C(t)} \alpha \, d\mathbf{x}}_{\text{increase in number of interfaces threaded}} - \underbrace{\int_{C(t)} \mathbf{S} \, d\mathbf{x}}_{\text{source of new interfaces}} \quad (2.2.5)$$

We can transform $|\alpha|v_n^\phi \Big|_{C^-}^{C^+} = \int_{C(t)} \nabla(|\alpha|v_n^\phi) \, d\mathbf{x}$.

Using that $C(t)$ is a material curve, we can write the mapping $d\mathbf{x} = \mathbf{F} \, d\mathbf{x}_0$ between the infinitesimal elements of $C(t)$ and its image C_0 in the reference. Then, the time derivative can be transformed to

$$\frac{d}{dt} \int_{C_0} \alpha \mathbf{F} \, d\mathbf{X} = \int_{C(t)} (\dot{\alpha} + \alpha \mathbf{L}) \, d\mathbf{x} \text{ where } \mathbf{L} \text{ is the spatial velocity gradient.}$$

This lets us localize to obtain:

$$\dot{\alpha} = \nabla(|\alpha|v_n^\phi) + \mathbf{S}(\mathbf{x}, t) - \alpha \mathbf{L} \quad (2.2.6)$$

Noting that the source is constrained by the above equation to be of the form, i.e. $\mathbf{S} = \nabla G + \alpha \mathbf{L}$, we can integrate the above equation to obtain:

$$|\nabla\phi|v_n^\phi + G = \dot{\phi} \quad (2.2.7)$$

The nucleation / source term G can be an arbitrary function of any of the fields in the problem, up to some weak limitations imposed by thermodynamics (discussed below). The term \mathbf{S} must be a gradient up to the term $\alpha \mathbf{L}$, and represents the fact that in a single-valued field ϕ , interfaces that nucleate must either terminate on the boundary or close on themselves but cannot end in the interior of the body.

We note certain important features of the evolution law that we have posed:

1. The kinetics of existing interfaces is constitutively prescribed through the interface velocity field v_n^ϕ , which can be a function of stress, strain, as well as any other relevant quantity, such as the work-

²A. Acharya gave a different argument for why the flux must have this final form that guided us, and also many useful discussions on Section 2.2.2.

conjugate to ϕ (the Eshelby / configurational force). This makes it trivial to obtain complex kinetics; for instance, if the interface is pinned below a critical value of the stress, we simply prescribe that v_n^ϕ is zero at all spatial points where the stress is below the critical value. Similarly, other kinds of nonlinear and complex kinetics can be readily incorporated.

2. Nucleation of new interfaces is prescribed through the source term in the balance law, and provides precise control on the nucleation process. For instance, we can prescribe that a source is activated only beyond some critical stress and stress rate; thus, for example, it is straightforward to model a nucleation process in which the critical nucleation stress is extremely sensitive to strain rate. In addition, the activation of the source can be completely heterogeneous and vary vastly from point to point.
3. The appearance of $|\nabla\phi|$ in the evolution is important to separate kinetics from nucleation: if we have a large driving force in a uniform phase far away from an interface, $|\nabla\phi|$ will remain 0 and therefore will not allow the kinetic term to play a role irrespective of driving force, stress, etc.

We note that an analogous idea to the conservation principle stated above is used in [Ach01] to obtain an evolution law for dislocations, and recently in [AD14, PAD14] for disclination dynamics. In [Ach01], by connecting the dislocation density to $\text{curl } \mathbf{F}$ and using the physical picture that these are line defects, a conservation law is posed by using that the rate of change of dislocations intersecting an arbitrary area element is related to the net flux of intersecting dislocations and the creation of intersecting dislocations. The conservation law that we have posed in this work builds on this picture, and the key point of departure of our work is the idea that the balance principle from [Ach01] can be extended from line defects detected by $\text{curl} \cdot$ to interfacial defects that are detected by $\nabla \cdot$. A further use of this approach are the standard continuum balances of mass, momentum, energy that are all posed with volumetric densities, and the appropriate quantity to be integrated over a volume is $\text{div} \cdot$.

In Appendix 2.A, we examine the relation between this conservation principle and Noether's theorem.

Balance Law in the Reference Configuration

The entire argument above was posed in the current configuration. Since the field ϕ relates to the state of material particles, it would be physically reasonable to alternatively pose the balance principle in the reference configuration. We examine this approach briefly.

In this section, quantities with subscripts of 0 denote referential objects. \mathbf{x}_0 is the referential pre-image of the material particle $\mathbf{x}(\mathbf{x}_0, t)$. We make the natural transformation that ϕ is the same in the reference and the current for a given material particle at a given time: $\phi_0(\mathbf{x}_0(\mathbf{x}, t), t) = \phi(\mathbf{x}, t)$. From standard manipulations of continuum mechanics, it follows that $\boldsymbol{\alpha}\mathbf{L} + \dot{\boldsymbol{\alpha}} = \mathbf{F}^{-T}\dot{\boldsymbol{\alpha}}_0$. We further make the identification that $\mathbf{S} = \mathbf{F}^{-T}\mathbf{S}_0 \Leftrightarrow G = G_0$.

Substituting in the balance principle (2.2.6), we can write:

$$\mathbf{F}^{-T}\dot{\boldsymbol{\alpha}}_0 = \mathbf{F}^{-T}\mathbf{S}_0 + \mathbf{F}^{-T}\nabla_{\mathbf{x}_0}(|\boldsymbol{\alpha}|v_n^\phi) \quad (2.2.8)$$

We have also used above that $\nabla_{\mathbf{x}} = \mathbf{F}^{-T}\nabla_{\mathbf{x}_0}$.

The natural transformation induced on the interface velocity field is obtained by requiring $|\boldsymbol{\alpha}|v_n^\phi = |\boldsymbol{\alpha}_0|v_{n_0}^\phi$. The result is the non-standard transformation $v_{n_0}^\phi\hat{\mathbf{n}}_0 = \mathbf{F}^{-1}v_n^\phi\hat{\mathbf{n}}$. This is deceptively simple, because the transformation between $\hat{\mathbf{n}}_0$ to $\hat{\mathbf{n}} \equiv \nabla\phi/|\nabla\phi|$ is not as a standard normal to a material surface. The final result can be compactly written $v_{n_0}^\phi = v_n^\phi (\hat{\mathbf{n}}_0\mathbf{F}^{-1}\mathbf{F}^{-T}\hat{\mathbf{n}}_0)^{\frac{1}{2}}$.

Using this further transformation of v_n^ϕ , we obtain the interface balance in the reference configuration:

$$\dot{\boldsymbol{\alpha}}_0 = \mathbf{S}_0 + \nabla_{\mathbf{x}_0}(|\boldsymbol{\alpha}_0|v_{n_0}^\phi) \quad (2.2.9)$$

This can be readily integrated once to obtain

$$\dot{\phi}_0 = G_0 + |\boldsymbol{\alpha}_0|v_{n_0}^\phi \quad (2.2.10)$$

There are two practical, though minor, advantages to the referential form of the balance principle. First, frame-indifference is readily seen to be satisfied. Second, the interpretation of $\mathbf{S}_0 = \nabla_{\mathbf{x}_0}G_0$ is simpler without the additional terms from the material derivative.

2.2.3 Thermodynamics and Dissipation

Following established ideas, we use the statement of the second law that the dissipation must be non-negative for every motion of the body to find the thermodynamic conjugate driving forces for kinetics and nucleation. The dissipation is defined as the deficit between the rate of external work done and the

increase in stored energy:

$$\mathcal{D} = \text{External working} - \frac{d}{dt} \left(\int_{\Omega_0} \left[\dot{W}(\mathbf{F}, \phi) + \frac{1}{2} \epsilon \frac{\partial \phi_0}{\partial x_{0i}} \frac{\partial \phi_0}{\partial x_{0i}} \right] d\Omega_0 + \frac{1}{2} \int_{\Omega_0} \rho_0 V_{0i} V_{0i} d\Omega_0 \right) \quad (2.2.11)$$

This can be manipulated to find the conjugates to v_n^ϕ and G .

$$\mathcal{D} = \text{External working} - \int_{\Omega_0} \left[\frac{\partial \dot{W}}{\partial F_{ij}} \frac{dF_{ij}}{dt} + \frac{\partial \dot{W}}{\partial \phi} \frac{d\phi}{dt} + \epsilon \frac{\partial \phi_0}{\partial x_{0i}} \frac{d}{dt} \frac{\partial \phi_0}{\partial x_{0i}} \right] d\Omega_0 - \int_{\Omega_0} \rho_0 V_{0i} \dot{V}_{0i} d\Omega_0 \quad (2.2.12)$$

Using $\frac{\partial F_{ij}}{\partial t} = \frac{\partial V_{0i}}{\partial x_{0j}}$ and integration-by-parts:

$$\begin{aligned} \mathcal{D} = & \text{External working} - \int_{\Omega_0} \frac{\partial}{\partial x_{0j}} \left(\frac{\partial \dot{W}}{\partial F_{ij}} V_{0i} \right) d\Omega_0 + \int_{\Omega_0} V_{0i} \left(\frac{\partial}{\partial x_{0j}} \frac{\partial \dot{W}}{\partial F_{ij}} - \rho_0 \dot{V}_{0i} \right) d\Omega_0 \\ & - \int_{\Omega_0} \left[\frac{\partial \dot{W}}{\partial \phi} \frac{d\phi}{dt} + \epsilon \frac{\partial \phi_0}{\partial x_{0i}} \frac{d}{dt} \frac{\partial \phi_0}{\partial x_{0i}} \right] d\Omega_0 \end{aligned} \quad (2.2.13)$$

The first integral above is exactly balanced by the external work done by boundary tractions³. The second integral is identically zero from balance of linear momentum. Therefore, the dissipation simplifies to:

$$\mathcal{D} = \int_{\Omega_0} \left[-\frac{\partial \dot{W}}{\partial \phi} + \epsilon \frac{\partial^2 \phi_0}{\partial x_{0i} \partial x_{0i}} \right] \frac{d\phi_0}{dt} d\Omega_0 - \int_{\partial \Omega_0} \epsilon \frac{\partial \phi_0}{\partial x_{0i}} N_{0i} \frac{d\phi}{dt} d\partial \Omega_0 \quad (2.2.14)$$

We continue to assume that there is no dissipation at the boundary, and hence use the boundary condition $\nabla_{\mathbf{x}_0} \phi_0 \cdot \mathbf{N}_0 = 0$. This also corresponds to the standard boundary condition used in phase-field models. In those models, taking the variation of the energy and moving terms to the boundary leads to $\nabla \phi \cdot \mathbf{n} = 0$ when there is no working on ϕ at the boundary. Physically, it implies a boundary kinetics that corresponds to the interface configuring itself instantaneously to always keep the boundary driving force zero, thereby not providing a dissipative mechanism. This can be noted from the expression for the driving force for the interface junction with boundary, f_{edge} , in the companion paper (Section on boundary kinetics); setting the terms t and ϵ_S to 0 there recovers the current model, and f_{edge} is precisely $\nabla \phi \cdot \mathbf{n}$.

We substitute the balance law $\dot{\phi}_0 = G_0 + |\alpha_0| v_{n0}^\phi$, to get:

$$\mathcal{D} = \int_{\Omega_0} \left[-\frac{\partial \dot{W}}{\partial \phi} + \epsilon \frac{\partial^2 \phi_0}{\partial x_{0i} \partial x_{0i}} \right] \left(G_0 + |\nabla_{\mathbf{x}_0} \phi| v_{n0}^\phi \right) d\Omega_0 \quad (2.2.15)$$

³We assume that there is no work done on ϕ at the boundary for now. We revisit this in the section on boundary kinetics in the companion paper.

Defining the driving force $f := - \left[-\frac{\partial \dot{W}}{\partial \phi} + \epsilon \frac{\partial^2 \phi_0}{\partial x_{0i} \partial x_{0i}} \right]$, we get:

$$\mathcal{D} = \int_{\Omega_0} f \left(G_0 + |\nabla_{\mathbf{x}_0} \phi| v_{n0}^\phi \right) d\Omega_0 \quad (2.2.16)$$

To ensure that dissipation is always non-negative, we need both fG_0 and $f|\nabla_{\mathbf{x}_0} \phi|v_{n0}^\phi$ to be non-negative. These are fairly easy conditions to satisfy in a material model. For kinetics, we choose the constitutive response of the form $v_{n0}^\phi = \frac{f}{|f|} \hat{v}_{n0}^\phi(|f|, \dots)$, where the constitutive response function \hat{v}_{n0}^ϕ can be any non-negative function of the arguments, and the list of arguments can consist of any of the field variables, as well as possibly nonlocal quantities. A similarly weak requirement holds for nucleation.

2.2.4 Formal Sharp-Interface Limit

We consider briefly the formal limit of the driving force in the sharp-interface limit $\epsilon = 0$. We emphasize that this is not rigorous, as the limit $\epsilon \rightarrow 0$ involves the delicate singular perturbation of a nonlinear hyperbolic equation.

We start with the dissipation expression ignoring the nucleation contribution:

$$\mathcal{D} = \int_{\Omega_0} -\frac{\partial \dot{W}}{\partial \phi} |\nabla_{\mathbf{x}_0} \phi| v_{n0}^\phi d\Omega_0 = \int_{\Omega_0} -\frac{\partial \dot{W}}{\partial \phi} \nabla_{\mathbf{x}_0} \phi \underbrace{\left(\frac{v_{n0}^\phi \nabla_{\mathbf{x}_0} \phi}{|\nabla_{\mathbf{x}_0} \phi|} \right)}_{=: \mathbf{v}_{n0}^\phi} d\Omega_0 \quad (2.2.17)$$

Adding and subtracting $\int_{\Omega_0} -\frac{\partial \dot{W}}{\partial \mathbf{F}} : \nabla_{\mathbf{x}_0} \mathbf{F} \cdot \mathbf{v}_{n0}^\phi d\Omega_0$, and also using that $\nabla_{\mathbf{x}_0} \dot{W} = \frac{\partial \dot{W}}{\partial \mathbf{F}} : \nabla_{\mathbf{x}_0} \mathbf{F} + \frac{\partial \dot{W}}{\partial \phi} \nabla_{\mathbf{x}_0} \phi$, we have

$$\mathcal{D} = - \int_{\Omega_0} \nabla_{\mathbf{x}_0} \dot{W} \cdot \mathbf{v}_{n0}^\phi d\Omega_0 + \int_{\Omega_0} \frac{\partial \dot{W}}{\partial \mathbf{F}} : \nabla_{\mathbf{x}_0} \mathbf{F} \cdot \mathbf{v}_{n0}^\phi d\Omega_0 \quad (2.2.18)$$

We now further assume the following: (i) the evolution is quasistatic, i.e. inertia is negligible; (ii) the phase boundary is flat and the fields are one-dimensional; and (iii) \mathbf{v}_{n0}^ϕ is constant in space. The assumptions (i) and (ii) allow us to assume that $\boldsymbol{\sigma} = \frac{\partial \dot{W}}{\partial \mathbf{F}}$ is constant in space and can be pulled out of the integral. Assumption (iii) is a direct consequence of assuming steady motion of the phase boundary as a traveling wave (Section 2.3), and allows us to pull \mathbf{v}_{n0}^ϕ out of the integral.

With these assumptions, we can write:

$$\mathcal{D} = - \left(\underbrace{\int_{\Omega_0} \nabla_{x_0} \dot{W} d\Omega_0}_{\llbracket \dot{W} \rrbracket \hat{n}} - \sigma : \underbrace{\int_{\Omega_0} \nabla_{x_0} \mathbf{F} d\Omega_0}_{\llbracket \mathbf{F} \rrbracket \otimes \hat{n}} \right) \cdot \mathbf{v}_{n_0}^\phi \quad (2.2.19)$$

which is identical to the driving force obtained by Abeyaratne and Knowles [AK06] in the quasistatic setting.

Given that we recover the classical driving force under these assumptions, it is reasonable to further expect that key properties of the classical theory, e.g. the Maxwell stress at which the driving force vanishes in quasistatics, are also captured correctly.

2.3 Traveling Waves in One Dimension

We investigate the behavior of traveling wave solutions in our model. These correspond to steadily moving interfaces.

For simplicity, we use a one-dimensional setting with linearized kinematics. For \dot{W} , we use the form:

$$\dot{W}(u_x, \phi) = \left(1 - H_l(\phi - 0.5)\right) \frac{1}{2} C(u_x - \varepsilon_1)^2 + H_l(\phi - 0.5) \frac{1}{2} C(u_x - \varepsilon_2)^2 \quad (2.3.1)$$

We use $\varepsilon_1 = 0$ and $\varepsilon_2 = 1$. The stress is $\sigma = \frac{\partial \dot{W}}{\partial (u_x)} = C(u_x - H_l(\phi - 0.5))$, and the driving force is $f = \delta_l(\phi - 0.5) \cdot (u_x - 0.5) + \epsilon \phi_{xx}$.

We search for traveling wave solutions of the form $u(x, t) = U(x - Vt)$ and $\phi(x, t) = \Phi(x - Vt)$ for a few different given kinetic relations. We substitute these into the balance of linear momentum and the evolution equation. Below, U' and Φ' denote derivatives of U and Φ . We assume that the kinetic response $\hat{v}_n^\phi(\dots)$ is a function of only the driving force f , and further that it is a monotone function and hence invertible.

From momentum balance, we obtain:

$$\begin{aligned} \rho u_{tt} = \sigma_x \Rightarrow V^2 \rho U'' = C \left\{ U'' - \delta_l(\Phi - 0.5) \Phi' \right\} &\Rightarrow (1 - M^2) U'' = \delta_l(\Phi - 0.5) \Phi' \\ \Rightarrow U' = \frac{H_l(\Phi - 0.5) + \tilde{c}_2}{1 - M^2} = \frac{H_l(\Phi - 0.5)}{1 - M^2} + c_2 \end{aligned} \quad (2.3.2)$$

where $c_2 \equiv \frac{\tilde{c}_2}{1 - M^2}$ is a constant of integration, and M is the Mach number. We see that as $M \rightarrow 1$, the derivative is unbounded unless $H_l(\phi - 0.5) + \tilde{c}_2 = 0$. The latter condition requires that Φ is constant in space, implying that only elastic waves and not phase interfaces are permitted at $M = 1$. As expected, this limitation is a consequence of momentum balance alone.

Next, from the evolution equation, we obtain:

$$\dot{\phi} = |\phi_x| \hat{v}_n^\phi(|f|) \Rightarrow -V \Phi' = |\Phi'| v_n^\phi \quad (2.3.3)$$

(2.3.3) implies that the interface velocity field v_n^ϕ is constant in space and time.

Using further that the kinetic response is a monotone function of f implies that the driving force field has to be a constant in space and time. Therefore, $f = \delta_l(\Phi - 0.5) \cdot (U' - 0.5) + \epsilon \Phi'' = \text{const.}$, and substituting for u' from (2.3.2) gives an ODE in Φ :

$$f = \text{const.} = \epsilon \Phi'' + \delta_l(\Phi - 0.5) \cdot \left(\frac{H_l(\Phi - 0.5)}{1 - M^2} - \frac{1}{2} - c_2 \right) \quad (2.3.4)$$

Given a value of M or alternatively V , we can solve this equation to obtain Φ . Also, given M , the value of f is obtained from the assumed kinetic response.

(2.3.4) is a nonlinear ODE because of $H_l(\Phi - 0.5)$ and $\delta_l(\Phi - 0.5)$. So we seek to find approximate solutions numerically using finite differences and least-squares minimization following [DB06]. Divide the domain of length $L = 1$ into N elements each of length $\Delta x = L/N$; the $N + 1$ grid points are denoted x_i . Discretize the ODE with as:

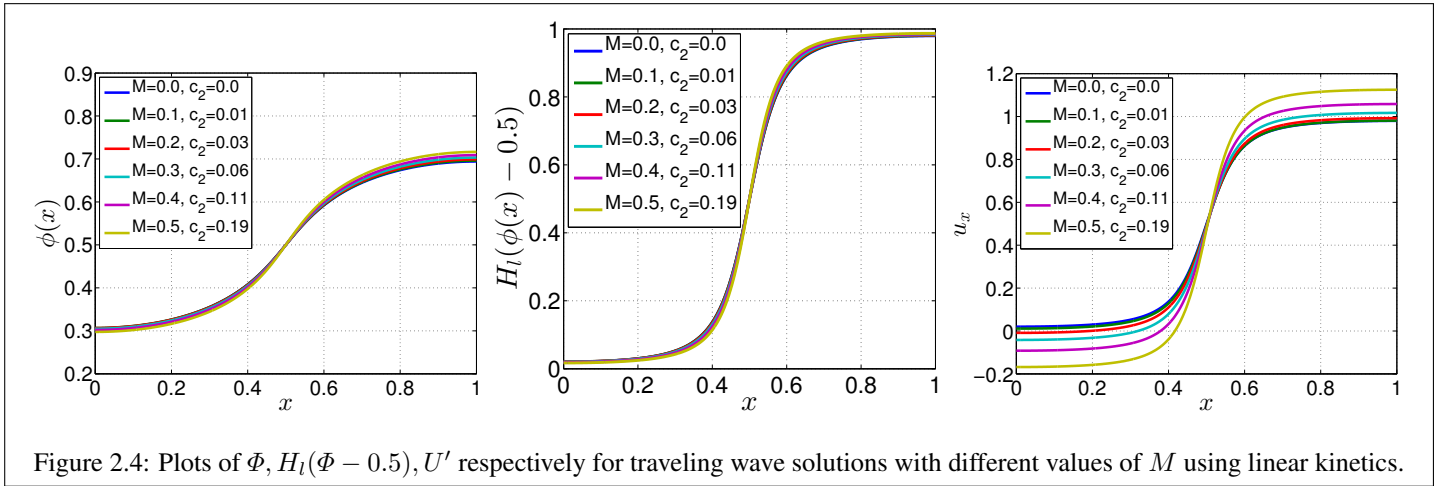
$$g(x_i) := \epsilon \frac{\Phi(x_{i+1}) - 2\Phi(x_i) + \Phi(x_{i-1}))}{(\Delta x)^2} + \delta_l(\Phi(x_i) - 0.5) \cdot \left(\frac{H_l(\Phi(x_i) - 0.5)}{1 - M^2} - \frac{1}{2} - c_2 \right) - f \quad (2.3.5)$$

Define the residue $\mathcal{R} := \sum_{i=2}^N |g(x_i)|^2$. To find Φ , we minimize \mathcal{R} with respect to the nodal values $\Phi_i := \Phi(x_i)$; at the completion of minimization, we evaluate \mathcal{R} to ensure that it is near 0 and we have not found

a local minimum. To prevent the solution algorithm from finding trivial single-phase solutions, we fix $\Phi|_{x=0.5} = 0.5$.

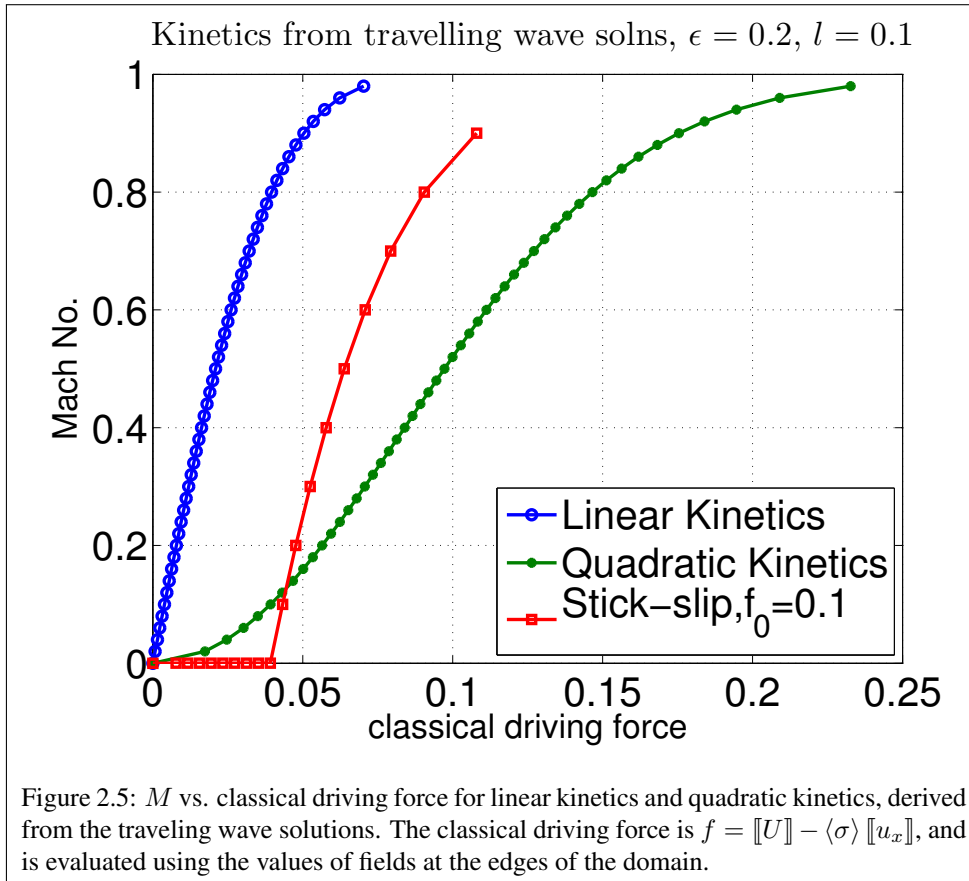
We note that there is an additional constant c_2 that is unknown. From classical sharp-interface analyses, we expect that the combination of momentum balance and kinetic relation should give us a unique solution in (2.3.4) once M is fixed. Examining (2.3.2), we can infer that it is related to the strains / stresses at $\pm\infty$, but it is not clear how exactly to find this explicitly. Therefore, we simply treat c_2 as an additional variable over which to minimize \mathcal{R} .

Fig. 2.4 plots the solutions for U and Φ for a linear kinetic relation. Qualitatively similar profiles are obtained for a quadratic kinetic relation.



We extract $(U')^\pm$, the limiting constant strains far from the interface, and use these to evaluate the classical driving force $\llbracket \dot{W} \rrbracket - \langle \sigma \rangle \llbracket U' \rrbracket$. Fig. 2.5 plots the *classical* driving force (not f) against M for solutions obtained for linear and quadratic kinetic relations. We find that the kinetic response that is specified through the response function \hat{v}_n^ϕ is reproduced in terms of the classical driving force. This supports the belief that our model provides the advantages of both the sharp-interface and the regularized-interface models without the disadvantages of either. We note that the classical kinetic relation deviates from the kinetic response function as $M \rightarrow 1$, but this is expected from linear momentum balance.

We emphasize an interesting difference between our model and existing phase-field models. In our model, the driving force field and the interface velocity field are both constant in space. Therefore, the relation between them is a simple relation between two scalar quantities, and the notion of a kinetic relation is well-defined. In existing phase-field models, the driving force field is large near an interface and goes to



zero away from the interface, i.e. it is a function of location. Therefore, there is no obvious unique scalar measure of the driving force that one can extract from this field; one could use the maximum value, or the mean value in some region, and so on. In this perspective, our model has the advantage that it has a closer link to the classical continuum model because there is a unique and obvious relation between driving force and interface velocity.

2.4 Dynamics of Interfaces in One Dimension

We examine the kinetics of phase interfaces through direct dynamic simulations. We solve linear momentum balance along with the evolution equation for ϕ in various configurations and with various choices for the kinetic response.

We use the following material model:

$$\dot{W}(u_x, \phi) = \left(1 - H_l(\phi - 0.5)\right) \frac{1}{2} C(u_x - \varepsilon_1)^2 + H_l(\phi - 0.5) \frac{1}{2} C(u_x - \varepsilon_2)^2 \quad (2.4.1)$$

$$\sigma = \frac{\partial \dot{W}}{\partial (u_x)} = \left(1 - H_l(\phi - 0.5)\right) C(u_x - \varepsilon_1) + H_l(\phi - 0.5) C(u_x - \varepsilon_2) \quad (2.4.2)$$

$$f = \delta_l(\phi - 0.5) \left(\frac{1}{2} C(u_x - \varepsilon_1)^2 - \frac{1}{2} C(u_x - \varepsilon_2)^2 \right) + \epsilon \phi_{xx} \quad (2.4.3)$$

$$\rho \ddot{u} = \sigma_x \quad (2.4.4)$$

$$\dot{\phi} = |\phi_x| v_n^\phi \quad (2.4.5)$$

The stored energy density near each well is quadratic with wells at $\varepsilon_1 = 0$ and $\varepsilon_2 = 1$.

We examine three different kinetic laws:

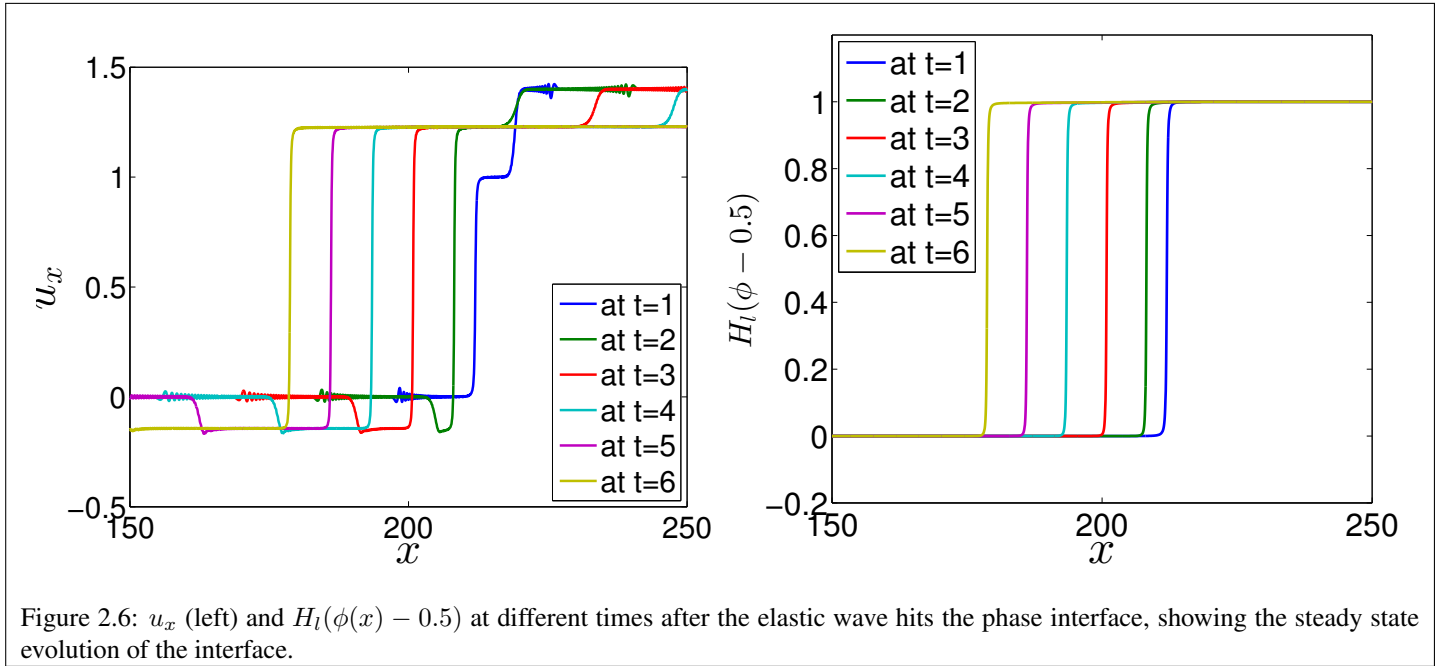
$$\hat{v}_n^\phi = \begin{cases} \text{sign}(f) \kappa |f| & \text{linear kinetics} \\ \text{sign}(f) \kappa |f|^2 & \text{quadratic kinetics} \\ 0 \text{ if } |f| < f_0 \text{ else } \text{sign}(f) \kappa \cdot (|f| - f_0) & \text{stick-slip kinetics} \end{cases} \quad (2.4.6)$$

and test if the direct dynamic simulations show a similar relation between interface velocity and classical driving force.

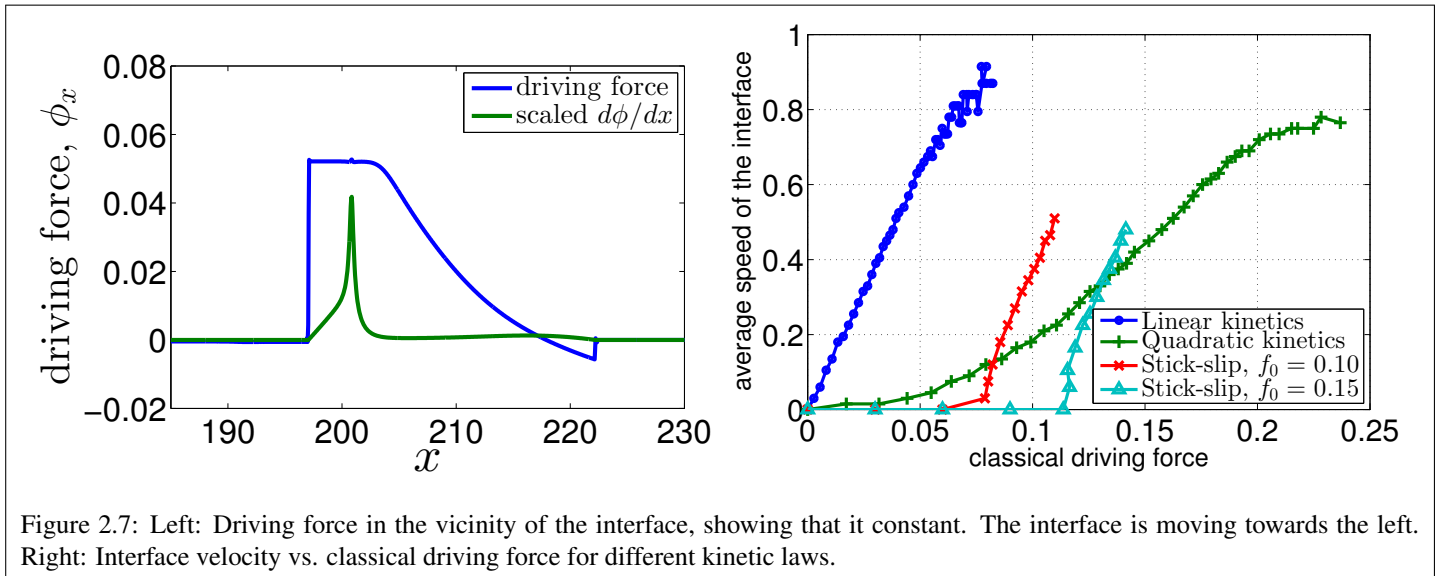
The configuration is a 1D bar with a phase interface at the center of the bar. The bar is fixed at the left end and a constant load P is applied at the right end. This causes an elastic wave to head towards the left from the right end. When the elastic wave hits the phase interface, it causes the interface to begin moving. Repeated calculations over a range of applied loads causes interfaces to propagate at a range of velocities.

Fig. 2.6 shows the evolution of the interface after the elastic wave hits it in the case of linear kinetics. It can be seen that the solution quickly reaches a steady-state evolution. The quadratic kinetics and the stick-slip kinetics above the sticking threshold display qualitatively similar evolution.

We note in Fig. 2.7 (left) the attractive feature of the model that the driving force field is constant in the vicinity of the interface. Consequently, v_n^ϕ is constant in that region, enabling the transport of the interface density without distortion of the interface shape. This also enables clear physical interpretations of the notion of driving force and interface velocity. To find the induced kinetics, we compute the classical



driving force and plot it against the interface velocity. Fig. 2.7 (right) shows the induced kinetics for the kinetic response functions in (2.4.6).



The induced kinetic relation follows quite well the kinetic response functions in (2.4.6) but the agreement gets worse as $M \rightarrow 1$. This is to be expected since balance of linear momentum does not permit supersonic interfaces irrespective of the driving force.

The stick-slip kinetic response permits evolution only if driving force exceeds a threshold value, and we

see the same induced behavior in terms of classical driving force. The precise threshold value is different, but the ratio of the threshold value is preserved for the two stick-slip kinetic laws that were tested in Fig. 2.7 (right).

Fig. 2.8 compares the kinetics derived from traveling wave solutions and direct dynamic simulations. For the same values of all parameters, the curves lie on top of each other, except near the sonic velocity where a steady traveling takes an extremely long time to develop. Therefore, it is more useful to compare with slightly different kinetics, and we observe that there is qualitative similarity between the traveling wave solutions and the dynamic simulations.

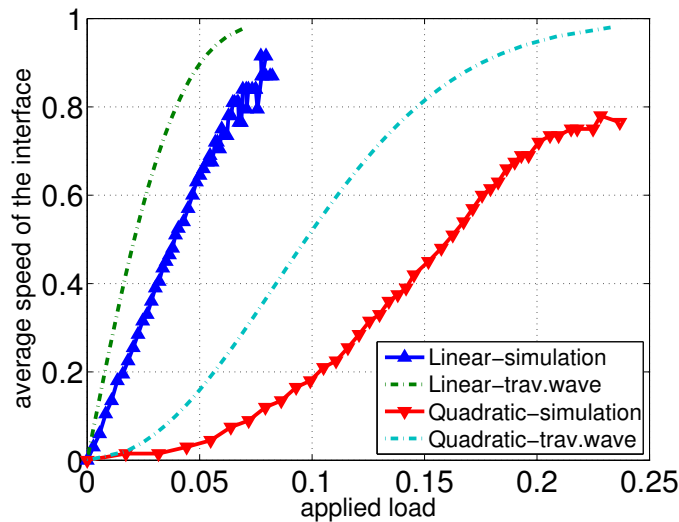


Figure 2.8: Comparison of linear and quadratic kinetics from dynamic simulations and traveling wave solutions. The chosen kinetic relations have different coefficients for the dynamics and traveling wave cases.

2.5 Effect of the Small Parameter l

In addition to the constitutive input in terms of \mathring{W} , \hat{v}_n^ϕ , G_0 , our model contains two small parameters: ϵ , the coefficient of $|\nabla\phi|^2$, and l , the parameter in the regularized Heaviside-like function H_l (see Fig. 2.1). There is a good physical understanding of ϵ as being related to the thickness of phase interfaces. We note that l provides a measure of the size (in strain space) of the unstable region between the stable phases, but the precise role in determining the induced kinetic relations is unclear. We examine this role by computing the induced kinetic relations for various values of l . We use both traveling waves with

linear kinetics and dynamic calculations with a stick-slip kinetic response. We use \dot{W} as in Section 2.4. Fig. 2.9 shows that the kinetics is quite sensitive to l . Ideally, we would like to see if there is convergence in any sense as $l \rightarrow 0$, but the energy is extremely steep as l becomes smaller and does not permit numerical simulations with confidence. From the calculations that we could confidently carry out, there appears to be no such convergence. However, while the kinetics is sensitive to l , the essential effect seems to be as a pre-multiplying coefficient that does not affect the shape of the kinetic response function. Therefore, a simple strategy to deal with this is to fix a given value of l that allows easy numerical simulations, and then calibrate the pre-multiplier in the kinetic response function to the desired value based on this fixed value of l . In other words, treat l as a fixed material parameter. In some ways, this is reminiscent of the behavior of standard regularized models in which the observed kinetics is very sensitive to the regularization parameters; the key difference is that the precise role of the regularization in setting the kinetics is typically opaque.

Additionally, an interesting observation from the dynamic calculations is that the relation between interface velocity and applied end load is fairly insensitive to l .

The linear kinetic relation in Fig. 2.9 also shows an interesting feature in relation to the competition between the linear kinetic response and the inability of the interface to go beyond $M = 1$. As $l \rightarrow 0$, we note that the kinetic relation remains linear for higher M ; this issue is further discussed in Section 2.6.

2.6 Competition Between Inertia and Dissipation

Phase interfaces in continuum mechanics provide an interesting demonstration of the competition between inertia and dissipation. Consider elastic shocks or their analog in gasdynamics: the behavior of these interfaces is almost completely constrained by momentum balance. Thermodynamics – in the sense of positive dissipation – typically serves only to select one of two possible solutions permitted by momentum balance. Typical phase interfaces are quite different from elastic shocks. Momentum balance provides only a weak constraint on the solutions, and there is a massive non-uniqueness that is left open. Non-equilibrium thermodynamics – in the form of a kinetic relation – selects the unique solution.

Regularized models of elastic shocks and phase interfaces also display this character. The addition of viscosity and gradient terms serves to regularize elastic shocks, but does not significantly change the

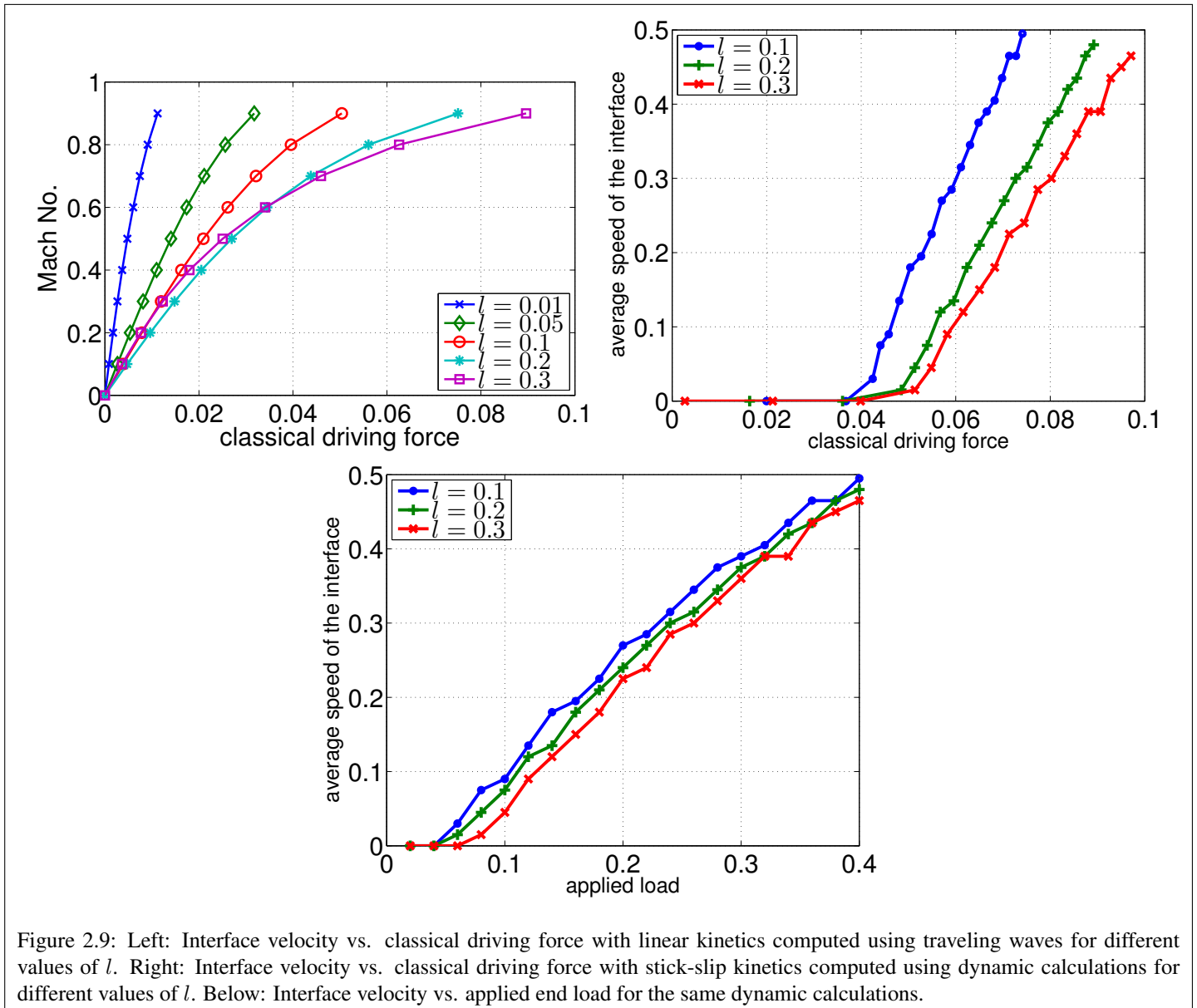


Figure 2.9: Left: Interface velocity vs. classical driving force with linear kinetics computed using traveling waves for different values of l . Right: Interface velocity vs. classical driving force with stick-slip kinetics computed using dynamic calculations for different values of l . Below: Interface velocity vs. applied end load for the same dynamic calculations.

kinetics if these regularizing mechanisms are sufficiently small. On the other hand, viscosity and gradient terms completely determine the kinetics of phase interfaces regardless of how small they may be. If one thinks of viscosity and these higher-order terms as related to dissipation, we see again the contrast between elastic shocks and phase interfaces.

In our model, this interplay may be observed in 2 ways. First, we are able to recover the classical continuum driving force only in the quasistatic limit without inertia⁴. Second, when we compare the prescribed kinetic response with the observed relation between classical driving force and interface velocity, we find

⁴Further assumptions are necessary, but not relevant to this discussion.

that the disagreement becomes larger as we approach the sonic velocity. Therefore, it is reasonable to consider the Mach number M as a measure of the relative dominance of inertia vs. dissipation; $M = 0$ corresponds to dissipation-dominance, and $M = 1$ corresponds to inertia-dominance⁵.

This brings us to an interesting example studied by [AK91b, Ros95]. Consider a 1D problem with the material model shown in Fig. 2.10. Let the elastic modulus of phase 1 be less than the modulus of phase 3, but let them have the same mass density. Therefore, the sonic speeds in these phases satisfy $c_1 < c_3$. For an interface moving at velocity v , define $M_1 := v/c_1$ and $M_3 := v/c_3$. Note that $M_3 < M_1$ for all v .

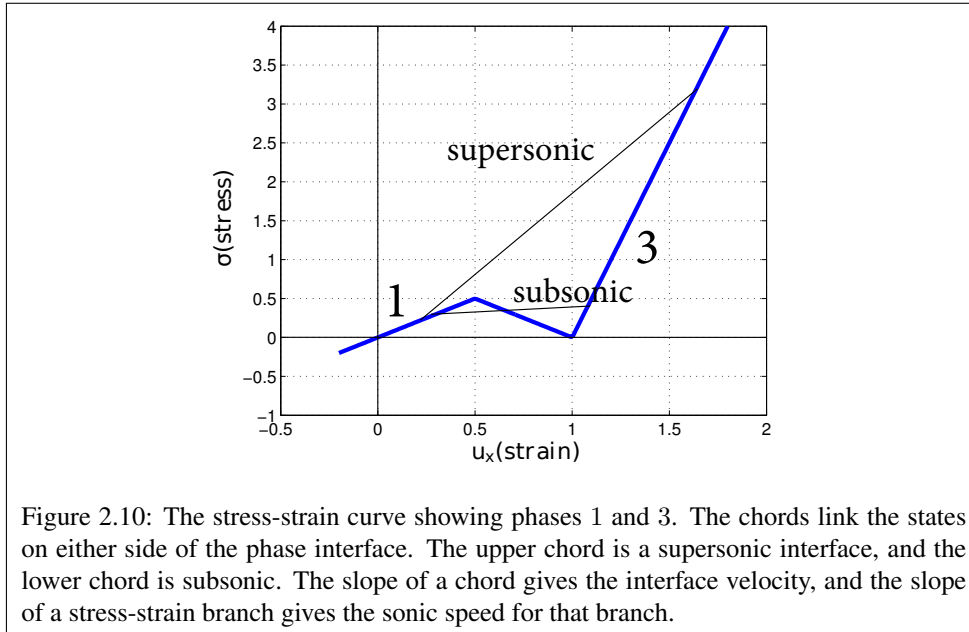


Figure 2.10: The stress-strain curve showing phases 1 and 3. The chords link the states on either side of the phase interface. The upper chord is a supersonic interface, and the lower chord is subsonic. The slope of a chord gives the interface velocity, and the slope of a stress-strain branch gives the sonic speed for that branch.

[AK91b, Ros95] consider, among various topics, a phase interface that bridges the phases 1 and 3. To briefly summarize their findings regarding this problem, they find that momentum balance permits this phase interface to have $M_1 > 1$ if it is propagating into phase 3. Further, when $M_1 < 1$, then the interface requires a kinetic relation for unique evolution, but when $M_1 > 1$ the interface *evolution is fully determined by momentum balance*. Note that $M_1 < 1$ is required when the interface propagates into phase 1, and $M_3 < 1$ always.

Therefore, an important challenge for the model that we have proposed is whether it can naturally capture this transition from dissipation-dominated evolution to inertia-dominated evolution. In other words, suppose we perform a dynamic calculation in which the velocity of the interface starts off subsonic, but at some point becomes supersonic. Will the model “automatically” know that the interface should not be

⁵We note also from Fig. 2.9 that smaller values of l correspond to increased dissipation-dominance.

governed by the kinetic response once it transitions to supersonic?

We examine this question using a combination of traveling wave analysis and dynamic calculations. We work with the following model:

$$\dot{W}(u_x, \phi) = \left(1 - H_l(\phi - 0.5)\right) \frac{1}{2} C_1 u_x^2 + H_l(\phi - 0.5) \frac{1}{2} C_3 (u_x - \varepsilon_3)^2 \quad (2.6.1)$$

$$\sigma = \frac{\partial \dot{W}}{\partial (u_x)} = \left(1 - H_l(\phi - 0.5)\right) C_1 u_x + H_l(\phi - 0.5) C_3 (u_x - \varepsilon_3) \quad (2.6.2)$$

where the stress-free strains are 0 and $\varepsilon_3 > 0$. The elastic moduli are C_1, C_3 with $C_1 < C_3$.

We use the traveling wave ansatz $u(x, t) = U(x - Vt)$, $\phi(x, t) = \Phi(x - Vt)$, $\sigma(x, t) = \Sigma(x - Vt)$ and similarly for other fields, with $V > 0$. Integrating $\rho \ddot{u} = \frac{d\sigma}{dx} \Rightarrow \rho V^2 U'' = \Sigma'$ once, we get:

$$\rho V^2 U' = \left(1 - H_l(\Phi - 0.5)\right) C_1 U' + H_l(\Phi - 0.5) C_3 \cdot (U' - \varepsilon_3) + \text{const.} \quad (2.6.3)$$

Using $M_1 = \frac{V}{(C_1/\rho)^{\frac{1}{2}}}$ and $M_3 = \frac{V}{(C_3/\rho)^{\frac{1}{2}}}$ and collecting the terms multiplying U' , we get:

$$U' = \frac{C - \varepsilon_3 M_1^2 H_l(\Phi - 0.5)}{M_3^2 (M_1^2 - 1) - (M_1^2 - M_3^2) H_l(\Phi - 0.5)} \quad (2.6.4)$$

We can get 3 useful results from (2.6.4):

1. Consider that $\Phi|_{-\infty} = 0, \Phi|_{+\infty} = 1$, and define $\epsilon^- \equiv U'|_{-\infty}, \epsilon^+ \equiv U'|_{+\infty}$. Evaluating (2.6.4) at $\pm\infty$ and subtracting gives $\epsilon^+ - \epsilon^- = \varepsilon_3 \frac{M_1^2}{M_3^2} \frac{1}{1 - M_1^2}$. The jump in ϵ is positive if $M_1 < 1$ and negative if $|M_1| > 1$. From the fact that we have phase 1 on the left, the jump in ϵ is expected to be positive.
2. Consider precisely $M_1 = 1$. We have $U' = \frac{C - \varepsilon_3 H_l(\Phi - 0.5)}{-(1 - M_3^2) H_l(\Phi - 0.5)}$. Since $\Phi|_{-\infty} = 0$, we require that $C = 0$ for this case to have U' bounded. Therefore, $U' = \frac{-\varepsilon_3 H_l(\Phi - 0.5)}{-(1 - M_3^2) H_l(\Phi - 0.5)}$, which implies that at a given spatial location, either (i) $U' = \frac{\varepsilon_3}{1 - M_3^2}$, or (ii) $H_l(\Phi - 0.5) = 0$. These conditions imply that the strain is constant in the vicinity of an interface in Φ , and the strain can transition from one phase to another only *away* from an interface in Φ . Our dynamic calculations, described below, show this feature that the interfaces in the U field and the Φ field are at different spatial locations as $M_1 \rightarrow 1$. It appears that the system responds to over-constraining by this mechanism of separating the evolution of ϕ from the evolution of u .
3. Recall that $M_3 < M_1$, and examine the denominator in (2.6.4) for $M_1 < 1$ and $M_1 \geq 1$. For all

values of $M_1 < 1$, the denominator is positive and therefore U' is bounded everywhere. On the other hand, when $M_1 \geq 1$, the denominator goes to 0 when $H_l(\Phi - 0.5) = \frac{M_3^2(M_1^2 - 1)}{M_1^2 - M_3^2} = \frac{M_1^2 - 1}{M_1^2/M_3^2 - 1}$. Using that $M_3 < 1$, we have that $0 < \frac{M_1^2 - 1}{M_1^2/M_3^2 - 1} < 1$. Noting that H_l takes values between 0 and 1, it follows that the condition $H_l(\Phi - 0.5) = \frac{M_1^2 - 1}{M_1^2/M_3^2 - 1}$ is satisfied at some spatial location(s) for every $M_1 \geq 1$. Therefore, our model will display unbounded strain at some point in the domain for interfaces that propagate at $M_1 > 1$.

We now examine this question through direct dynamic calculations. While the traveling wave framework has already ruled out existence of supersonic interfaces in our model, it is based on the assumption of steadily-propagating interfaces. Dynamic simulations enable us to probe the transient behavior as interfaces accelerate towards the sonic speed. Essentially, we expect that the dynamics will not tend to a steady traveling wave state because such a state has been shown above to not exist.

We consider a material model with $C_3/C_1 = 2.25 \Rightarrow M_3 = M_1/1.5$. Fig. 2.11 (top) shows the initial state with a stationary interface and a compressive shock approaching from the right. The other plots in Fig. 2.11 show the evolution of ϕ and u_x . We find that (1) the interface in ϕ moves extremely rapidly, and is in fact significantly above sonic with respect to all wave speeds in the problem!, but (2) the interface in u_x moves completely independently of the ϕ -interface, and is subsonic with respect to both phases. The ϕ -interface carries a small elastic wave with it, but this can be considered as the response to a supersonic moving external load rather than as a supersonic wave.

In conclusion, it appears that our model does not handle the transition of phase interfaces from regimes where a kinetic relation is required, to regimes where a kinetic relation would overconstrain the evolution. Our model simply does not allow supersonic transitions of the type studied in [AK91b, Ros95]. However, it is encouraging that the model does not produce spurious seemingly-realistic solutions, but provides some warning. That is, if we observe that the interfaces in ϕ and u do not have the same spatial location, or if there are no steady traveling wave-like solutions, it is likely that the evolution is over-constrained and has transitioned from dissipation-dominated to inertia-dominated.

We show in Appendix 2.B that the standard phase-field models suffers from this same deficiency.

Finally, we note another example of the tension between inertia and dissipation: in [PB03], they find that certain phase interfaces in continuum string models also do not require an additional kinetic relation for

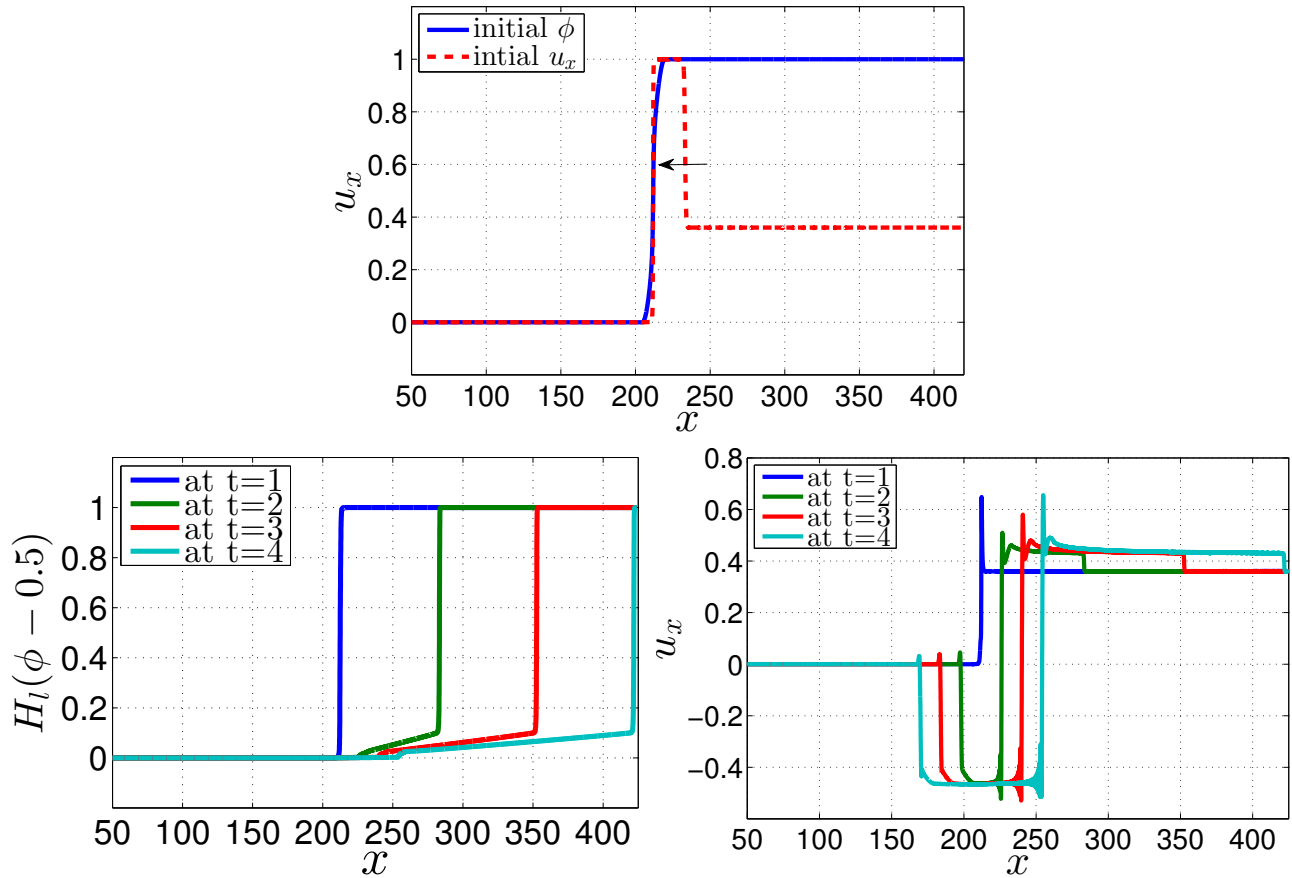


Figure 2.11: Top: A stationary interface as a compressive elastic wave approaches from the right. Left: The evolution of $H_l(\phi - 0.5)$ shows the phase interface in ϕ . Right: The evolution of u_x shows the phase interface in u_x . The key point is that the evolution of phase interfaces in ϕ and u_x are decoupled.

unique evolution.

2.7 Discussion

We have presented the formulation and characterization of a phase-field model that has non-singular interfaces yet allows for transparent prescription of kinetics and nucleation of interfaces. The key elements are a re-parametrization of the energy and an evolution law that enables us to separate nucleation from kinetics. In standard phase-field approaches, these are mixed together in an extremely opaque manner. For instance, a uniform phase can nucleate a new phase through the kinetic equation, and there is no separate nucleation equation. This mixing between kinetics and nucleation makes calibration extremely challenging. In addition, standard phase-field models do not have a direct connection between evolu-

tion of ϕ and the kinetics of interfaces, and nucleation is completely opaque. In our formulation, the calibration of nucleation and kinetics is simple and transparent.

We find two positive indications regarding our model: (i) a formal limit of the kinetic driving force recovers the classical continuum sharp-interface driving force of Abeyaratne and Knowles; (ii) examining interfaces as traveling waves in our model, we find that the driving force is constant in space, unlike the variational derivative of standard phase-field models. The latter result implies that kinetic relations – i.e., a relation between velocity and driving force – is a well-defined notion in our model, and provides confidence in both the re-parametrized energy and the evolution statement. In addition, our re-parametrization of the energy modifies barriers in a drastic way, but preserves the structure of the energy away from the barriers. However, we recall that the driving force in the classical setting [AK06] depends only on the end-states on either side of the interface and not on the details of the barrier. The information about the barrier is retained in our model through the kinetics and nucleation that we prescribe.

In the companion paper, we present a number of examples characterizing our model in two dimensions. Our approach could be criticized as introducing extra equations and parameters that are not used in traditional phase-field models. Is this a disadvantage of our approach, since it becomes more complex, with more fitting parameters required from experiment, MD, etc.? In other words, have we sacrificed model simplicity for model flexibility? For instance, standard phase-field models with only a handful of parameters and energy minimization-driven kinetics have been proven remarkably effective for many applications in materials science. However, it is our opinion that while standard phase-field models are certainly very simple, that is because the many significant assumptions related to kinetics and nucleation that are present are simply not made explicit. Our model could be made just as simple, for instance, by assuming that we have linear kinetics and that nucleation occurs at some arbitrarily-chosen value of the driving force. This would provide a model that is just as simple and easy to formulate as a standard phase-field model. But even in the setting that we wish to use only a handful of parameters, our model makes transparent the assumptions that we are making on kinetics and nucleation.

An important open problem for our formulation is the inability to handle supersonic phase interfaces that do not require kinetics to obtain a unique evolution; in fact, prescription of kinetics overconstrains the evolution in the classical setting. We find that our model cannot describe such supersonic interfaces in a traveling-wave setting corresponding to steady propagation, and dynamic calculations show strange

behavior in these settings. We further find that standard phase-field models also have this deficiency. Regularized models that are based on adding viscosity and strain-gradients to the stress-response can correctly describe this interface [Ros95]. But strain-gradient models have an important disadvantage compared to phase-field models. Strain-gradient models do not use a phase-field at all but work exclusively with the displacement field. The strain-gradients then impose severe smoothness requirements on the displacement field, making it challenging for finite elements in higher dimensions. In contrast, phase-field models – both the existing approaches as well as our formulation – require only the usual levels of smoothness because the gradients are on ϕ and only of second-order, and finite element implementations are commonplace, e.g. [XB08, SL07, YD12].

Ongoing extensions of this work are as follows:

1. The extension to 3 or more phases is straightforward following the ideas presented here. This is an important capability for realistic problems, and is a focus of our ongoing work.
2. Our model extends the domain of stable phases, and allows them to exist in regions of strain space that should correspond to unstable phases. This is not an ideal situation, and our ongoing work aims to remedy this by appropriately using nucleation criteria.
3. Phase-field models for fracture are gaining in popularity. Our ongoing work aims to extend the work presented here to that setting to enable dynamic fracture calculations. In addition, we find that traveling wave analyses of the type presented in Appendix 2.B are providing much insight into the behavior of supersonic cracks in the existing phase-field models of fracture, e.g. [BVS⁺12].
4. We have used finite elements for the elasticity and finite differences for the evolution of ϕ . However, the evolution of ϕ comes from a conservation principle, which can provide important advantages for robust numerical implementations such as a natural weak form [Tra09]. The development of such a scheme may be a useful future extension.

2.A Connection to Noether’s Theorem

A seminal observation by Noether was that conservation principles in physics often have their roots in continuous symmetries. For instance, conservation principles for linear momentum, angular momentum, and energy can be shown to arise from the facts that the energy of an isolated body is independent of trans-

lations in space, rotations in space, and translations in time respectively. A concrete and extremely useful manifestation of Noether's principle is in [KS72], where they show that the essential path-independent properties of the J -integral of fracture mechanics are related to the application of Noether's theorem. The idea can be roughly summarized as the procedure: (i) find the Lagrangian or action corresponding to the equation, and then (ii) take the variation with respect to the transformations mentioned above.

We briefly examine here if a similar procedure provides any insight into the the conservation principle for interfaces. For simplicity, we consider the one-dimensional setting with the interface velocity field being a constant that we set to 1, i.e. our evolution equation is simply $\phi_t = \phi_x$. Write the action $A = \int \int \frac{1}{2} (\phi_t^2 \phi_x - \phi_x^2 \phi_t) dx dt$. We have constructed A by trial-and-error, using [Whi65] as a starting point. Subscripts x and t refer to space and time derivatives respectively. We take the variation of A by using the perturbation $\phi \rightarrow \phi + \epsilon \eta$, and evaluating $\left. \frac{dA}{d\epsilon} \right|_{\epsilon=0} = 0$ provides:

$$\phi_t \phi_{xt} - \phi_{xx} \phi_t - \phi_x \phi_{xt} + \phi_{tt} \phi_x + \phi_t \phi_{xt} - \phi_x \phi_{xt} = 0 \quad (2.A.1)$$

We have assumed that ϕ is sufficiently smooth for all derivatives to exist.

The Euler-Lagrange equation is a very nonlinear PDE and possibly has non-unique solutions. However, we observe that $\phi_t = \phi_x$ is a solution, and also $\phi_t = \phi_x \Rightarrow \phi_{tt} = \phi_{xx} = \phi_{xt}$. Further, we observe that $\phi_{tt} = \phi_{xx}$ by itself, without assuming $\phi_t = \phi_x$, does not appear to be a solution. Therefore, this action is promising in that it provides the first-order wave equation but not the second-order equation. The Hamiltonian is computed from the Legendre transform $\int \left(\phi_t \frac{\partial L}{\partial \phi_t} - L \right) dx$ to be $\frac{1}{2} \phi_t^2 \phi_x$.

We examine then the effect of enforcing invariance under translations of the form $t \rightarrow t + \epsilon$ and $x \rightarrow x + \epsilon$. Unfortunately, these do not provide any further insights. This is not too surprising, because Noether's theorem typically does not provide new evolution laws, but rather can provide conserved quantities that are already implied by the original evolution laws; e.g., given the force-acceleration equation for an isolated system of particles, Noether's principle can show that the total momentum is conserved.

2.B Non-existence of Supersonic Interfaces in Standard Phase-field Models

We consider a 1D phase-field model with energy as follows:

$$\int_{\Omega} W(\phi) + \frac{1}{2}C(\phi) (\nabla u - \epsilon_0(\phi))^2 + \frac{1}{2}\kappa \left(\frac{\partial \phi}{\partial x} \right)^2 \quad (2.B.1)$$

where W is a nonconvex energy density with multiple wells. Using the standard gradient-flow assumption, the evolution equations are:

$$\rho \ddot{u} = \frac{\partial}{\partial x} [C(\phi) (\nabla u - \epsilon_0(\phi))], \quad \dot{\phi} = \frac{dW}{d\phi} + \kappa \frac{\partial^2 \phi}{\partial x^2} \quad (2.B.2)$$

The context of the calculation here is based on the discussion in Section 2.6. Analysis of classical continuum models [AK90] and strain-gradient models [Ros95] show the possibility of interfaces that are supersonic with respect to the softer phase. But our model does not admit such interfaces, and requires that interfaces are subsonic with respect to both phases. We examine this question in the context of the standard phase-field model (2.B.1), (2.B.2). We note that setting the elastic modulus $C(\phi) > 0$ to be an explicit function of the phase parameter allows the moduli – and hence the sonic velocities – of the phases to be different.

We now analyze just the momentum balance equation from (2.B.2). Assuming a traveling wave framework, we write $u(x, t) = U(x - Vt)$, $\phi(x, t) = \Phi(x - Vt)$. This gives us $\rho V^2 U'' = [C(\Phi) (U' - \epsilon_0(\Phi))]'$. Integrating once, we get $\rho V^2 U' = C(\Phi) (U' - \epsilon_0(\Phi)) + D$. We rearrange to write:

$$U' = \frac{D - \epsilon_0(\Phi)}{1 - M^2(\Phi)} \quad (2.B.3)$$

where $M(\Phi) := \frac{V}{(C(\Phi)/\rho)^{\frac{1}{2}}}$ is the local Mach number.

Let $C(\phi)$ be a continuous function of its argument ϕ ⁶. It follows that $M(\Phi)$ is a continuous function of Φ . Now, consider a phase interface; such an interface involves a transition from $\Phi = 0$ to $\Phi = 1$, with Φ being continuous in its argument. Therefore, if $M(\Phi) > 1$ at any point in space corresponding to the softer phase, and $M(\Phi) < 1$ at any point in space corresponding to the stiffer phase, then $M = 1$ at some point in the domain. Further, U' is unbounded at the point where $M = 1$. Hence, phase-field models

⁶Assuming that $C(\phi)$ is not continuous would require us to explicitly track the discontinuity in numerical calculations, thereby destroying the essential advantage of phase-field approaches.

cannot support steadily-propagating phase interfaces that are supersonic with respect to the softer phase.

Chapter 3

Two-dimensional characterization and boundary kinetics

3.1 Introduction

In the companion paper, we presented the formulation and one-dimensional characterization of a phase-field model focused on structural transformations and twinning. The key new feature of our model is the ability to transparently and easily prescribe complex nucleation and kinetic behavior of microstructural interfaces. While the one-dimensional setting provides a simplified arena to transparently understand and characterize certain aspects, many essential features of structural transformations and twinning are inherently higher-dimensional. In particular, elastic compatibility is trivial in one dimension, but can be central to the behavior of interfaces in 2 and 3 dimension [BJ87, BJ92, Bha03a].

The key issue can be illustrated in a simple example. Consider a one-dimensional setting with a material that has two stress-free strains ε_1 and ε_2 . Given traction-free boundary conditions, any spatial arrangement of ε_1 and ε_2 will satisfy both equilibrium as well as elastic compatibility. On the other hand, consider a 2D or 3D system with phases given by stress-free stretches U_1 and U_2 , and with traction-free boundaries. If these do not satisfy the kinematic compatibility condition – i.e. there is no solution Q, a, n to the equation $QU_1 - U_2 = a \otimes n$ – then the only stress-free solutions are either uniformly U_1 or uniformly U_2 in the entire domain. Any solution with both phases will involve stresses or elastodynamics, or both.

The focus of this paper is to characterize the model in 2 dimensions where the kinetics and nucleation of interfaces interacts strongly with complex stress fields. These stress fields can arise when phases are not stress-free compatible. They can also emerge during the nucleation process even if the phases are stress-free compatible; from the equation $QU_1 - U_2 = \mathbf{a} \otimes \mathbf{n}$, we note that only specific rotations and interface directions are stress-free, and the nucleation process is unlikely to follow precisely that loading path. The examples that we consider in this paper include both of these possible effects.

Some of the specific examples, and the motivations for considering them, are as follows.

First, we examine the effect of a non-monotone kinetic relation both in 1D and 2D. Previous work analyzing non-monotone kinetic relations has shown extremely interesting features such as the natural emergence of stick-slip behavior [RK97]. That motivates us to study this example; an important caveat however is that [RK97] use a driving force that is a non-monotone function of interface velocity, whereas we are restricted to setting the interface velocity to be a non-monotone function of the driving force. Possibly for this reason, we do not observe as rich a behavior as [RK97].

Second, we present the formulation of a model that can display anisotropic kinetics; while we use a simple functional form of anisotropy, it is readily generalizable to more complex settings. A key motivation for this example is that twin boundary propagation is extremely anisotropic [AV03].

Third, we present the formulation of a model that displays stick-slip behavior of interfaces, i.e., it requires a finite value of driving force to initiate motion. This is a universal feature of microstructural interfaces, but is challenging to incorporate in standard phase-field models. Recent approaches in higher dimensions use spatially-oscillating imposed stress fields [LL07, LLP10]. In these strategies, it is not clear how – or even if it is possible – to incorporate the anisotropy of the stick-slip threshold that is widely observed. An additional challenge is the requirement of a fine discretization to resolve the imposed stress field.

Fourth, we examine the question of nucleation in 1D and 2D, through the vehicle of computing hysteresis loops. We demonstrate that it is simple and transparent to impose complex nucleation criteria that are rate-dependent as well as different for the forward and reverse transformation. This is a particular advantage of our model over existing phase-field approaches; in the latter, nucleation criteria are adjusted in an *ad-hoc* manner by modifying barriers in the energy landscape. Modifying barriers can have consequences on both reverse and forward transformations, is extremely unsystematic, and cannot allow for complex

nucleation criteria based on rates and stress measures such as hydrostatic stress.

Finally, we examine the competition between nucleation and kinetics by varying the relative rates of these processes. This provides a powerful tool to systematically examine the effect of different types of microstructure evolution on the final microstructure.

We also extend our model to the kinetics of the junction lines that form at the intersection of microstructural interfaces and material surfaces such as free surfaces. In general, junction lines can be considered as distinct defects with their own kinetics, though coupled to the interface kinetics through the evolution of the stress field. Experimental measurements, many of which are on the surface of a specimen, will therefore largely probe the junction kinetics and not the interface kinetics. Hence, it is important to construct a model that can incorporate a distinct kinetics for junction lines. In analogy to the formulation in the companion paper, we develop a model that allows for the independent prescription of the kinetics of the junction lines, while at the same time treating them as regularized non-singular defects. Our approach builds on previous work by [SB98] that treats interfaces and junctions as singular objects. Our point of departure is to treat these defects in a regularized setting while still allowing for the independent prescription of interface and junction kinetics.

For a list of notation, we refer to the companion paper.

3.1.1 Organization

The paper is organized as follows.

- In Section 3.2, we briefly recall our proposed model that is described in greater detail in the companion paper.
- In Section 3.3, we outline the formulation of a 2D energy density that we use in many of the subsequent 2D calculations.
- In Section 3.4, we examine the effect of non-monotone kinetic response in 1D and 2D.
- In Section 3.5, we demonstrate the formulation of anisotropic kinetic laws in 2D.
- In Section 3.6, we examine twinning interfaces with stick-slip kinetics in 2D.
- In Section 3.7, we demonstrate – in 1D and 2D – the formulation of complex nucleation criteria that includes rate-dependent critical nucleation stresses, as well as independent prescription of forward

and reverse nucleation stresses, without modifying the energy barriers.

- In Section 3.8, we demonstrate imposing hydrostatic stress-dependence of twin nucleation, in addition to usual shear-stress dependence.
- In Section 3.9, we examine the competition between nucleation and kinetics in a twinning transformation.
- In Section 3.10, we examine the prescription of a kinetics associated with the junctions between interfaces and specimen boundaries.
- In Section 3.11, we review our work.

3.2 Summary of the Proposed Phase-Field Model

Our starting point is to assume that the strain energy density $W(\mathbf{F})$, the kinetic relation for interfaces, and the nucleation behavior of interfaces, are well-characterized and available. Our approach then takes this information, and formulates a phase-field model that reproduces the elastic response and the kinetic and nucleation behavior of interfaces. The governing equations of our model are as follows.

The energy density has the form:

$$\dot{W}(\mathbf{E}, \phi) = (1 - H_l(\phi - 0.5)) \psi_1(\mathbf{E}) + (H_l(\phi - 0.5)) \psi_2(\mathbf{E}) \quad (3.2.1)$$

where H_l is a smooth function that resembles the Heaviside. The functions ψ_1 and ψ_2 have the form:

$$\psi_A(\mathbf{E}) = W(\mathbf{E}_A) + \underbrace{\boldsymbol{\sigma}_T}_{\equiv \frac{\partial W}{\partial \mathbf{E}} \Big|_{\mathbf{E}_A}} : (\mathbf{E} - \mathbf{E}_A) + \frac{1}{2} (\mathbf{E} - \mathbf{E}_A) : \underbrace{\mathbf{C}_T}_{\equiv \frac{\partial^2 W}{\partial \mathbf{E} \partial \mathbf{E}} \Big|_{\mathbf{E}_A}} : (\mathbf{E} - \mathbf{E}_A) \quad (3.2.2)$$

$\psi_A (A = 1, 2)$ approximates the behavior of W near the states \mathbf{E}_1 and \mathbf{E}_2 .

The total energy is then:

$$\int_{\Omega_0} \left(\dot{W} + \frac{1}{2} \epsilon |\nabla \phi|^2 \right) d\Omega_0 \quad (3.2.3)$$

The displacement field evolves through momentum balance:

$$\text{div}_{\mathbf{x}_0} \left(\frac{\partial \dot{W}(\mathbf{F}, \phi)}{\partial \mathbf{F}} \right) = \rho_0 \ddot{\mathbf{x}}(\mathbf{x}_0, t) \quad (3.2.4)$$

In quasistatics, the inertial contribution is set to 0.

The phase field evolution is governed by the conservation law posed in the companion paper:

$$|\nabla\phi|v_n^\phi + G = \dot{\phi} \quad (3.2.5)$$

G is a constitutively-prescribed nucleation term, and v_n^ϕ is the interface velocity field – completely distinct from the material velocity field – through which the kinetic relation is prescribed.

For further details, we refer to the companion paper.

3.3 Formulation of a Two-Dimensional Energy for Twinning

We perform a number of 2D calculations for twinning in the subsequent sections. Here, we outline certain aspects that are common to all those calculations, such as the formulation of $\mathring{W}(\mathbf{E}, \phi)$.

The form of \mathring{W} is:

$$\mathring{W}(\mathbf{E}, \phi) = (1 - H_l(\phi - 0.5)) \frac{1}{2}(\mathbf{E} - \mathbf{E}_1) : \mathbf{C} : (\mathbf{E} - \mathbf{E}_1) + H_l(\phi - 0.5) \frac{1}{2}(\mathbf{E} - \mathbf{E}_2) : \mathbf{C} : (\mathbf{E} - \mathbf{E}_2) \quad (3.3.1)$$

Both \mathbf{E}_1 and \mathbf{E}_2 are the stress-free states because $\boldsymbol{\sigma}_T = 0$. Both wells are at the same height, i.e., $\mathring{W}(\mathbf{E}_1, 0) = \mathring{W}(\mathbf{E}_2, 1) = 0$. This is appropriate for twinning, but perhaps not so for other transformations. The relative height of the wells is important because it appears directly in the driving force, and is trivial to change if appropriate.

We have assumed for simplicity that the moduli \mathbf{C} are the same in each twin, and additionally assumed that \mathbf{C} is isotropic. It should be noted that neither of these assumptions are appropriate in real materials [Cla10, Kal98]. However, it is trivial to incorporate physically-appropriate forms for \mathbf{C} in the energy formulated above when required.

For twinning, consider the transformation stretch tensors:

$$\mathbf{U}_1 = \begin{bmatrix} \alpha & 0 \\ 0 & \beta \end{bmatrix}, \mathbf{U}_2 = \begin{bmatrix} \beta & 0 \\ 0 & \alpha \end{bmatrix}, \quad \alpha = 1 - 0.1042, \beta = 1 + 0.09659 \quad (3.3.2)$$

\mathbf{E}_1 and \mathbf{E}_2 are computed from $\mathbf{F}_1 = \mathbf{U}_1$ and $\mathbf{F}_2 = \mathbf{U}_2$. The stress-free compatible interfaces between these wells have normals $\frac{1}{\sqrt{2}} \begin{pmatrix} 1 \\ 1 \end{pmatrix}$ and $\frac{1}{\sqrt{2}} \begin{pmatrix} 1 \\ -1 \end{pmatrix}$.

In certain cases, we rotate the specimen by $\pi/12$ radians with respect to the coordinate axes. In that case, the compatible interfaces are oriented with normal $\frac{1}{2} \begin{pmatrix} \sqrt{3} \\ 1 \end{pmatrix}$ and $\frac{1}{2} \begin{pmatrix} -1 \\ \sqrt{3} \end{pmatrix}$. The reason is that an interface that is inclined at a large angle will feel the effects of the loading on the right boundary of the domain quite differently at different points along its length. On the other hand, an interface aligned perfectly normal to the top and bottom boundaries of the domain will not have any shear stress in the direction tangent to the interface at the junction between the interface and the domain boundary. Some level of shear stress is required for evolution on the boundary/interface junction (Section 3.10). The angle that we have chosen balances between these competing reasons.

3.4 Non-Monotone Kinetic Laws

Non-monotone kinetic laws have been predicted to show extremely complex and interesting behavior, e.g. [RK97]. However, in that literature, the driving force is taken as a function of interface velocity. In the case where it is non-monotone, it is not invertible to obtain the interface velocity as a function of driving force. In our case, we assume that the interface velocity is a non-monotone function of driving force. We briefly present the results of calculations in 1D and 2D, but the summary is that there is no complex and unexpected behavior as observed in [RK97]. We have verified after the calculations that the level of driving force was appropriate to access the non-monotonic portion of the kinetic response.

3.4.1 1D Non-Monotone Kinetics

We use the following material model:

$$\dot{W}(u_x, \phi) = \left(1 - H_l(\phi - 0.5)\right) \frac{1}{2} C(u_x - \varepsilon_1)^2 + H_l(\phi - 0.5) \frac{1}{2} C(u_x - \varepsilon_2)^2 \quad (3.4.1)$$

$$\sigma = \frac{\partial \dot{W}}{\partial (u_x)} = \left(1 - H_l(\phi - 0.5)\right) C(u_x - \varepsilon_1) + H_l(\phi - 0.5) C(u_x - \varepsilon_2) \quad (3.4.2)$$

$$f = \delta_l(\phi - 0.5) \left(\frac{1}{2} C(u_x - \varepsilon_1)^2 - \frac{1}{2} C(u_x - \varepsilon_2)^2 \right) + \epsilon \phi_{xx} \quad (3.4.3)$$

$$\rho \ddot{u} = \sigma_x \quad (3.4.4)$$

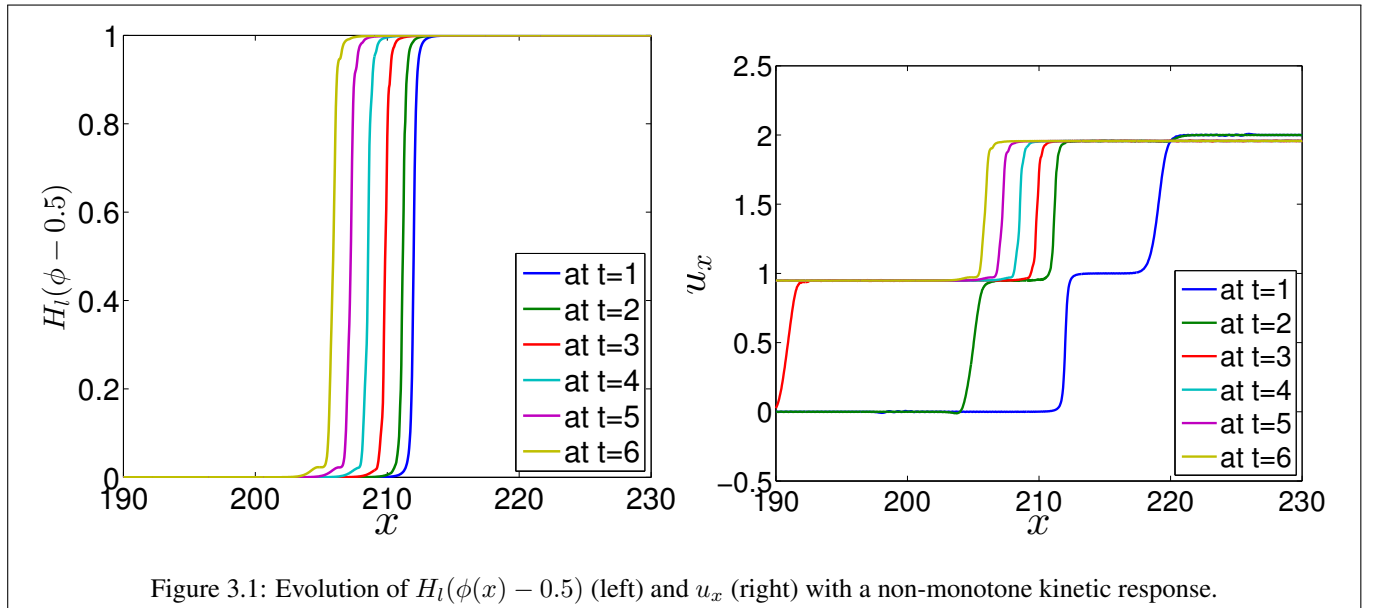
$$\dot{\phi} = |\phi_x| v_n^\phi \quad (3.4.5)$$

The stored energy density near each well is quadratic with wells at $\varepsilon_1 = 0$ and $\varepsilon_2 = 1$.

The kinetic response is chosen to be non-monotonic:

$$\hat{v}_n^\phi = \begin{cases} |f| \cdot (0.1 - |f|) & \text{if } |f| < 0.075 \\ 0.075 \cdot (0.1 - 0.075) & \text{if } |f| \geq 0.075 \end{cases} \quad (3.4.6)$$

Fig. 3.1 shows the evolution of ϕ and u_x which are qualitatively similar to the calculations with simpler kinetic response functions.



3.4.2 2D Non-Monotone Kinetics

We examine 2 settings with non-monotone kinetics; first, a problem with a stress-free compatible interface, and second, where there is necessarily stress around the interface. The reasoning to test both cases is that it is possible that elastic compatibility will dominate the evolution, and therefore testing both cases will let us compare the role of kinetics. We compare a linear kinetic response and a non-monotone kinetic response. For the latter, we use the same kinetic response as in 1D from (3.4.6).

We first examine the case of stressed interfaces using a square plate where a circular region near the center has a second phase. The energy is described in Section 3.3, and for the incompatible wells we use:

$$\mathbf{U}_1 = \begin{bmatrix} 1 & 0 \\ 0 & 1 \end{bmatrix}, \mathbf{U}_2 = \begin{bmatrix} \beta & 0 \\ 0 & \alpha \end{bmatrix}, \quad \alpha = 1 - 0.1042, \beta = 1 + 0.09659 \quad (3.4.7)$$

Fig. 3.2 shows the evolution through $F_{11} - 1$ at various times for the linear and non-monotone kinetic responses respectively. While there are quantitative differences, there are no obvious qualitative differences, and further there is no complex behavior in the non-monotone case.

The previous calculation leaves open the possibility that the kinetics is possibly complex but that momentum balance simply dominates due to the stresses that are necessarily present. Therefore, we briefly examine a problem with a stress-free compatible interface. The energy is described in Section 3.3, and we use \mathbf{E}_1 and \mathbf{E}_2 as described there, with the rotated sample. We consider a 2D rectangular plate fixed at the left edge, and traction-free at the top and bottom edges. A stress free compatible phase interface exists in the plate initially. A constant tensile load is then applied at the right edge. Fig. 3.3 shows the initial configuration, and the configuration after some evolution has occurred for both linear and non-monotone kinetics.

3.5 Anisotropic Kinetics in Two Dimensions

We consider the role of anisotropic kinetics in a 2D transformation. To isolate the role of anisotropy in the kinetics, we keep all other effects isotropic. Therefore, we use the energy described in Section 3.3,

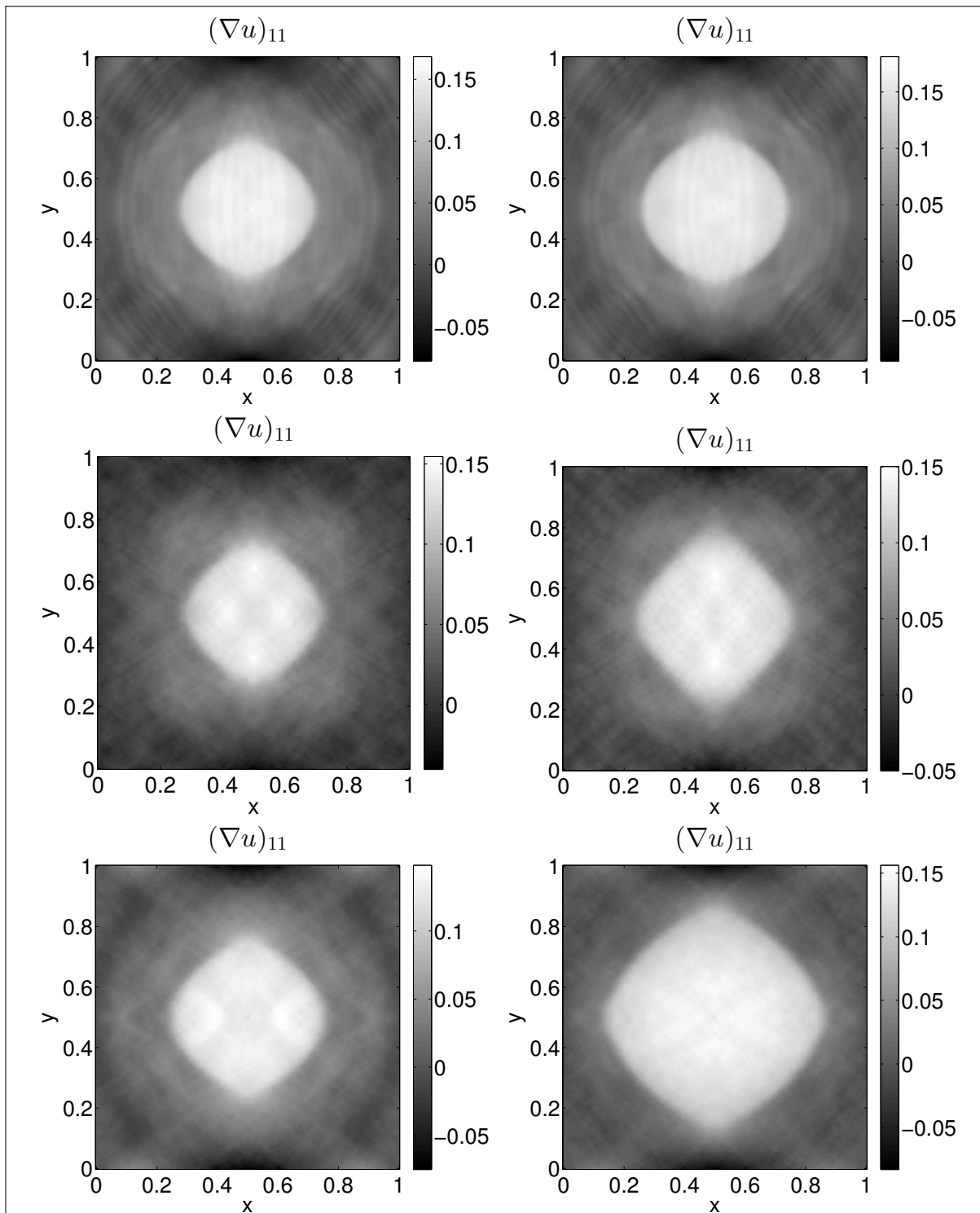
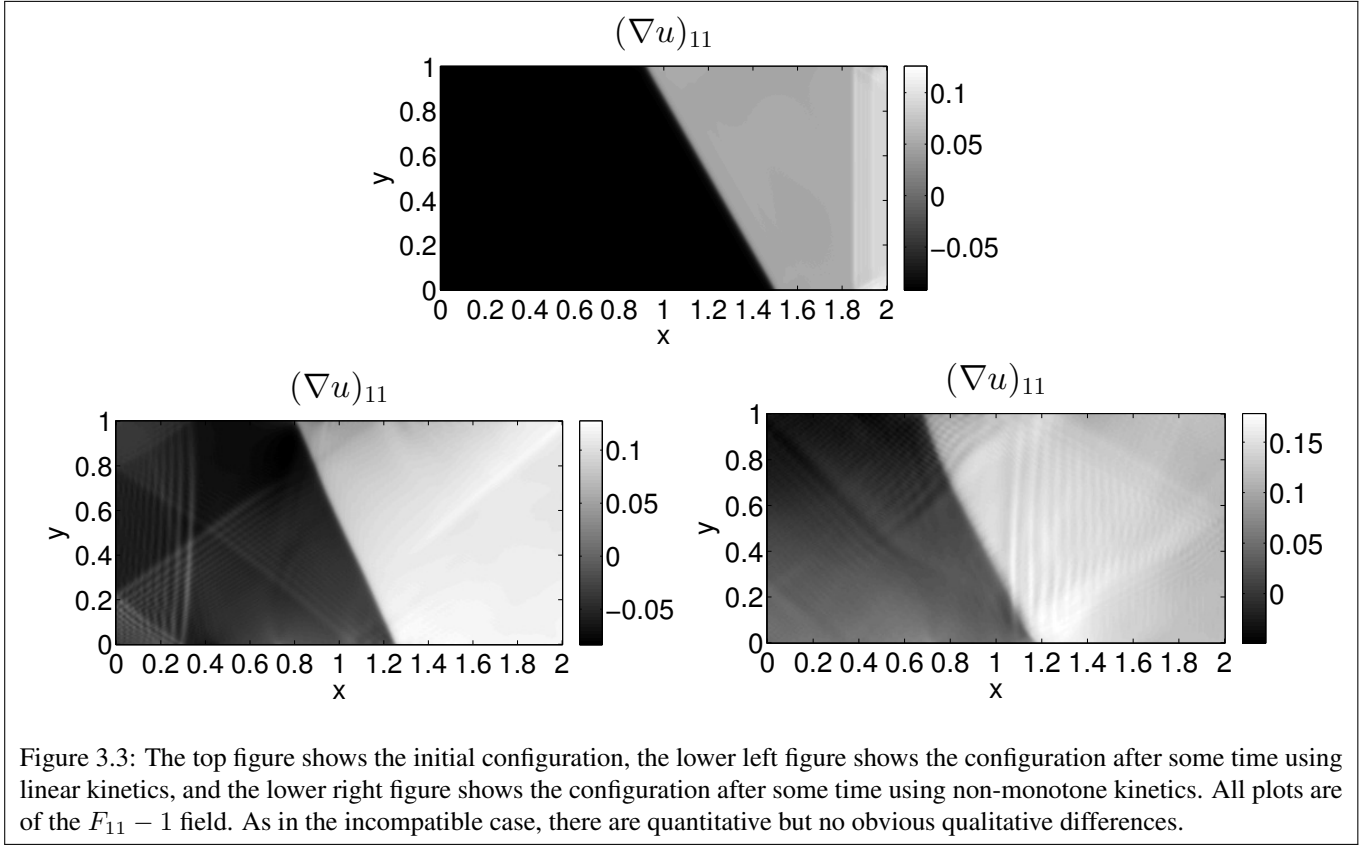


Figure 3.2: The left column is the evolution with linear kinetics, and the right column is the evolution with non-monotone kinetics, with snapshots of the $F_{11} - 1$ field taken at the same time for both processes. The phases are not stress-free compatible. The top row, at small times, is fairly similar. As evolution progresses, there are quantitative but not qualitative differences.



but with stress-free wells:

$$\mathbf{U}_1 = \alpha \mathbf{I} \quad \text{and} \quad \mathbf{U}_2 = \beta \mathbf{I}, \quad \text{with } \alpha = 1.05, \beta = 1.1 \quad (3.5.1)$$

These wells not stress-free compatible.

We consider a square domain with a hydrostatic loading applied on the boundary. The material is entirely in a single phase, but the new phase nucleates as the loading increases. To force the nucleation to occur away from the boundaries, we make the source term heterogeneous, and of the form:

$$G(\phi, \boldsymbol{\sigma}, \mathbf{x}) = \begin{cases} A_{0-1} H_l(1 - \phi) & \text{if } |\boldsymbol{\sigma}_{11} + \boldsymbol{\sigma}_{22}| > \sigma_0 \text{ and } |\mathbf{x}| < 0.1 \\ 0 & \text{otherwise} \end{cases} \quad (3.5.2)$$

A_{0-1} is a constant characteristic of the $0 - 1$ reaction, and $H_l(1 - \phi)$ ensures that the 1-phase is created only when we are not already in the 1-phase, i.e., the nucleation term turns off when the 1-phase has nucleated. The nucleation term is only active in a circle centered around the middle of the domain, and is only active when the hydrostatic stress $|\boldsymbol{\sigma}_{11} + \boldsymbol{\sigma}_{22}|$ is above a critical stress σ_0 . We have not allowed

for the reverse transformation, but it is trivial to add this if required. The nucleation term and the loading both maintain the circular symmetry in the problem.

The kinetic response is $\hat{v}_n^\phi(f) = \text{sign}(f)\kappa |f| \left| \frac{\nabla\phi}{|\nabla\phi|} \cdot \mathbf{d}_m \right|$, where $\mathbf{d}_m = \frac{\sqrt{3}}{2}\mathbf{e}_1 + \frac{1}{2}\mathbf{e}_2$ is a distinguished material direction that sets the anisotropy. Recall that $\frac{\nabla\phi}{|\nabla\phi|}$ sets the normal to the interface. Therefore, the kinetic response depends on the relative orientation of the interface to \mathbf{d}_m , and interface velocity goes to 0 along directions normal to \mathbf{d}_m .

The evolution of the deformation is shown in Fig. 3.4.

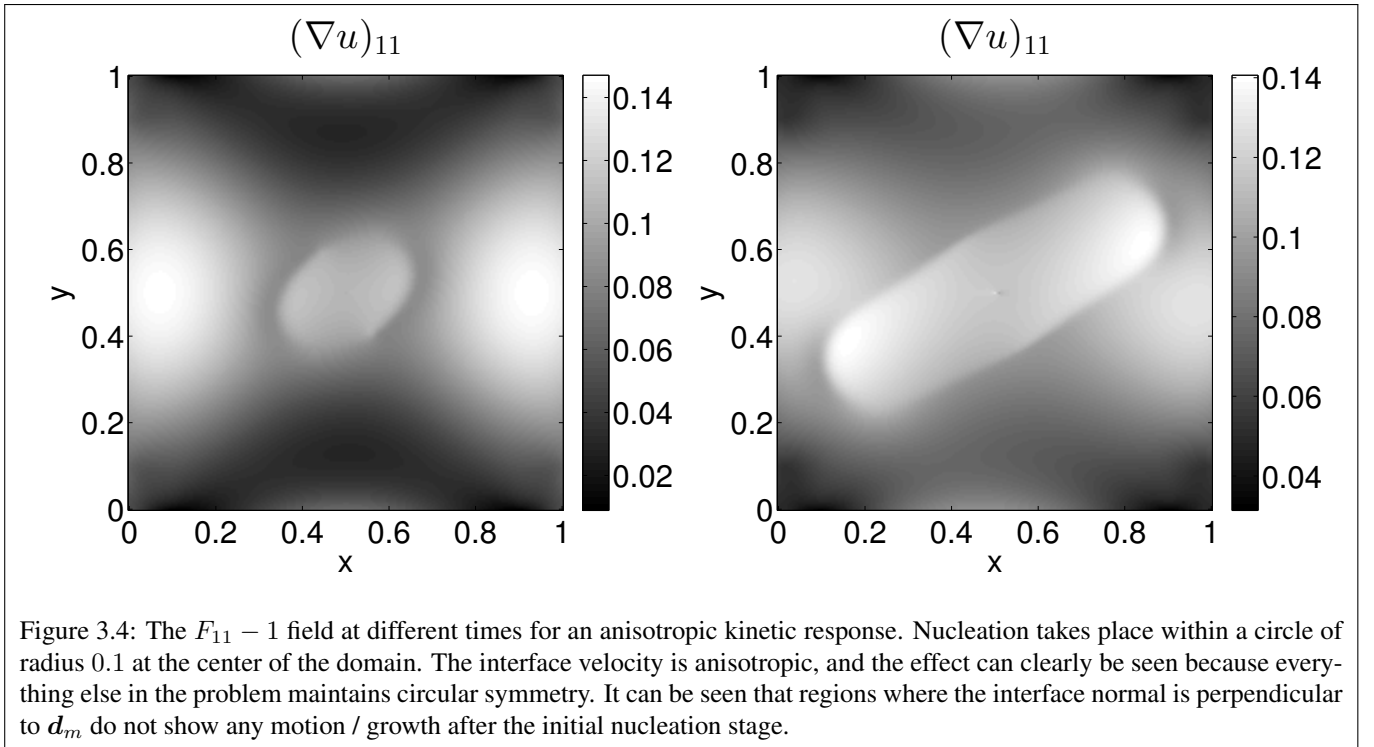


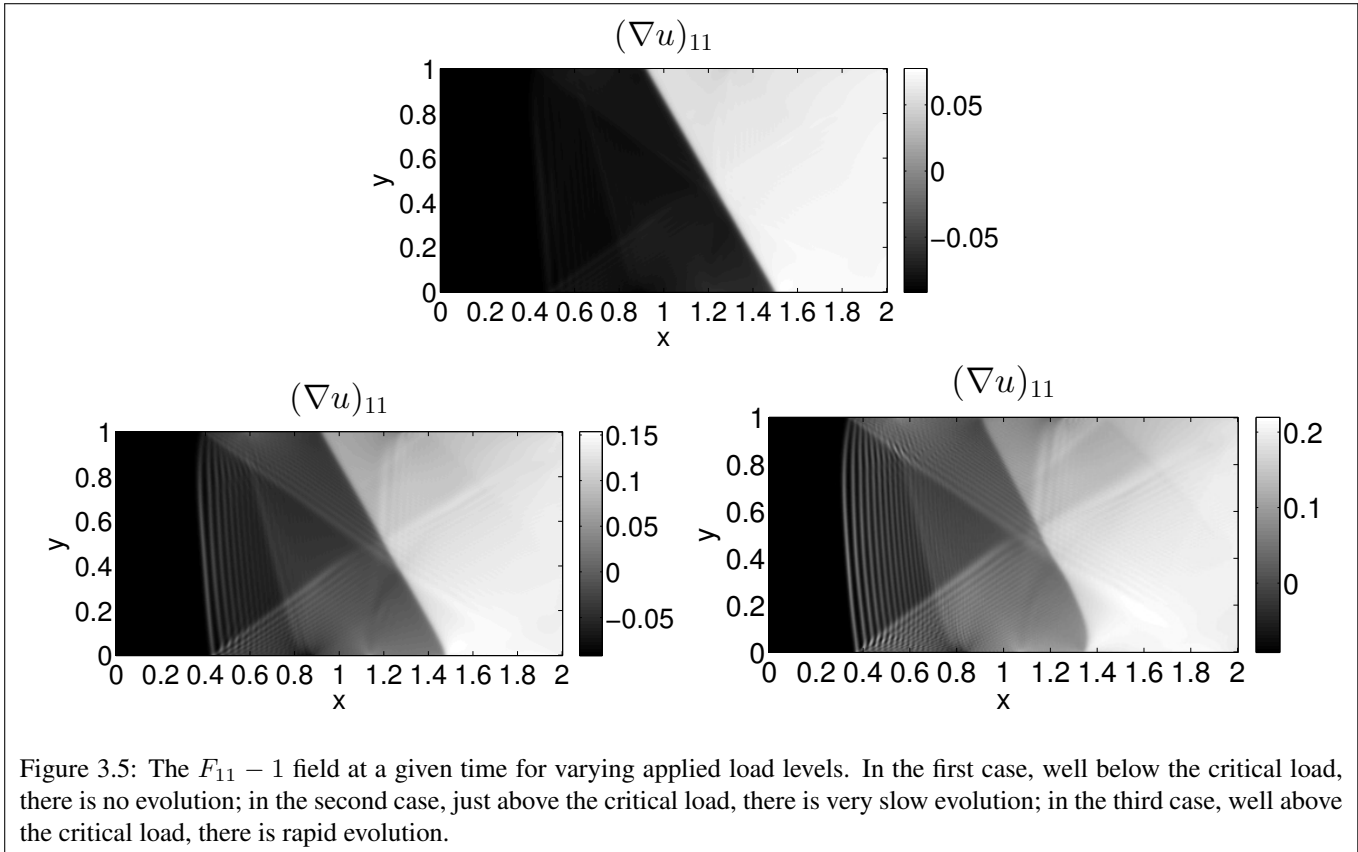
Figure 3.4: The $F_{11} - 1$ field at different times for an anisotropic kinetic response. Nucleation takes place within a circle of radius 0.1 at the center of the domain. The interface velocity is anisotropic, and the effect can clearly be seen because everything else in the problem maintains circular symmetry. It can be seen that regions where the interface normal is perpendicular to \mathbf{d}_m do not show any motion / growth after the initial nucleation stage.

3.6 Stick-slip Twinning Kinetics

We examine the evolution of twinning interfaces in 2D using stick-slip kinetics using the energy described in Section 3.3 with the rotated specimen. We consider a 2D rectangular plate fixed at the left edge, and traction-free at the top and bottom edges. A stress-free compatible phase interface exists in the plate initially. A constant tensile load is then applied at the right edge.

We use a stick-slip kinetic response: $\hat{v}_n^\phi = 0$ if $|f| < f_0$ and $\hat{v}_n^\phi = \kappa \text{sign}(f) (|f| - f_0)$ if $|f| \geq f_0$. We examine the evolution of the interface for a number of applied load levels. Fig. 3.5 shows the $F_{11} - 1$

field some time after evolution has commenced, for different load levels. We find that we are able to impose stick-slip easily and effectively through the kinetic response listed above in 2D as well.



3.7 Rate-Dependent and Asymmetric Nucleation

We examine the prescription of complex nucleation rules in our formulation. In this section, we demonstrate two key features: (1) that we transparently incorporate complex nucleation behavior such as rate-dependence; and (2) that we can tailor the nucleation stress easily without any modifications to the energy but purely through the activation of the source term G . We perform calculations in 1D and 2D to show the ability of the model to separate kinetics and energetics from nucleation. An additional feature that we demonstrate is that we can independently prescribe the forward and reverse nucleation stresses; i.e., given a completely symmetric energy landscape, we are able to induce nucleation in one direction at a certain critical stress, but the reverse transformation is induced at a completely independent critical value of the stress.

This gives us a powerful approach to prescribe complex nucleation criteria. For instance, in the 1D calculation described below, we are able to change the nucleation stress by a factor of 3 for a change of 4% in the loading rate.

3.7.1 Rate-Dependent and Asymmetric Nucleation in One Dimension

We use the same energy \mathring{W} as in Section 3.4.1 with linear kinetics. This energy is quadratic around the stress-free strains 0 and 1, corresponding to phase 1 and phase 2. The elastic moduli is the same in both phases.

The nucleation criterion is specified as follows:

$$G(x) = \begin{cases} (1 - H_l(\phi - 0.6)) & \text{if } \sigma(x) > \sigma_{1 \rightarrow 2} \\ H_l(\phi - 0.4) & \text{if } \sigma(x) < \sigma_{2 \rightarrow 1} \\ 0 & \text{else} \end{cases} \quad (3.7.1)$$

The term $(1 - H_l(\phi - 0.6))$ ensures consistency with thermodynamics in that it turns off the nucleation source for the transformation $1 \rightarrow 2$ when we are in phase 2. Similarly, $H_l(\phi - 0.4)$ turns off the source for the reverse transformation $2 \rightarrow 1$ when we are in phase 1.

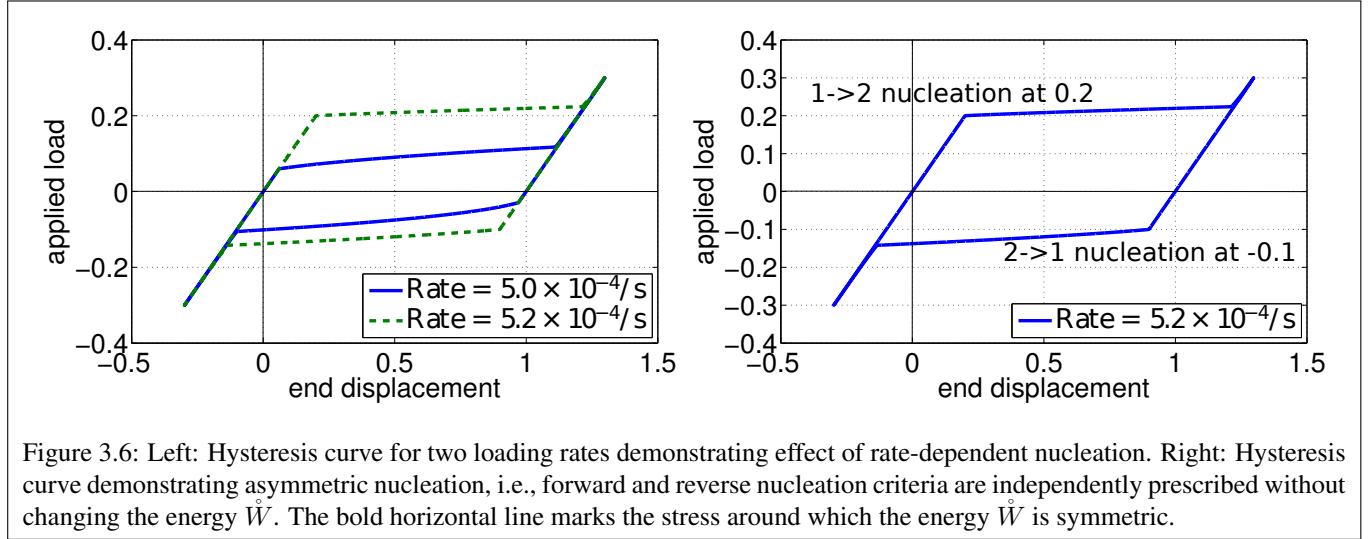
For clarity of presentation, we have simplified the nucleation definitions to be piece-wise. However, this would require us to track precisely the point at which the stress reaches the critical value. Therefore, in implementation, we use a regularized version of these definitions, both in this section and elsewhere. The key distinction between the regularization that we have used in the nucleation and kinetics, vs. the usual regularization of displacement fields, is that in our case the observed nucleation and kinetics are *not* sensitive to the regularization.

Asymmetry in the forward and reverse transformations is readily prescribed by using different values for the forward and reverse threshold stresses $\sigma_{1 \rightarrow 2}$ and $\sigma_{2 \rightarrow 1}$.

Rate-dependence is prescribed by making the threshold stresses functions of the loading rate. We use:

$$\sigma_{1 \rightarrow 2} = \begin{cases} 0.06 & \text{if } \dot{\varepsilon} < 5.1 \times 10^{-4} s^{-1} \\ 0.2 & \text{if } \dot{\varepsilon} \geq 5.1 \times 10^{-4} s^{-1} \end{cases} \quad \text{and } \sigma_{2 \rightarrow 1} = \begin{cases} -0.03 & \text{if } \dot{\varepsilon} < 5.1 \times 10^{-4} s^{-1} \\ -0.1 & \text{if } \dot{\varepsilon} \geq 5.1 \times 10^{-4} s^{-1} \end{cases} \quad (3.7.2)$$

We demonstrate this nucleation criterion by computing an entire hysteresis loop, starting with the forward transformation from phase 1 to phase 2, and then the reverse transformation back to phase 1 (Fig. 3.6). This loop is computed by simply evolving the kinetic equation for ϕ while solving the quasistatic (i.e., without inertia) momentum balance as the evolution proceeds.



As we notice from Fig. 3.6, we are able to precisely set the nucleation stress in a direct and transparent manner. In addition, we are able to change the nucleation stress by a factor of 3 for a change in loading rate of 4%.

3.7.2 Rate-Dependent and Asymmetric Nucleation in Twinning

We demonstrate here the possibility of allowing rate-dependence and asymmetry in nucleation for a twinning transformation. While twinning is typically expected to be symmetric, this calculation serves as a demonstration that asymmetry in nucleation can be readily introduced in 2D even when everything else in the problem is symmetric.

We use the energy for twinning described in Section 3.3 with linear kinetics. The nucleation criterion is specified as follows:

$$G = \begin{cases} (1 - H_l(\phi - 0.8)) & \text{if } \mathbf{a} \cdot \boldsymbol{\sigma} \mathbf{b} > \sigma_{1 \rightarrow 2} \\ H_l(\phi - 0.2) & \text{if } \mathbf{a} \cdot \boldsymbol{\sigma} \mathbf{b} < \sigma_{2 \rightarrow 1} \\ 0 & \text{else} \end{cases} \quad (3.7.3)$$

It resembles closely the 1D version. The key difference from 1D is that the scalar stress is here replaced

by the shear traction magnitude on the planes oriented at $\pi/12$. Hence, this is essentially a critical resolved shear stress (CRSS) type of nucleation criterion, with the difference being that we can set $\sigma_{2 \rightarrow 1}$ and $\sigma_{1 \rightarrow 2}$ to completely distinct values.

Asymmetry and rate-dependence are prescribed by following exactly the 1D approach of making $\sigma_{2 \rightarrow 1}$ and $\sigma_{1 \rightarrow 2}$ different from each other and rate-dependent. For simplicity, we set the rate-dependence through the 11-component of the nonlinear strain measure. For realistic calculations, a model based on an objective rate would be appropriate.

Fig. 3.7 shows the hysteresis loop that demonstrates both asymmetry and rate-dependence of our evolution law.

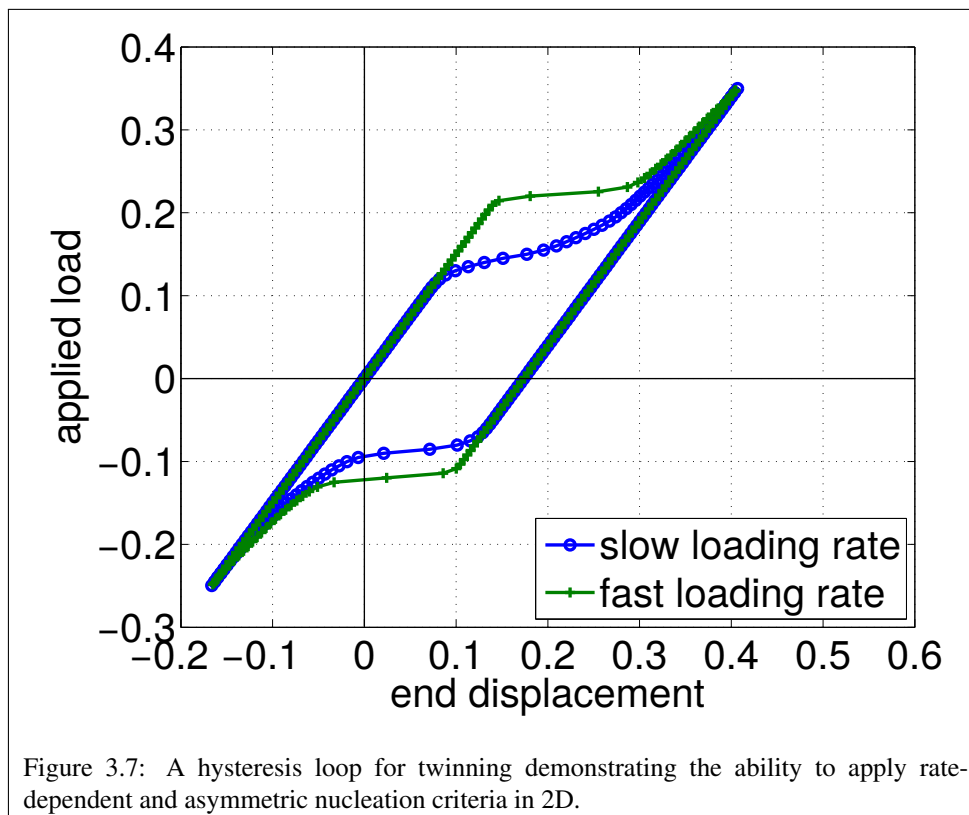


Figure 3.7: A hysteresis loop for twinning demonstrating the ability to apply rate-dependent and asymmetric nucleation criteria in 2D.

3.8 Imposing Principal Normal Stress- and Shear Stress- Dependent Nucleation for Twinning

Defect nucleation and kinetics typically do not depend exclusively on the driving force. E.g., recent studies of dislocation motion in BCC metals show that other stress components can be important in addition to the shear-related driving force [GBV08, GRBV08]. Motivated by these studies, we examine twin nucleation within our model, where the nucleation criterion has a dependence on the maximum principal stress, in addition to the critical resolved shear stress (CRSS) for twin nucleation. While this nucleation criterion is not motivated by any specific observations in experiments or atomistics, it serves as a toy model to demonstrate the transparent specification of complex nucleation criteria.

The elastic energy is as described in Section 3.3, with the unrotated specimen. We use simple linear kinetics. Our nucleation criterion is as follows:

$$G(\phi, \boldsymbol{\sigma}) = \begin{cases} A_{0 \rightarrow 1} H_l(0.6 - \phi) & \text{if } |\mathbf{b} \cdot \boldsymbol{\sigma} \mathbf{a}| > \tau_{CRSS} \text{ and } \max\{|\sigma_{principal}|\} > \sigma_0 \\ 0 & \text{otherwise} \end{cases} \quad (3.8.1)$$

$A_{0 \rightarrow 1}$ is a constant which controls the rate of nucleation. $H_l(0.6 - \phi)$ causes nucleation to be active when $\phi < 1$ and “turns off” when ϕ is close to 1. To prevent nucleation near the boundaries, G is active only in a circle of radius 0.35 centered at the middle of the domain and 0 elsewhere.

The CRSS character is built into the nucleation stress through the condition $|\mathbf{b} \cdot \boldsymbol{\sigma} \mathbf{a}| > \tau_{CRSS}$. The vectors $\mathbf{a} = \frac{1}{\sqrt{2}} \begin{pmatrix} 1 \\ 1 \end{pmatrix}$ and $\mathbf{b} = \frac{1}{\sqrt{2}} \begin{pmatrix} -1 \\ 1 \end{pmatrix}$ are the twin normal and shear direction, thereby resolving the shear stress in the direction appropriate for twin nucleation. We note that it is direct and transparent to have the nucleation stress have CRSS character as in the equation. It is equally direct to add a dependence on the hydrostatic stress state if required; in our example, we have taken a simple dependence that requires a minimum level of the principal stress. More complex pressure-sensitive nucleation responses can be easily incorporated in our model.

We examine the behavior of this nucleation response through the interaction of an elastic wave with the residual stress field around an inclusion. A square 2D single-phase domain is considered with a circular non-transforming elastic inclusion at the center. The elastic inclusion is stress-free at $\mathbf{F} = \mathbf{I}$ but the

surrounding matrix has $\mathbf{F} = \mathbf{U}$; therefore, the interface between the inclusion and the matrix sets up a stress field. A shear at – or above – the critical level required by the CRSS criterion would not cause nucleation unless there is also sufficiently large principal stress. The residual stress field around the misfitting inclusion provides this stress.

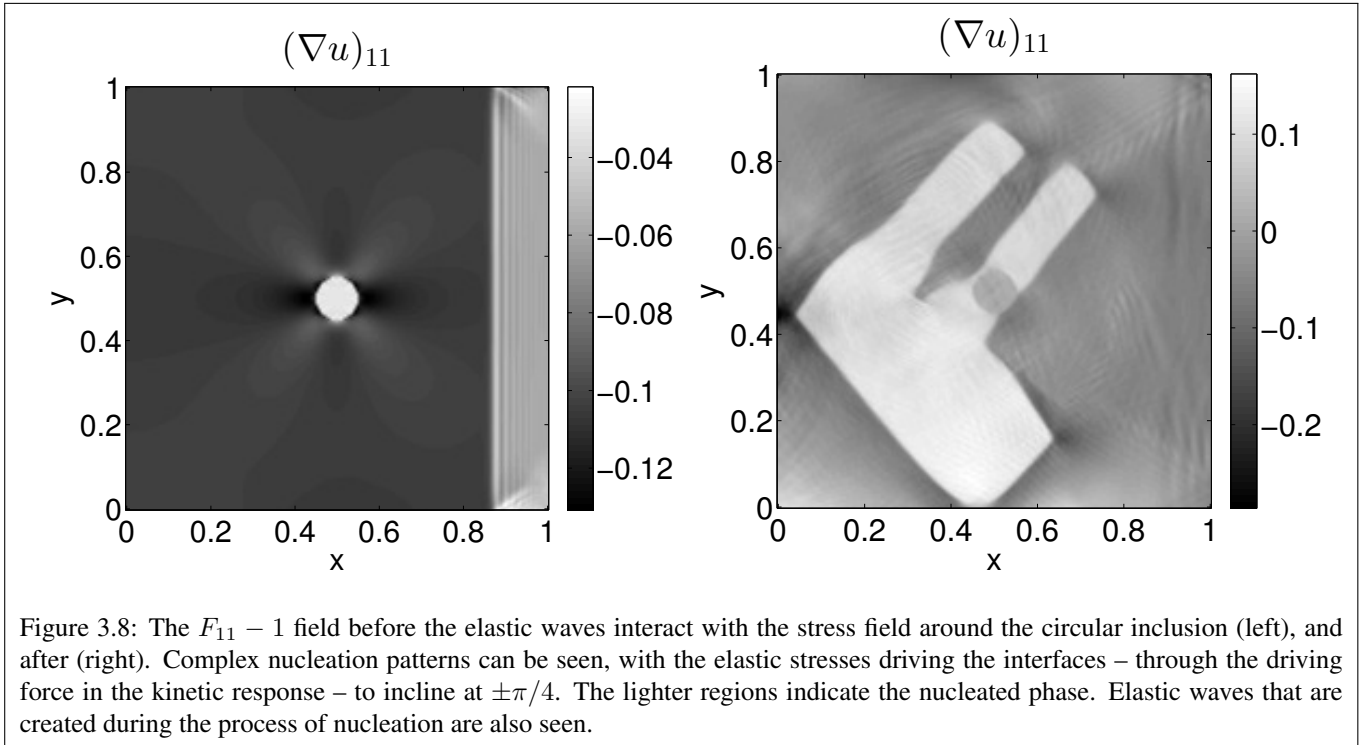
The specimen is fixed on the left boundary, traction-free at the top and bottom, and a constant load is applied to the right. This load results in an elastic wave which interacts with the stress field around the inclusion and leads to nucleation when the critical conditions are satisfied (Fig. 3.8).

The inclusion is elastic in the sense that it has a finite elastic modulus. However, it has only a single stress-free deformation state at $\mathbf{F} = \mathbf{I}$. Therefore, \dot{W} in the inclusion is independent of ϕ , and the energy has only the term $\frac{1}{2}\epsilon|\nabla\phi|^2$ that depends on ϕ . Therefore, the evolution of ϕ is diffusion-driven within the inclusion, and interacts with the matrix through the value of ϕ on the boundary. Physically the evolution of ϕ within the inclusion has no meaning, but it nonetheless affects the evolution in the matrix through the interaction on the inclusion-matrix boundary. Therefore, the ideal strategy would be to not define ϕ at all within the inclusion and use a separate boundary kinetic equation that reflects the physics of the interface interacting with the inclusion-matrix boundary (see Section 3.10). A simpler approach may be to define the kinetics within the inclusion in such a way as to mimic the correct physics at the inclusion-matrix boundary. For now, we have ignored these issues and simply evolved ϕ based on $\frac{1}{2}\epsilon|\nabla\phi|^2$.

3.9 Competition Between Nucleation and Kinetics in Twinning

We examine the competition between kinetics and nucleation in the evolution of microstructure. We use precisely the same material model, specimen geometry and inclusion, and loading conditions as in Section 3.8. Recalling that G is a nucleation rate, we examine the effect of a large nucleation rate and a small nucleation rate, while keeping the kinetic response the same in both cases. Varying the nucleation rate simply involves changing the value of $A_{0\rightarrow 1}$ in (3.8.1).

The results of the calculations are shown in Fig. 3.9. A key qualitative difference is that when the nucleation rate is smaller, we find that the microstructure is finer as compared to the larger nucleation rate. Heuristically, it appears that the high nucleation rate enables the formation of larger nuclei that quickly coalesce to form relatively coarse-microstructure. For lower nucleation rates, the microstructure



takes longer to develop and there are a number of smaller nuclei. We note that the total area of the transformed regions is smaller when the nucleation rate is lower, as may be expected.

3.10 Boundary Kinetics

The most widely-used boundary condition (BC) on ϕ in standard phase-field modeling imposes $\nabla\phi \cdot \mathbf{N} = 0$ on $\partial\Omega$. Among other things, it forces the interface to be normal to the boundary in the vicinity of the boundary, and it does not associate a kinetics to the evolution on the boundary beyond that which is driven by the evolution in the bulk. However, as [SB98, SB00, SB99] examined in the sharp-interface setting, it is possible to associate a separate kinetics to the junction line (or junction point in 2D) of the interface with the boundary. Along the junction line, we require not only the normal interface velocity field v_n^ϕ , but also the interface velocity component that is tangent to the boundary. As illustrated in Fig. 3.10, the boundary velocity can have a profound effect on the evolution on the interior. It also controls the surface evolution of ϕ , and ignoring the effect of boundary kinetics can potentially lead to errors in analyzing experiments that are based only on surface measurements.

In this section, we use the interface balance principle to deduce a kinetic law for the regularized junction

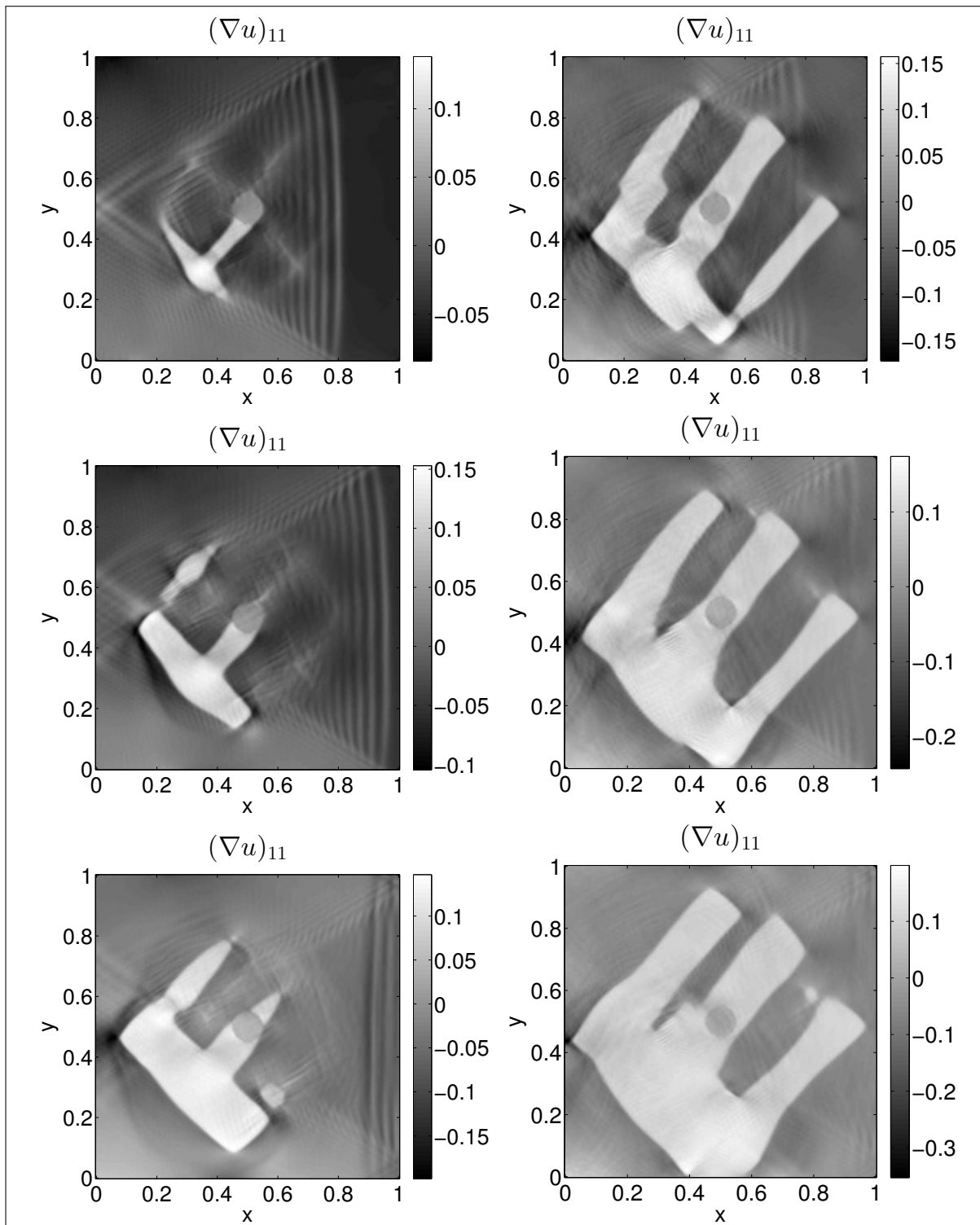
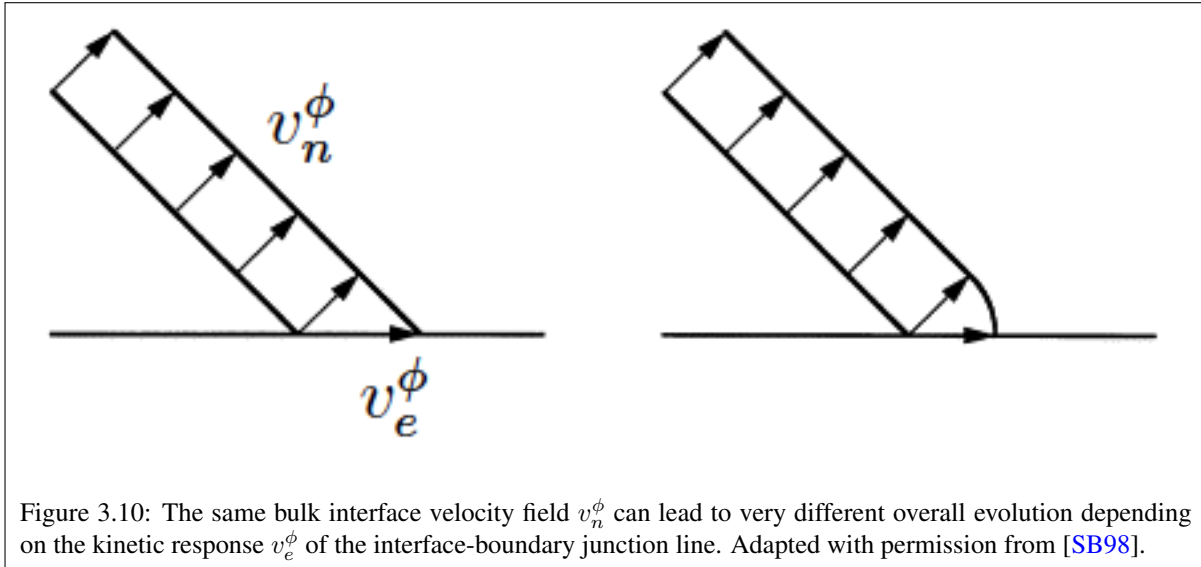


Figure 3.9: The $F_{11} - 1$ field as the elastic waves interact with the stress field around the circular inclusion, causing nucleation and growth. The lighter regions indicate the nucleated phase. The left column is the evolution with small nucleation rate ($A_{0 \rightarrow 1} = 2$), and the right column is the evolution with large nucleation rate ($A_{0 \rightarrow 1} = 20$). The plots show snapshots taken at the same time for both processes.



lines, and apply the formulation to some illustrative calculations.

3.10.1 Formulation of Boundary Kinetics

Following closely the balance principle posed in the companion paper, we consider the flux of interfaces that thread a curve, with the only difference being that in this case the curve is restricted to lie on the boundary. Hence, the kinetic law is the same as the bulk, $\dot{\phi} = |\nabla\phi|v_e^\phi + G_e$, with the gradient operator here interpreted as restricted to the boundary. As with v_n^ϕ , the edge velocity v_e^ϕ can be an arbitrary function of any arguments as long as it satisfies positive dissipation. To ensure positive dissipation, as well as identify the thermodynamic conjugate driving force, we re-examine the dissipation statement, but augment the energy to account for the boundary working.

We start by rewriting the energy to include an “elastic energy on the boundary”:

$$\int_{\Omega_0} \dot{W}(\mathbf{F}, \phi) + \int_{\Omega_0} \frac{1}{2}\epsilon|\nabla\phi|^2\alpha + t \int_{\partial\Omega_0} \dot{W}(\mathbf{F}, \phi) + \int_{\partial\Omega_0} \frac{1}{2}\epsilon_S|\nabla_S\phi|^2 \quad (3.10.1)$$

∇_S is the gradient on the surface.

The first surface integral is the “elastic energy on the boundary”. The constant t that multiplies it has dimensions of length, and is required for dimensional consistency. Heuristically, it can be considered a measure of the distance that the surface effects penetrate into the bulk.

The term containing ϵ_S regularizes the interface-boundary junction. In principle, it is possible for the elastic energy on the boundary to drive the interface to become singularly sharp at the junction, and this term prevents that. Physically, it allows for the junction to have a width that can differ from the width of interfaces in the bulk. We use ϵ_S to define $t \sim \epsilon_S/\epsilon$ which has dimensions of length.

For notational convenience, we write the energy in (3.10.1) as $V[\mathbf{u}, \phi] + S[\mathbf{u}, \phi]$, where V consists of the volume integrals and S consists of the surface integrals. We write the kinetic energy also as a sum of a volume integral and surface integral:

$$K = K_v + K_s = \int_{\Omega_0} \frac{1}{2} \rho \mathbf{V} \cdot \mathbf{V} + t \int_{\partial\Omega_0} \frac{1}{2} \rho \mathbf{V} \cdot \mathbf{V} \quad (3.10.2)$$

We now examine dissipation to obtain the thermodynamic conjugate driving forces for the the bulk and the edge interface velocities. Recall that \mathcal{D} is the difference between rate of external working and the rate of change of stored energy. Computing \mathcal{D} gives us precisely the same result as the dissipation calculations in the companion paper, except that we have the additional contribution from the surface terms in the stored energy. This additional contribution is $-\frac{d}{dt}(S[\mathbf{u}, \phi] + K_s)$, and can be simplified as follows:

$$\frac{d}{dt}(S + K_s) = t \int_{\partial\Omega_0} \left(\frac{\partial \dot{W}}{\partial \mathbf{F}} : \dot{\mathbf{F}} + \rho \mathbf{V} \cdot \dot{\mathbf{V}} \right) + t \int_{\partial\Omega_0} \frac{\partial \dot{W}}{\partial \phi} \dot{\phi} - \int_{\partial\Omega_0} \epsilon_S \nabla_S \dot{\phi} \cdot \nabla_S \phi \quad (3.10.3)$$

The first term above vanishes as follows. Following precisely the calculations in the companion paper, we can write $\dot{\mathbf{F}}$ as the material velocity gradient. Using integration-by-parts and the divergence theorem, we obtain balance of linear momentum which consequently vanishes, and another term that is a total derivative integrated over the closed region $\partial\Omega_0$ and therefore is set to 0.

The last term above can be written as $\int_{\partial\Omega_0} \epsilon_S \dot{\phi} \operatorname{div}_S \nabla_S \phi$, as well as another term that is a total derivative integrated over the closed region $\partial\Omega_0$ and therefore goes to 0.

We can now write the dissipation \mathcal{D} . It consists of the same expressions as in the dissipation without bulk

contributions (see companion paper), and with the additional remaining nonzero terms from (3.10.3):

$$\mathcal{D} = \underbrace{- \int_{\Omega_0} \left[\frac{\partial \dot{W}}{\partial \phi} + \epsilon (\operatorname{div} \nabla \phi) \right] \dot{\phi}}_{\text{Bulk contributions}} - \underbrace{\int_{\partial \Omega_0} \left[\epsilon \nabla \phi \cdot \mathbf{N} - t \frac{\partial \dot{W}}{\partial \phi} + \epsilon_S \operatorname{div}_S \nabla_S \phi \right] \dot{\phi}}_{\text{Surface contributions}} \quad (3.10.4)$$

We use the bulk and boundary balance laws to replace $\dot{\phi}$ by $|\nabla \phi| v_n^\phi$ and $|\nabla \phi| v_e^\phi$ to obtain the thermodynamic conjugates to v_n^ϕ and v_e^ϕ as the bulk and edge driving forces:

$$f_{bulk} := - \frac{\partial \dot{W}}{\partial \phi} + \epsilon \operatorname{div} \nabla \phi, \quad f_{edge} := -t \frac{\partial \dot{W}}{\partial \phi} + \epsilon_S \operatorname{div}_S \nabla_S \phi - \epsilon \nabla \phi \cdot \mathbf{N} \quad (3.10.5)$$

The expression for f_{edge} has some similarities to the sharp-interface version [SB98], in much the same way as f_{bulk} has similarities to the classical driving force on an interface.

We have ignored the source G^e above, but it provides a natural avenue to control nucleation of new interfaces on the boundary.

3.10.2 Faceting of a Flat Stressed Interface

We consider the energy in Section 3.3 using the unrotated specimen. As noted there, the stress-free compatible twin interfaces are oriented at $\pm\pi/4$. Here, we begin with an interface oriented vertically, and examine the evolution driven by the stress field. As expected, the interface facets to locally align along the stress-free compatible directions. However, we examine the effect of two contrasting choices of the boundary kinetics: (1) linear boundary kinetics that matches the linear bulk kinetics, and (2) pinned on the boundary with linear bulk kinetics. We fix the left face of the specimen, and leave the other faces traction-free.

Fig. 3.11 shows the initial condition for both cases, and the final equilibrium state. An interesting result when the interface is pinned on the boundary is that the orientation of the interface at the boundary is exactly the opposite of the interface orientation in the bulk. Experimental probes of microstructure at the surface could completely mis-estimate the bulk microstructure.

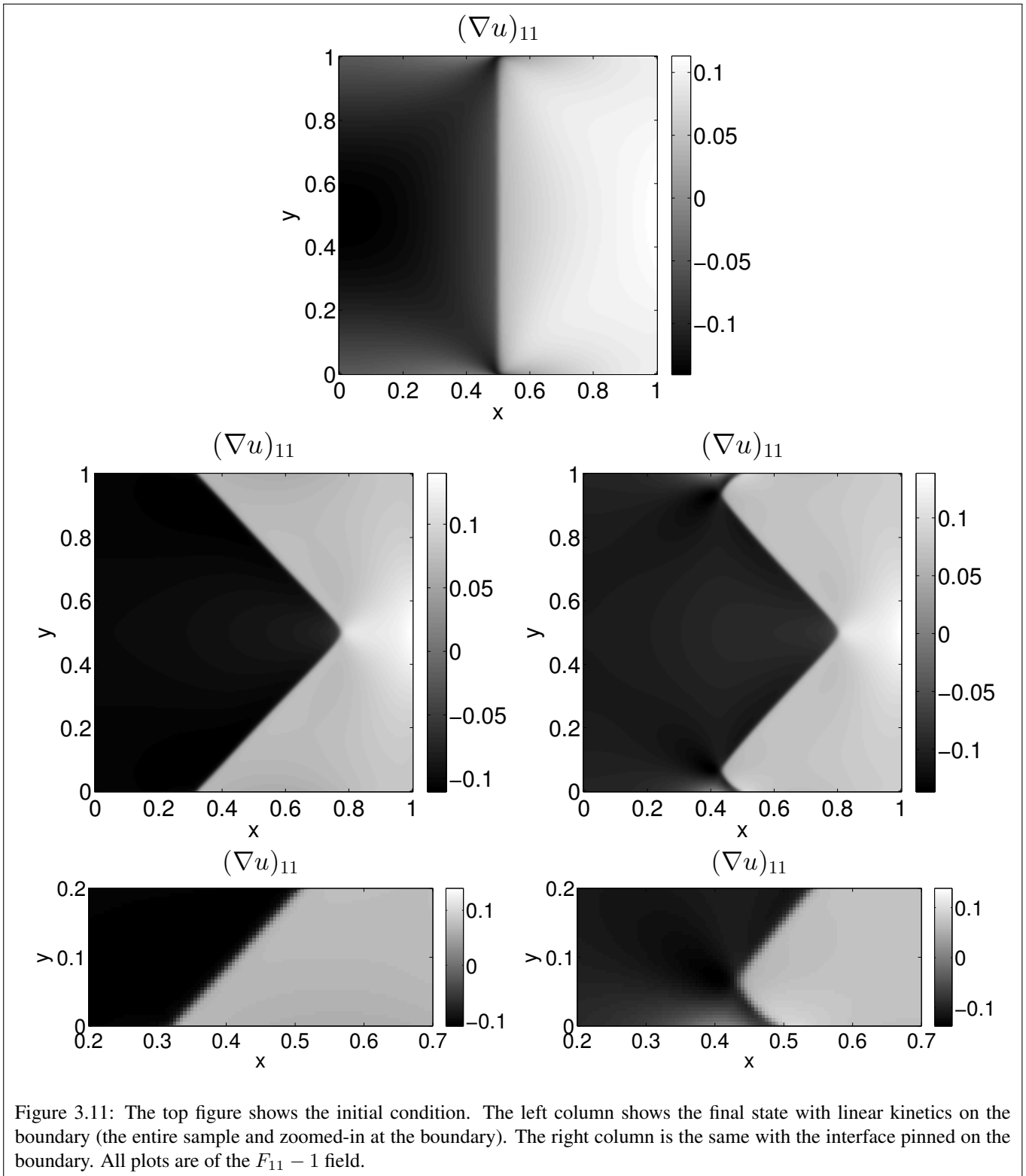


Figure 3.11: The top figure shows the initial condition. The left column shows the final state with linear kinetics on the boundary (the entire sample and zoomed-in at the boundary). The right column is the same with the interface pinned on the boundary. All plots are of the $F_{11} - 1$ field.

3.10.3 Competition Between Bulk and Boundary Kinetics

We compare the evolution of a stress-free compatible interface for 3 different cases: when the boundary kinetics is (i) slower, (ii) the same, and (iii) faster, than the bulk kinetics. For both bulk and boundary kinetics, we use a linear dependence on driving force, and change only the leading coefficient multiplying them. The ratios of the coefficients are 0.4 (boundary slower than bulk), 1.0 (boundary and bulk are the same), and 1.6 (boundary faster than bulk).

We use the material described in Section 3.3 with the rotated specimen. The initial configuration with the stress-free compatible interface for all 3 cases is the same and shown in Fig. 3.12. A constant tensile load is applied at the right face of the domain, and this causes the interface to begin to move. The top and bottom faces are traction-free, and the left end is clamped. The results from the 3 cases are shown in Fig. 3.12.

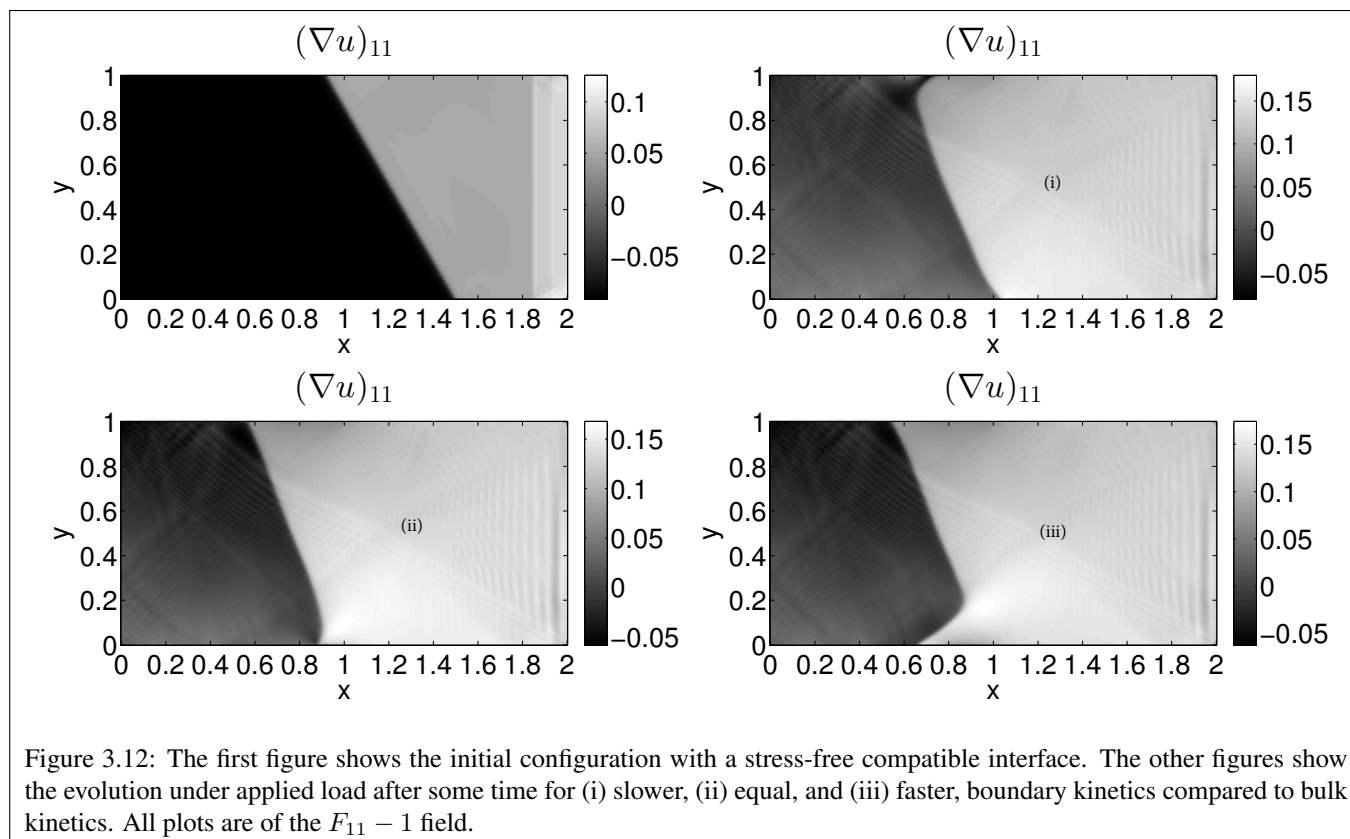


Figure 3.12: The first figure shows the initial configuration with a stress-free compatible interface. The other figures show the evolution under applied load after some time for (i) slower, (ii) equal, and (iii) faster, boundary kinetics compared to bulk kinetics. All plots are of the $F_{11} - 1$ field.

3.10.4 A Singularity In Boundary Kinetics

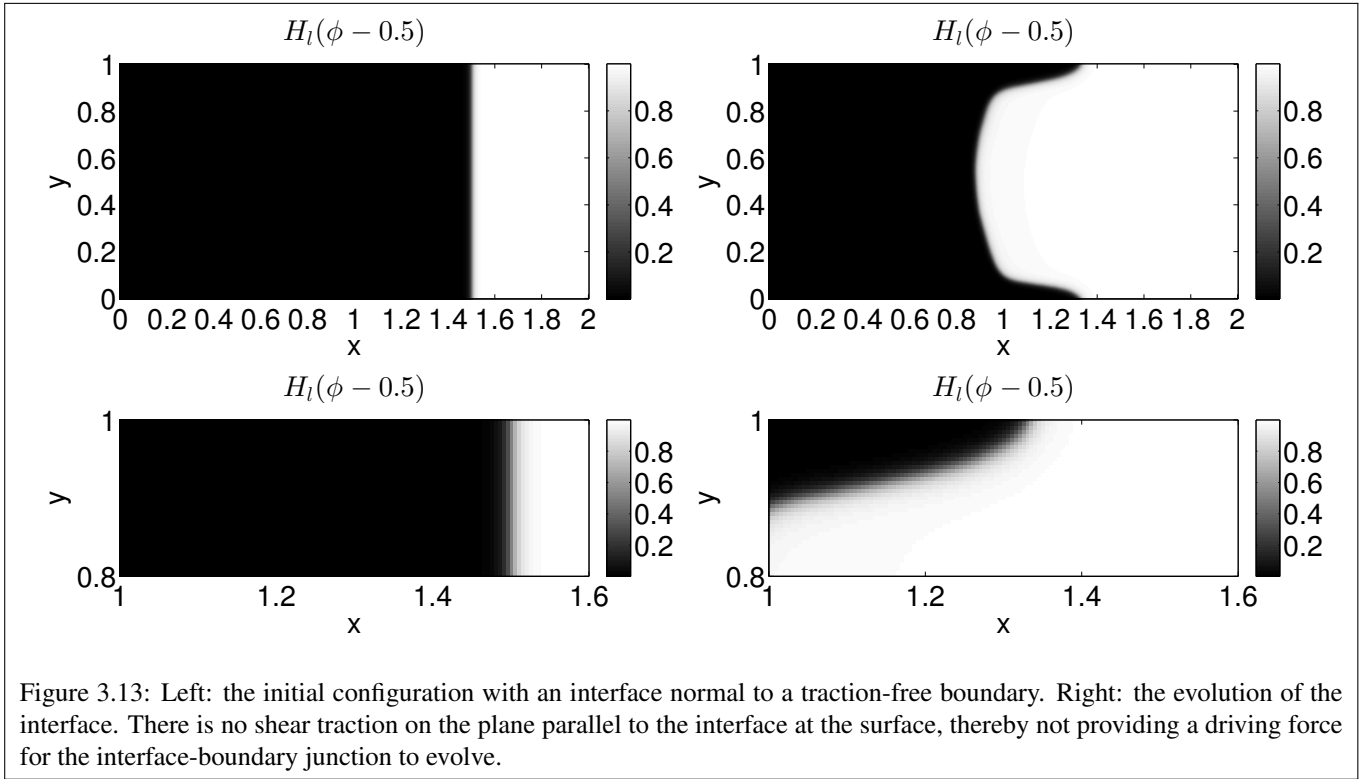
The simplest boundary kinetic relation is to assume that the edge velocity field v_e^ϕ is a function of only the driving force f_{edge} . However, we discuss here a simple but realistic example where this can lead to unexpected and likely-unphysical results.

Consider the energy in Section 3.3 for twinning, but with the specimen oriented such that the stress-free twin interface is vertical. The interface is normal to the boundary on the top and bottom faces which are traction-free. We apply a shear force on the right face while the left face is held fixed.

These phases in this problem are related by a shear, and hence the driving force for transformation is directly proportional to the shear traction on the plane that is parallel to the interface. Therefore, a simple choice of linear kinetics – in the bulk as well as on the boundary – will set the interface velocity roughly proportional to the local value of the shear traction on the interface.

However, the top and bottom faces of the domain are traction-free; therefore, the shear stresses along the interface at the top and bottom faces are 0. The boundary driving force then largely vanishes, except for a small contribution due to the regularization parameters ϵ and ϵ_S . Fig. 3.13 shows the time evolution of the interface in the vicinity of the boundary. We find the unexpected development of an extremely curved interface as the interface in the interior moves forward while the interface-boundary junction barely moves. The presence of ϵ and ϵ_S prevent this extremely curved interface from becoming completely singular. With this regularization, the interface moves slowly along the boundary as the large curvature leads to contributions from the higher-order derivatives.

While this regularization keeps the problem from becoming singular, it does not seem physically attractive for the evolution to be dominated by ad-hoc regularization terms. An approach that may perhaps provide more physically-meaningful evolution is to set the boundary kinetics based on $\nabla\phi \cdot \mathbf{N}$; recall that the typical boundary condition in standard phase-field methods is $\nabla\phi \cdot \mathbf{N} = 0$. However, as pointed out previously, this will drive the interface to be normal to the boundary in the vicinity of the boundary.



3.11 Discussion

We have presented the 2D characterization of a phase-field model – formulated in the companion paper – that has non-singular interfaces yet allows for transparent prescription of kinetics and nucleation of interfaces. A number of examples displaying complex kinetics and nucleation are seen to be easily and transparently attacked by our approach. We have also extended the phase-field framework to allow for the prescription of an independent kinetics for the junction line between an interface and a material surface.

Our formulation allows us to prescribe both kinetics and nucleation independently. From various numerical calculations, we find that microstructure patterns and mechanical response can be very sensitive to the kinetics, particularly for stick-slip and anisotropic kinetics. Both stick-slip and anisotropic kinetics are key elements in many physical situations of interest. Standard phase-field does not handle stick-slip well when it is imposed by simply stopping the evolution when the driving force is below some critical value [LLP10], but it is unclear if this difficulty is due to the energy structure or the evolution law. Non-monotone kinetic relations, however, were found not to provide any complex behavior.

We find that nucleation plays an extremely significant role in the development of microstructure patterns

and mechanical response. We have presented a number of examples to show the transparent and easy prescription of complex nucleation rules in our formulation. These nucleation rules can involve various components of stress and strain, their rates, nonlocal quantities, and so on. We emphasize that the nucleation criteria that we have used are toy models to enable the demonstration that we can readily and transparently incorporate an extremely broad range of nucleation criteria. In addition to enabling calibration to experiment or atomic calculations, this capability enables us to systematically probe the roles of different physical mechanisms for nucleation. Recently, [BT10, WBT10] presented a first-principles-motivated statistical model of twin nucleation in HCP materials. While we have only examined deterministic nucleation in this work, it is straightforward to replace the deterministic source term in our evolution law by a statistical object that incorporates the insights from [BT10, WBT10].

An important work with an alternative approach to the goal of numerical simulations of interface kinetics and nucleation is [HRL99]. They use a level-set like approach but with a careful approach to regularization that aims to preserve the sharp-interface kinetics. While there are many similarities between our work and theirs, there are also some key differences. In our approach, we aim to formulate a model with certain key features such as regularized interfaces and the ability to prescribe nucleation and kinetics. Their approach, however, is to develop a careful and sophisticated numerical method that reproduces the sharp-interface model. A further difference appears to be the relative ease of numerical implementation of our model compared to that approach, but this could change.

Phase-field methods have largely been restricted to linear elastic models. This has the advantage that the elastic problem has nice properties such as existence, uniqueness etc. While we have used a nonlinear deformation model in some of our calculations, it is convex (and quadratic) in the nonlinear strain for a fixed value of ϕ ; we note that convexity in the nonlinear strain measure chosen here does not guarantee these nice properties [Cia88]. Other recent phase-field models with large-deformation elasticity include [PL13, CK11, Lev14].

Our extension to incorporate boundary kinetics provides an interesting contrast with standard phase-field models. In those models, the phase-field evolution has roughly the character of a diffusion equation if one considers the highest derivatives: $\dot{\phi} = F(\phi) + \text{div } \nabla \phi$ where $F(\phi)$ is the nonconvex term. Neumann boundary conditions are universally used for ϕ ; from (3.10.5), setting $t = 0, \epsilon_S = 0$ to recover the standard phase-field models, we can recognize that Neumann boundary conditions are a specific choice

of boundary kinetics that adapts the configuration instantaneously to always achieve zero driving force. Our use of boundary kinetics is roughly equivalent to time-dependent Dirichlet BCs, with the time-dependence being related to the fields in a complex and nonlinear fashion.

Chapter 4

Analysis of lamellar twins

4.1 Introduction

Twins often form needle like structures, for e.g. see figures 2 and 3 in [CMZ⁺06]. We discuss the reason behind formation of such structures.

Given two compatible 3D wells U_i and U_j , there exists exactly two solutions to the equation $QU_i - U_j = \mathbf{a} \otimes \mathbf{n}$. Consider a cube of this material which is uniformly in phase one and the second phase nucleates near the center of this cube at certain time. According to elasticity, incompatibly oriented part of the interface will have higher stresses than interfaces aligned along compatible directions. The inclusion of second phase may grow in all directions however, the incompatible directions will grow either faster or slower than the compatible directions because of the difference in the stress fields. We think, this asymmetry in stress fields might responsible for faster evolution of incompatible part of the interface resulting in formation of needle-like structures during twinning.

If one reduces the 3D problem into a 2D setting with two in-plane displacement components, i.e., either the plane-stress or plane-strain case, then that will put both the compatible directions in the 2D frame of view. Therefore in this setting there can be an inclusion of second phase completely embedded in first phase with compatible interface everywhere, which is never possible in 3D setting. The reason is while reducing 3D problem into 2D we assume that all fields are equilibrated in the third direction. Which is same as assuming the second phase inclusion extends throughout the thickness with the same cross-section. Now because the interface is compatible everywhere, in other words there is no region where the

inclusion of second phase is incompatible with the outer first phase, there will be no needle-like structure forming. The corners will still be incompatible and will have high stresses, but they cannot evolve rapidly because the resulting geometry of interface will be energetically even more expensive. We present a 2D calculation demonstrating this behaviour in 4.3.

The 3D problem can be reduced into a 2D setting with only one out-of-plane displacement component also, i.e., the antiplane setting. In this situation there can be at-most only one compatible direction in the frame of view. Hence, if there is a closed interface separating two phases then some part of it will not be compatible, thus breaking the symmetry and causing high stresses which might lead to needle-like structures. Similar problem was attempted by [HRL99] using level-set method and needle-like structures were seen. We attempt twinning in antiplane setting and study the effect of anisotropic kinetics in 4.4.1 and curvature dependent kinetics in 4.4.2.

4.2 Formulation

The detailed formulation is described in [AD15a]. Briefly, our starting point is to assume that the strain energy density $W(\mathbf{F})$, the kinetic relation for interfaces, and the nucleation behavior of interfaces, are well-characterized and available. Our approach then takes this information, and formulates a phase-field model that reproduces the elastic response and the kinetic and nucleation behaviour of interfaces. The governing equations of our model are as follows.

The energy density has the form:

$$\mathring{W}(\mathbf{E}, \phi) = (1 - H_l(\phi - 0.5)) \psi_1(\mathbf{E}) + (H_l(\phi - 0.5)) \psi_2(\mathbf{E}) \quad (4.2.1)$$

where H_l is a smooth function that resembles the Heaviside. The functions ψ_1 and ψ_2 have the form:

$$\psi_A(\mathbf{E}) = W(\mathbf{E}_A) + \underbrace{\boldsymbol{\sigma}_T}_{\equiv \frac{\partial W}{\partial \mathbf{E}} \Big|_{\mathbf{E}_A}} : (\mathbf{E} - \mathbf{E}_A) + \frac{1}{2} (\mathbf{E} - \mathbf{E}_A) : \underbrace{\mathbf{C}_T}_{\equiv \frac{\partial^2 W}{\partial \mathbf{E} \partial \mathbf{E}} \Big|_{\mathbf{E}_A}} : (\mathbf{E} - \mathbf{E}_A) \quad (4.2.2)$$

$\psi_A (A = 1, 2)$ approximates the behavior of W near the states \mathbf{E}_1 and \mathbf{E}_2 .

The total energy is then:

$$\int_{\Omega_0} \left(\dot{W} + \frac{1}{2} \epsilon |\nabla \phi|^2 \right) d\Omega_0 \quad (4.2.3)$$

The displacement field evolves through momentum balance:

$$\operatorname{div}_{\mathbf{x}_0} \left(\frac{\partial \dot{W}(\mathbf{F}, \phi)}{\partial \mathbf{F}} \right) = \rho_0 \ddot{\mathbf{x}}(\mathbf{x}_0, t) \quad (4.2.4)$$

In quasistatics, the inertial contribution is set to 0.

The phase field evolution is governed by the conservation law posed in the companion paper:

$$|\nabla \phi| v_n^\phi + G = \dot{\phi} \quad (4.2.5)$$

G is a constitutively-prescribed nucleation term, and v_n^ϕ is the interface velocity field – completely distinct from the material velocity field – through which the kinetic relation is prescribed.

For further details, we refer to the earlier paper [[AD15a](#)].

4.3 Twinning under plane-strain

Configuration is a 2D square plate of unit dimensions. It is fixed at left edge, top and bottom edges are traction free. Traction is applied on the right edge. Both the phases are isotropic and have same stiffness ($\mathbf{C}_1 = \mathbf{C}_2$). Kinetics is assumed to be linear and isotropic. Anisotropic kinetics can be obtained as $\hat{v} = \kappa |f| g(\hat{\nabla} \phi \cdot \mathbf{a})$ where, \mathbf{a} is some material direction and $g(\cdot)$ is a non-negative function. We do not attempt anisotropic kinetics in this setting because it is not intuitive or justifiable physically.

The wells for the two phase are chosen to be:

$$\mathbf{U}_1 = \begin{bmatrix} 1 & 0 \\ 0 & 1 \end{bmatrix}, \mathbf{U}_2 = \begin{bmatrix} 1 & 0 \\ 0.5 & 1 \end{bmatrix} \quad (4.3.1)$$

The compatible directions corresponding to these wells are:

$$\mathbf{n}_1 = \begin{pmatrix} 1 \\ 0 \end{pmatrix} \quad \mathbf{n}_2 = \begin{pmatrix} 0.24 \\ 0.97 \end{pmatrix} \quad (4.3.2)$$

These \mathbf{n} 's are the solution to the twinning equation $\mathbf{Q}\mathbf{U}_2 - \mathbf{U}_1 = \mathbf{a} \otimes \mathbf{n}$.

Nucleation criterion is chosen to be:

$$G = H_l(r - 0.1) \quad \text{if} \quad |\sigma_{12}| > 0.01 \quad (4.3.3)$$

where r is distance from $(0.75, 0.5)$.

The elasticity tensor is:

$$\lambda \mathbf{I} \otimes \mathbf{I} + 2\mu \mathcal{I}$$

For the calculations we chose $\lambda = 0$. If the above quadratic energy is used with large strains, stress can become unbounded at large but finite strain when $\lambda \neq 0$. Hence, the corners of the nucleated phase can cause numerical difficulties so we can avoid this by choosing $\lambda = 0$. This is equivalent to assuming Poisson's ratio = 0. Shear and tensile traction is applied on the right edge at $t = 0$ which sends an elastic wave towards the left. This wave cause nucleation and then the second phase evolves. Results are shown in Fig. 4.1.

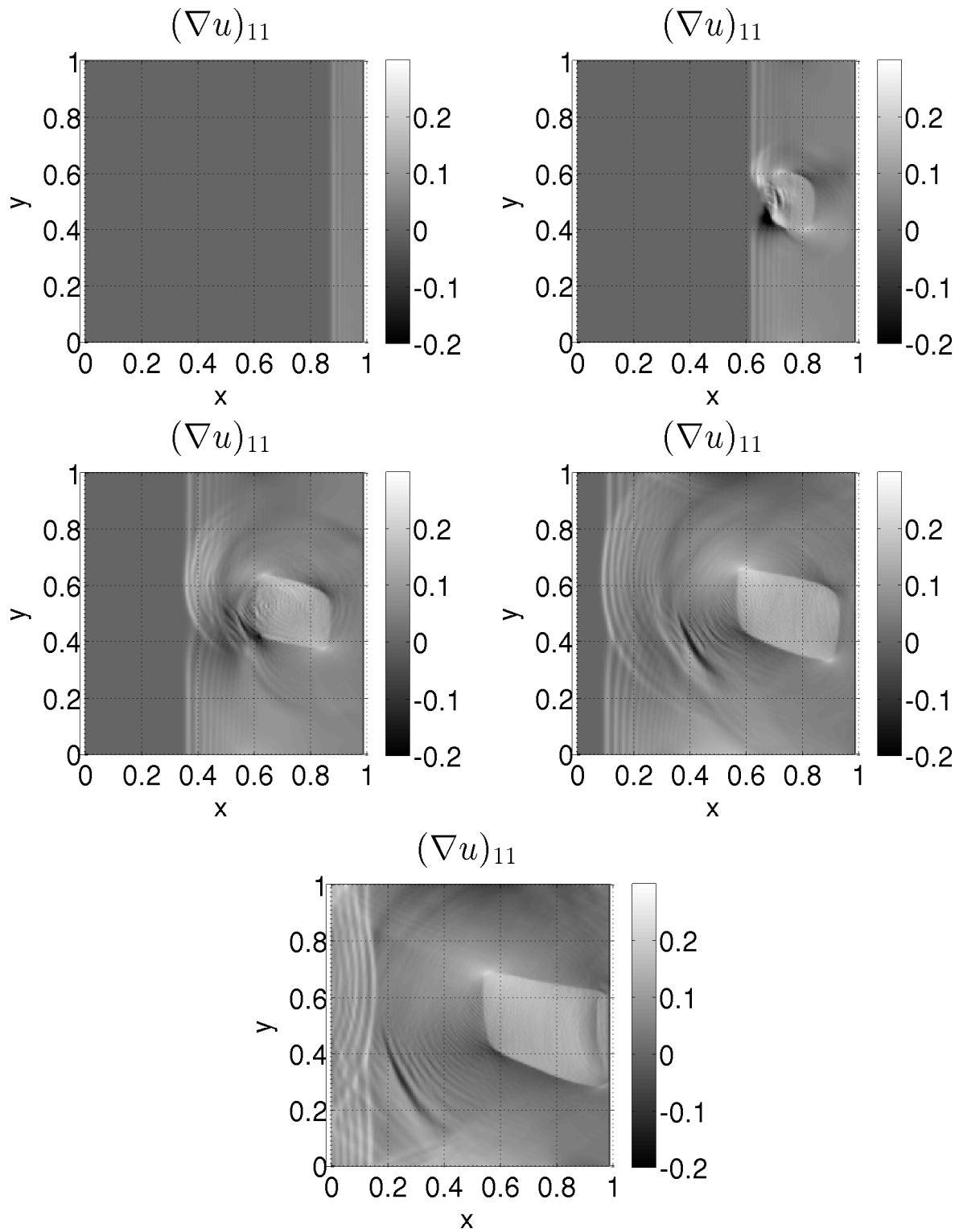


Figure 4.1: $(\nabla u)_{11}$ at different times ($t=1,3,5,7,9$). The compatible directions are e_2 .

From the results it is clear that no matter what the loading is, both the interfaces (interfaces parallel to n_1 and parallel to n_2) will experience similar order of driving force and therefore it is difficult to expect

needle-like structure in this setting. The driving force on the two interfaces might be slightly different but there is no reason why one would have significantly higher driving force than other unless some kind of asymmetry is explicitly modelled.

Anisotropic kinetics might be used to make one interface grow faster than other and might lead to needle like structure. But, there is no physical reason why one compatible interface should have kinetics different from the other compatible interface.

Also, note that the upper left corner looks more stressed than the bottom left one. The rotation, Q in the twinning equation is different for the two solutions. This rotation varies rapidly (in space) from Q_1 to Q_2 near the corners causing high stresses.

4.4 Twinning calculations in antiplane formulation

As described in [TR01], the incompatible direction should have more twinning dislocations than the compatible directions to accommodate deformation and hence the kinetics can be significantly different for twin motion along compatible and incompatible directions. In the calculations below we explore this possibility of formation of needle-like structures. We find that isotropic kinetics is not sufficient for these shapes. As explained earlier and in [TR01], because tip of the twin is expected to be different from the rest of the interface it is intuitive that kinetics of the tip is different from the rest so we test anisotropic kinetics and curvature dependent kinetics. We report that anisotropic results in formation of these type of structures but curvature dependence does not.

The configuration is 2D square plate of unit size. There is only one component displacement field which is in the out of plane direction, call it u . Strain is $\boldsymbol{\varepsilon} = \{u_{,1}, u_{,2}\}$. Energy for each phase near their respective wells is of the form:

$$W_i(\boldsymbol{\varepsilon}) = \frac{1}{2}\mu|\boldsymbol{\varepsilon} - \boldsymbol{\varepsilon}_{0i}|^2 \quad (4.4.1)$$

Note that this form of energy means that material is isotropic in antiplane setting. A more general form of energy which incorporates anisotropic elasticity might also be used however we perform all the calculations assuming isotropic elasticity, see [TR94] for a discussion. Elastic anisotropy might also be helpful in formation of these particular kind of structures because it might cause higher driving force for

the incompatibly oriented interface, but we do not explore that question here.

4.4.1 Isotropic and anisotropic kinetics

The two phases have wells at $\epsilon_{01} = \mathbf{0}$ and $\epsilon_{02} = \{0.0, 0.5\}$, which means the compatible direction is $\mathbf{n} = \mathbf{e}_2 = \{0, 1\}$. The plate has displacement boundary condition on all edges, $u = ky$, $k = 0.35$. A circular nucleation site is present at $(0.98, 0.5)$, its radius is ≈ 0.05 .

The forms of isotropic kinetics(4.4.2) and anisotropic kinetics (4.4.3) are below:

$$\hat{v} = \kappa|f| \tag{4.4.2}$$

$$\hat{v} = \kappa|f| \left(0.1 + \frac{|\nabla\phi \cdot \mathbf{a}|}{|\nabla\phi|} \right) \tag{4.4.3}$$

In the above (4.4.3), there are two terms in the brackets. The first term is isotropic because it does not have any dependence on $\nabla\hat{\phi}$ and the second term is the anisotropic part. There can be more sophisticated expressions to incorporate anisotropic kinetics but we choose this form for its simplicity. It models faster kinetics for the interface oriented along \mathbf{a} direction, thus making \mathbf{a} a preferred direction. In the calculations below the preferred direction is chosen to be perpendicular to the compatible direction, i.e., $\mathbf{a} = \mathbf{e}_1$. Fig.4.2 shows the difference between isotropic and anisotropic kinetics.

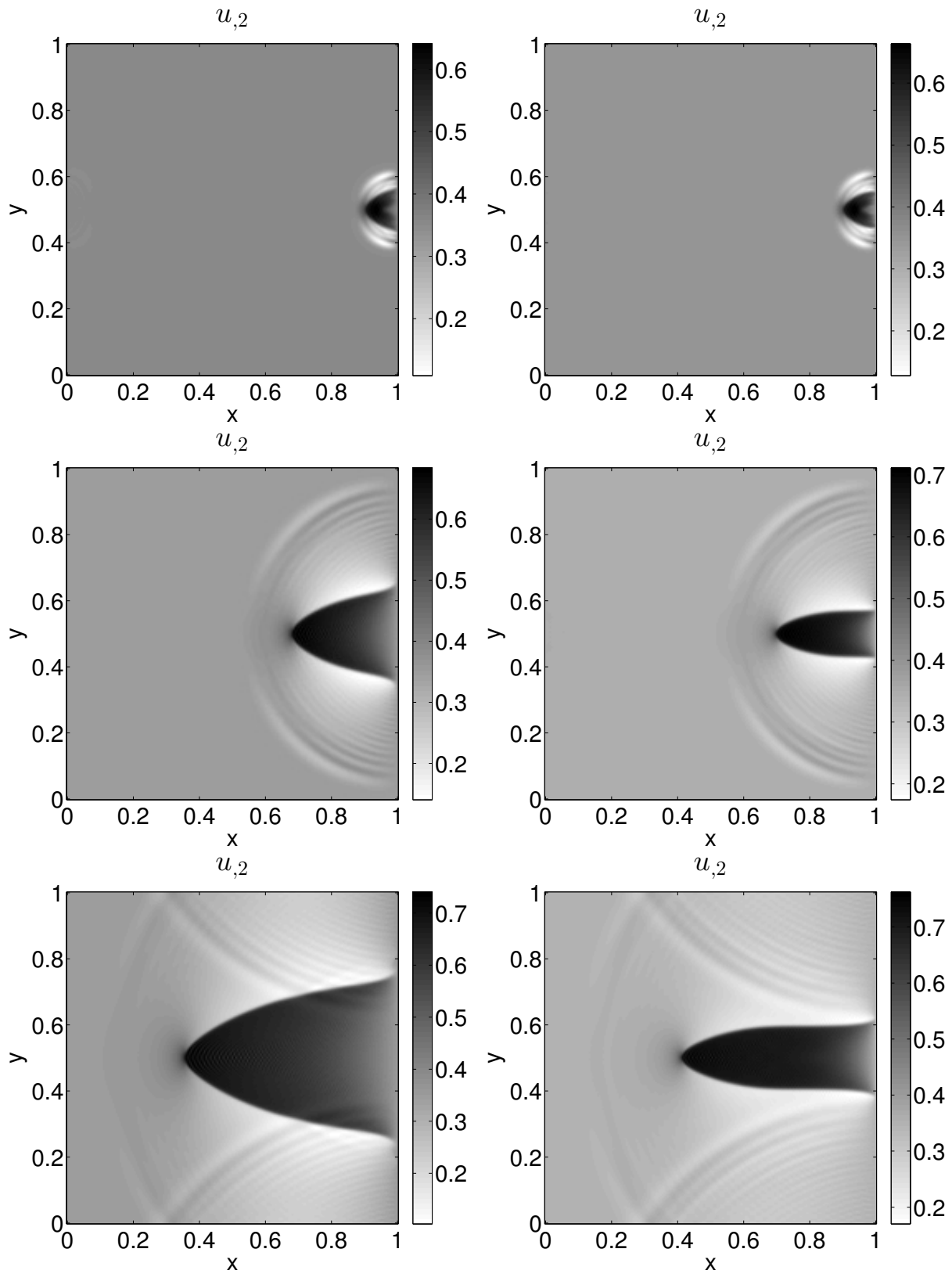


Figure 4.2: u_2 at different times ($t=1,5,10$). The compatible direction is e_2 . Left column corresponds to isotropic kinetics, right column corresponds to anisotropic kinetics: $\hat{v} = \kappa|f|(0.1 + |\nabla\phi \cdot e_1|/|\nabla\phi|)$

4.4.2 Curvature dependent kinetics

The configuration is same as in 4.4.1, i.e., a 2D square plate of unit size with displacement boundary condition on all edges, $u = ky$, $k = 0.35$. Nucleation site is at $(0.98, 0.5)$, its radius is ≈ 0.05 . The wells are at $\varepsilon_{01} = \mathbf{0}$ and $\varepsilon_{02} = \{0.0, 0.5\}$, which means the compatible direction is $\mathbf{n} = \mathbf{e}_2 = \{0, 1\}$. Calculations show the evolution when kinetics is curvature dependent.

Curvature dependent kinetic law :

$$\hat{v} = \kappa|f| \left(0.1 + \frac{|\nabla \mathbf{n}^T \cdot \mathbf{t}|}{50.0} \right) \quad (4.4.4)$$

where, \mathbf{n} is the normalized gradient of phase field, i.e., $\mathbf{n} = \nabla\phi/|\nabla\phi|$, and \mathbf{t} is the tangent to interface, orthogonal to \mathbf{n} .

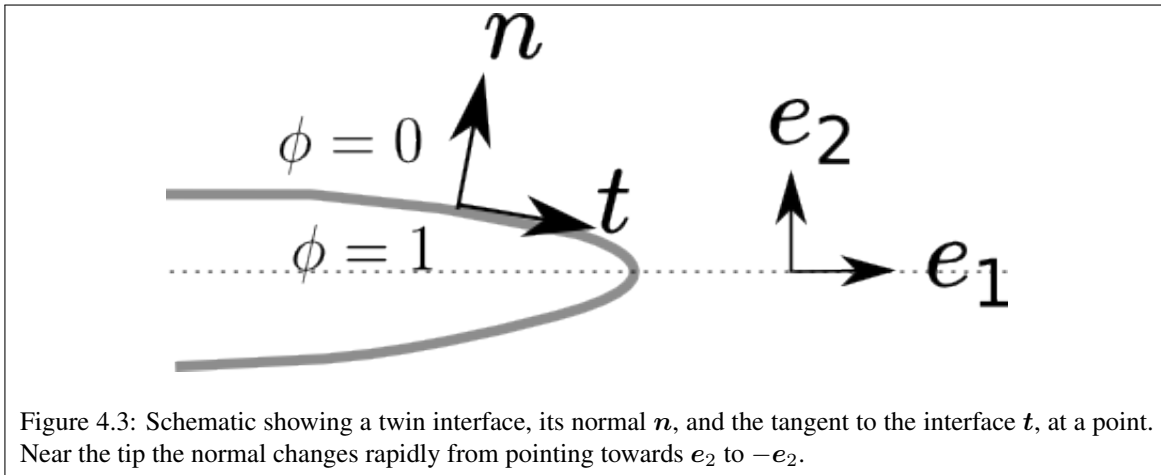


Figure 4.3: Schematic showing a twin interface, its normal \mathbf{n} , and the tangent to the interface \mathbf{t} , at a point. Near the tip the normal changes rapidly from pointing towards \mathbf{e}_2 to $-\mathbf{e}_2$.

The tip of the twin is the region of the interface where it bends or curves a lot, in other words the region where the normal to the interface varies rapidly. $\mathbf{n} = \hat{\nabla}\phi$ is the normal to the interface and therefore its gradient contains the information about the curvature but since it is a second order tensor we cannot use it directly. We need a scalar out of $\nabla \mathbf{n}$ which tells us the curvature. Intuitively the invariants of determinant or some other expression can be used as a measure of curvature. There are so many choices possible because we demand very little, i.e., an expression which becomes high when there sharp change in \mathbf{n} . Here we use $|\nabla \mathbf{n}^T \cdot \mathbf{t}|$ as the measure. Note that:

The reason for choosing $\nabla \mathbf{n}^T \cdot \mathbf{t}$, as a measure of curvature is as follows: For an arbitrary vector \mathbf{r} , $\nabla \mathbf{n}^T \cdot \mathbf{r}$ represents change in \mathbf{n} if we move along \mathbf{r} . An example of this is if $\mathbf{r} = \mathbf{n}$:

$$\begin{aligned}\mathbf{n} \cdot \mathbf{n} &= n_i n_i = 1 \\ \Rightarrow \nabla(\mathbf{n} \cdot \mathbf{n}) &= 2n_{i,j}n_i = \nabla \mathbf{n}^T \cdot \mathbf{n} = \mathbf{0}\end{aligned}$$

Which makes sense because \mathbf{n} does not change if we move along \mathbf{n} (only the magnitude of $\nabla\phi$ changes not the direction).

In 2D there is only one tangent corresponding to a normal but in 3D setting there will be a plane corresponding to a normal and therefore infinitely many \mathbf{t} vectors. In that situation one can use curvature defined in terms of invariants of curvature tensor.

Note that $|\nabla \mathbf{n}^T \cdot \mathbf{t}|$ is not a bounded function. So either we can use a function of the form $|\nabla \mathbf{n}^T \cdot \mathbf{t}|/(1 + |\nabla \mathbf{n}^T \cdot \mathbf{t}|)$ or, as in the above equation (4.4.4). We used isotropic/anisotropic kinetics calculations to see the value this term achieves at the tip of the needle structure and used that value to normalize the curvature term so that it reaches a maximum of 1.

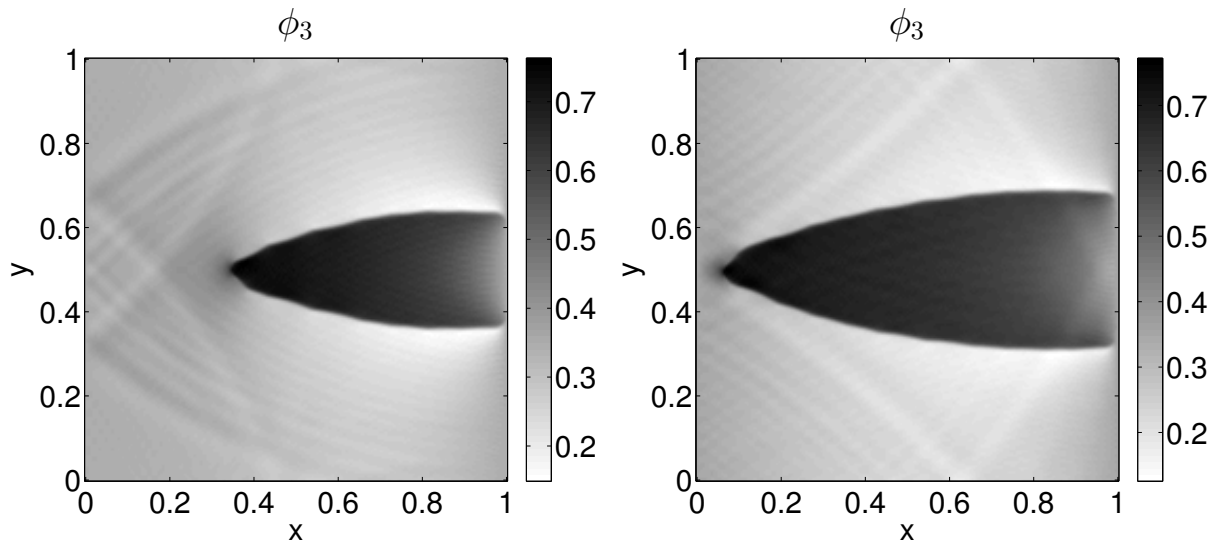


Figure 4.4: $\hat{v} = \kappa f\left(0.1 + \frac{|\nabla \mathbf{n}^T \cdot \mathbf{t}|}{50.0}\right)$. Figure showing u_2 at two different times during the evolution of twin. This form of curvature dependence does give needle like structure but the the phase interface is "wiggly".

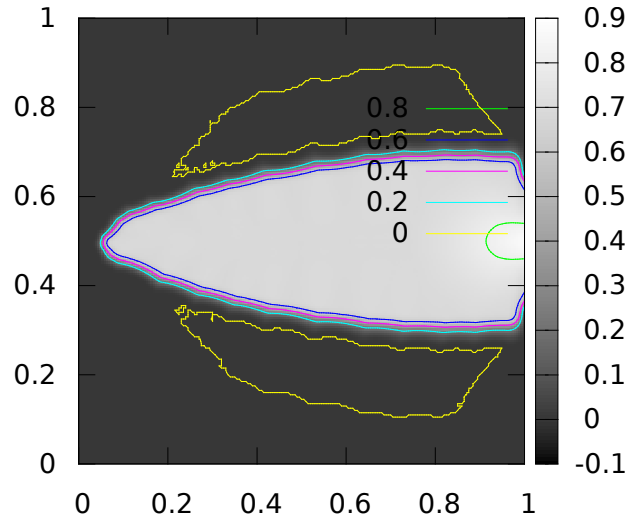


Figure 4.5: Same as the second picture in Fig.4.4 but with contour plots highlighting the wiggly interface.

Fig. 4.4 shows the results where the nucleated second phase evolves to form needle like structure however the tip and the interface are "wiggly". This feature is more clear in the plots of ϕ with contours in Fig.4.5. One could explain formation of the rugged features by saying that elasticity (or the initial and boundary conditions on u) wants the second phase to grow but kinetics can allow its growth only when the curvature is high. So, though this wiggled interface costs more elastic energy, together with the faster growth of second phase it becomes favourable.

4.5 Twin crossing grain boundary

Given a material with stored energy density $W(\mathbf{F})$, the strain energy density of a grain (rotated by orthogonal tensor \mathbf{R}) of this material will have a transformed strain energy density $\tilde{W}(\mathbf{F})$ related to $W(\mathbf{F})$ by the relation:

$$\tilde{W}(\mathbf{F}) = W(\mathbf{F}\mathbf{R}) \quad (4.5.1)$$

If the energy of a phase is $W(\mathbf{F}) = \frac{1}{2}(\mathbf{E} - \mathbf{E}_0) : \mathbf{C} : (\mathbf{E} - \mathbf{E}_0)$, energy of the rotated grain is:

$$\begin{aligned}
 \tilde{W}(\mathbf{F}) &= W(\mathbf{F}\mathbf{R}) \\
 &= \frac{1}{2}(\mathbf{R}^T \mathbf{E} \mathbf{R} - \mathbf{E}_0) : \mathbf{C} : (\mathbf{R}^T \mathbf{E} \mathbf{R} - \mathbf{E}_0) \\
 &= \frac{1}{2} \mathbf{R}^T (\mathbf{E} - \tilde{\mathbf{E}}_0) \mathbf{R} : \mathbf{C} : \mathbf{R}^T (\mathbf{E} - \tilde{\mathbf{E}}_0) \mathbf{R} \\
 &= \frac{1}{2} C_{ijkl} (\mathbf{R}^T (\mathbf{E} - \tilde{\mathbf{E}}_0) \mathbf{R})_{ij} (\mathbf{R}^T (\mathbf{E} - \tilde{\mathbf{E}}_0) \mathbf{R})_{kl} \\
 &= C_{ijkl} R_{mi} R_{nj} R_{pk} R_{ql} (E - \tilde{E}_0)_{mn} (E - \tilde{E}_0)_{pq}
 \end{aligned} \tag{4.5.2}$$

where, $\tilde{\mathbf{E}}_0 = \mathbf{R}\mathbf{E}_0\mathbf{R}^T$ represents the rotated eigenstrain or strain well for the phase. The transformed stiffness tensor has components $\tilde{C}_{mnpq} = C_{ijkl} R_{mi} R_{nj} R_{pk} R_{ql}$. To model grains one can either use the transformed stiffness tensor and eigenstrain, or just keep the same \mathbf{C} and \mathbf{E}_0 and use the transformed strain $\tilde{\mathbf{E}}$. Both the ways are equivalent as shown above in (4.5.2).

For our calculations we work in the antiplane setting for the earlier explained reasons. Further we assume the stiffness tensor \mathbf{C} to be isotropic. Although a single grain would hardly ever be isotropic we still assume they are for demonstration purposes. Eigenstrain is different for the original and the rotated grain which makes grains behave differently even though the stiffness tensor is isotropic.

A rotation of angle θ about an axis pointing out of plane of this paper can be written as:

$$\mathbf{R} = \begin{bmatrix} \cos\theta & \sin\theta & 0 \\ -\sin\theta & \cos\theta & 0 \\ 0 & 0 & 1 \end{bmatrix} \tag{4.5.3}$$

The out of plane small strain tensor under this rotation transforms as:

$$\tilde{\boldsymbol{\varepsilon}} = \{\gamma_1 \cos\theta - \gamma_2 \sin\theta, \gamma_2 \cos\theta + \gamma_1 \sin\theta\} \tag{4.5.4}$$

This can be obtained by computing $\tilde{\mathbf{E}} = \mathbf{R}^T \mathbf{E} \mathbf{R}$, considering only out-of-plane displacement and then linearising.

Therefore the energy for two grains is:

$$W_{g1}(\boldsymbol{\varepsilon}) = \frac{1}{2}\mu|\boldsymbol{\varepsilon} - \boldsymbol{\varepsilon}_1|^2 \quad (4.5.5)$$

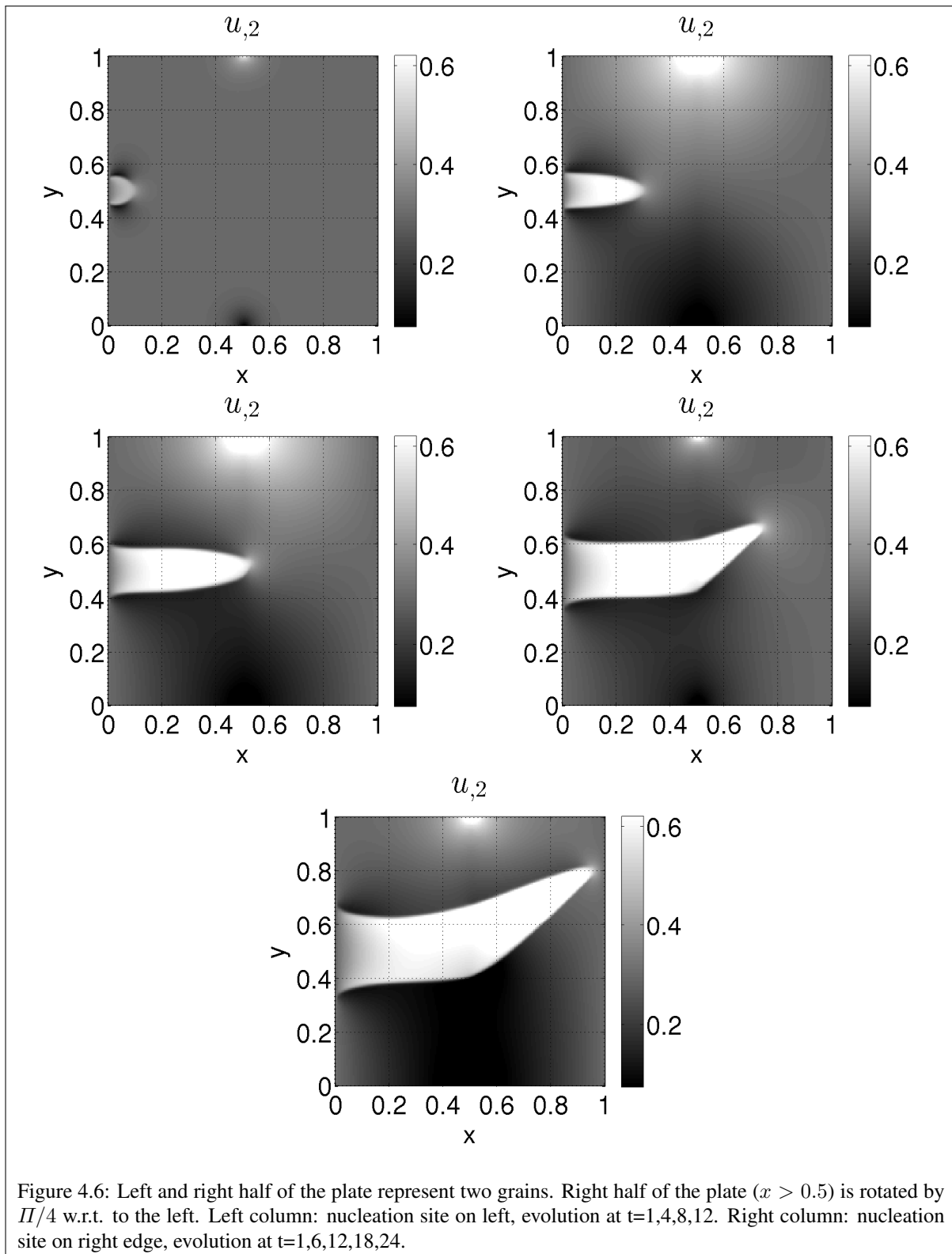
$$W_{g2}(\boldsymbol{\varepsilon}) = \frac{1}{2}\mu|\tilde{\boldsymbol{\varepsilon}} - \boldsymbol{\varepsilon}_1|^2 \quad (4.5.6)$$

Apart from energy, the kinetic law and nucleation criteria are also constitutive laws which will transform according to rotation \mathbf{R} . An isotropic kinetic law will have no effect. If the kinetic law is anisotropic then it must depend upon $\nabla\phi$, therefore $\hat{v} = \hat{v}(|f|, \nabla\phi)$. The transformed kinetic law can be obtained as:

$$\tilde{\hat{v}}(|f|, \nabla\phi) = \hat{v}(|f|, \mathbf{R}\nabla\phi) \quad (4.5.7)$$

Grain boundary is located at $x = 0.5$, the grains on the two sides differ by 45° . There is only one nucleation site at $(0.02, 0.5)$ of radius ≈ 0.05 which gets activated with any nonzero stress. We perform dynamic calculations with small amount of viscosity to suppress elastic waves reflecting from domain and grain boundaries. The purpose of this calculation is to show that the model can capture the proper shape of a growing twin therefore an exact nucleation criteria is not required.

Since the orientation of twinning direction or compatibility direction is a consequence of the strain wells, we expect that when the twin lamella crosses the grain boundary, it bends by 45° .



No nucleation at the grain boundary, the twin goes through the boundary and bends in the direction elasticity predicts.

Chapter 5

Extension of the model for n -phases

5.1 Introduction

We extend our phase-field method for the case when there can be three or more possible phases. For a problem involving just two phases, one phase parameter, ϕ is sufficient to identify the phase of the material point. For $n \geq 3$ possible phases, we need $(n - 1)$ phase parameters or n parameters with a constraint $\sum \phi_i = 1$. A total of ${}^n C_2$ kinds of interfaces are possible and in the most general situation each interface can have its own kinetics, completely independent of the other phases.

The problems with phase-field methods for the case of three or more phases is well known in the phase-field community (for e.g. see [LR15]). One common approach to impose the constraint on sum of phase fields is via Lagrange multiplier, however this has issues. For e.g. [SP99] discuss that treating each ϕ_i to be independent and using Lagrange formalism to impose the constraint mixes time scales of n -phase problem. They define interface fields $\Psi_{\alpha\beta} = \phi_\alpha - \phi_\beta$ and call this generalized coordinates in ${}^n C_2$ -dimensional space. Writing evolution law for generalized coordinates eliminates Lagrange multiplier from their formulation but we are not aware of any work reporting the problem couples with elasticity and its numerics. [BJM12] discuss that the Lagrange multiplier formulation does not reduce to the standard two-phase problem when $N = 2$ and also that it leads to growth of spurious extra phases. [LR15] do not impose the constraint using Lagrange multiplier instead they add energy penalty to avoid any three phases being simultaneously non-zero at a point. This resolves the problem of growth of spurious phases. However in this approach too, the evolution of ${}^n C_2$ kinds of interfaces is governed by $(n - 1)$ constitutive

laws and therefore the kinetics of a particular kind of interface depends upon all the $(n - 1)$ parameters in a non-transparent way.

The motivation and details of our model when there are only two phases is described in [AD15a]. Briefly, we defined $\nabla\phi$ to represent the only kind of interface possible between two phases. A geometric balance law for interfaces was formulated to obtain the evolution equation for ϕ . Finally we formulated the energy such that when phase parameter is away from the transition region the energy is independent of ϕ . This ensured that elasticity and phase-field were coupled just enough that the resulting driving force governed kinetics but did not cause unwanted nucleation.

For the problem with n phases, we define n phase-fields $\{\phi_i\}$ with $i = 1$ to n . A material point \mathbf{x} in i -th phase is represented as $\phi_i(\mathbf{x}) = 1, \phi_j(\mathbf{x}) = 0, \forall j \neq i$.

It is possible to write evolution equation for each ϕ_i the same way as we did for the the only phase field in the two-phase problem. This would require imposition of the constraint on sum of all phase fields using Lagrange multiplier in the energy. However, recall that the $\nabla\phi$ in our balance law physically represents an interface between two phases but in the case multiphase problem $\nabla\phi_i$ does not represent a particular interface. A nonzero $\nabla\phi_i$ only indicates an interface between i -th and any other phase. So, we define a function $f_{ij}(\phi_1, \phi_2, \dots, \phi_n)$ to represent an $i - j$ interface. Total possible kinds of interfaces is nC_2 so we introduce nC_2 such functions and write balance law for each kind of interface. Physically every kind of interface can have its own kinetics and nucleation criteria and this approach allows us to prescribe constitutive laws for each type of interface independently.

In the next section we formulate an energy which has the essential features necessary to keep the kinetic law or the kinetic term from causing any nucleation. In the original model in [AD15a], the energy we used did not enforce the phase fields to be either 0 or 1, rather it only kept ϕ away from 0.5. In the multiphase calculations, we found that it is important to drive all phase parameters to 0 or 1 otherwise there can be growth of unphysical phase configurations, i.e., three or more phase-fields being non-zero at the same point. We achieve this by adding a non-convex potentials for each ϕ_i in the energy functional.

5.2 Formulation for more than two phases: Energy and Balance law

If we want to study phases transformation with just two phases (or two energy wells) then just one variable ϕ is sufficient because $\phi = 0$ and $\phi = 1$ can describe the two phases. If there are three or more phases then we need more fields to represent all the phases/interfaces. If there are n possible phases then the total number of different types of interfaces possible is ${}^n C_2$.

5.2.1 Balance law

We define n phase field variables: $\phi_i(\mathbf{x})$ with $i = 1, 2, \dots, n$. At any point i -th phase is represented by $\phi_i = 1$ and $\phi_j = 0$ for $j \neq i$. For any i and j , $f_{ij} = \nabla(\phi_i - \phi_j)$ represents interface between i th and j th phases. f_{ij} will transition when ϕ_i and ϕ_j are transitioning, however it will also transition when there is an $i - k$ interface. The basic requirement for the function f_{ij} is that it transitions only when there is an $(i - j)$ interface, in other words $\nabla f_{ij} \neq 0$ iff there is an $(i - j)$ interface. One choice could be $\phi_i \nabla \phi_j - \phi_j \nabla \phi_i$, however there is no simple function whose gradient is this. Therefore, writing a balance law for such a function will make the evolution equation highly nonlinear in phase parameters therefore we choose the linear form for this paper. We use f_{ij} to represent interface and write balance law for each kind of interface. For e.g. if we have three possible phases then there can be three kinds of interfaces and the balance laws for them can be written as:

$$\overline{\dot{\phi}_1 - \phi_2} = \mathbf{v}_{12} \cdot (\nabla \phi_1 - \nabla \phi_2) + G_{12} \quad (5.2.1a)$$

$$\overline{\dot{\phi}_2 - \phi_3} = \mathbf{v}_{23} \cdot (\nabla \phi_2 - \nabla \phi_3) + G_{23} \quad (5.2.1b)$$

$$\overline{\dot{\phi}_3 - \phi_1} = \mathbf{v}_{31} \cdot (\nabla \phi_3 - \nabla \phi_1) + G_{31} \quad (5.2.1c)$$

Note that G_{12} represents nucleation of phase-1 in phase-2 as well as of nucleation of phase-2 in phase-1. v_{ij} represent the kinetic law for $i - j$ interface.

Using the above three equations (5.2.1) we want to find rate laws for ϕ_1 , ϕ_2 and ϕ_3 . However the system cannot be solved to find unique equations for $\dot{\phi}_1$, $\dot{\phi}_2$ and $\dot{\phi}_3$. Reason being they are not independent

equations, one can compute the determinant of the matrix of coefficients of $\dot{\phi}_i$'s as shown below to check that it comes out to be zero:

$$\begin{vmatrix} 1 & -1 & 0 \\ 0 & 1 & -1 \\ -1 & 0 & 1 \end{vmatrix} = 0 \quad (5.2.2)$$

This is expected because there is one more condition that needs to be imposed which ensures that only one of the ϕ 's is 1 at any point at any time. So we have:

$$\phi_1 + \phi_2 + \phi_3 = 1 \quad (5.2.3)$$

or,

$$\dot{\phi}_1 + \dot{\phi}_2 + \dot{\phi}_3 = 0 \quad (5.2.4)$$

Using equations (5.2.1) and (5.2.4), we can find rate laws for each of the ϕ_i s:

$$3\dot{\phi}_1 = \mathbf{v}_{12} \cdot (\nabla\phi_1 - \nabla\phi_2) - \mathbf{v}_{31} \cdot (\nabla\phi_3 - \nabla\phi_1) + G_{12} - G_{31} \quad (5.2.5a)$$

$$3\dot{\phi}_2 = \mathbf{v}_{23} \cdot (\nabla\phi_2 - \nabla\phi_3) - \mathbf{v}_{12} \cdot (\nabla\phi_1 - \nabla\phi_2) + G_{23} - G_{12} \quad (5.2.5b)$$

$$3\dot{\phi}_3 = \mathbf{v}_{31} \cdot (\nabla\phi_3 - \nabla\phi_1) - \mathbf{v}_{23} \cdot (\nabla\phi_2 - \nabla\phi_3) + G_{31} - G_{23} \quad (5.2.5c)$$

Also note that in both (5.2.1) and (5.2.5) $\mathbf{v}_{ij} \cdot (\nabla\phi_i - \nabla\phi_j)$ can be replaced by $v_{ij}|\nabla\phi_i - \nabla\phi_j|$.

Evolution law for $n = 4$ phases

$$4\dot{\phi}_1 = v_{12}|\nabla\phi_1 - \nabla\phi_2| + v_{13}|\nabla\phi_1 - \nabla\phi_3| + v_{14}|\nabla\phi_1 - \nabla\phi_4| + G_{12} + G_{13} + G_{14} \quad (5.2.6a)$$

$$4\dot{\phi}_2 = v_{21}|\nabla\phi_2 - \nabla\phi_1| + v_{23}|\nabla\phi_2 - \nabla\phi_3| + v_{24}|\nabla\phi_2 - \nabla\phi_4| + G_{21} + G_{23} + G_{24} \quad (5.2.6b)$$

$$4\dot{\phi}_3 = v_{31}|\nabla\phi_3 - \nabla\phi_1| + v_{32}|\nabla\phi_3 - \nabla\phi_2| + v_{34}|\nabla\phi_3 - \nabla\phi_4| + G_{31} + G_{32} + G_{34} \quad (5.2.6c)$$

$$4\dot{\phi}_4 = v_{41}|\nabla\phi_4 - \nabla\phi_1| + v_{42}|\nabla\phi_4 - \nabla\phi_2| + v_{43}|\nabla\phi_4 - \nabla\phi_3| + G_{41} + G_{42} + G_{43} \quad (5.2.6d)$$

Note that $v_{ij} = -v_{ji}$ and $G_{ij} = -G_{ji}$.

5.2.2 Energetics

Let the elastic energy of each phase is $\Psi_i(\mathbf{E})$, where \mathbf{E} is the strain tensor. Ignoring the diffusion term for now, we can write the energy of this multi-phase system to be:

$$\mathring{W}(\mathbf{E}, \phi_1, \phi_2, \phi_3) = H_l(\phi_1 - 0.5)\Psi_1(\mathbf{E}) + H_l(\phi_2 - 0.5)\Psi_2(\mathbf{E}) + H_l(\phi_3 - 0.5)\Psi_3(\mathbf{E}) \quad (5.2.7)$$

The diffusion term or the energy penalty which keeps ϕ_i to form sharp interfaces should be:

$$\frac{1}{2}\epsilon|\nabla\phi_1|^2 + \frac{1}{2}\epsilon|\nabla\phi_2|^2 + \frac{1}{2}\epsilon|\nabla\phi_3|^2 \quad (5.2.8)$$

Also note that if we write diffusion term to penalize the "interfaces", that too would give the same diffusion term:

$$\frac{1}{2}\epsilon|\nabla(\phi_1 - \phi_2)|^2 + \frac{1}{2}\epsilon|\nabla(\phi_2 - \phi_3)|^2 + \frac{1}{2}\epsilon|\nabla(\phi_3 - \phi_1)|^2 = \frac{1}{2}\epsilon \left(\sum_{i=1}^3 |\nabla\phi_i|^2 - \sum_{i \neq j} \nabla\phi_i \cdot \nabla\phi_j \right) \quad (5.2.9)$$

Using the fact $\sum \phi_i = 1 \Rightarrow \sum \nabla\phi_i = 0 \Rightarrow |\sum \nabla\phi_i|^2 = 0 \Rightarrow \sum_{i=1}^3 |\nabla\phi_i|^2 = -\sum_{i \neq j} \nabla\phi_i \cdot \nabla\phi_j$, we have

$$\frac{1}{2}\epsilon \left(\sum_{i=1}^3 |\nabla\phi_i|^2 - \sum_{i \neq j} \nabla\phi_i \cdot \nabla\phi_j \right) = \epsilon \sum_{i=1}^3 |\nabla\phi_i|^2 \quad (5.2.10)$$

which is same as (5.2.8).

In our earlier work on two phase systems there was no term in the energy to drive ϕ to zero or one. A transition region was characterized by ϕ near 0.5 and ϕ sufficiently above or below 0.5 characterized the two phases. Width of the transition region was dependent upon the small parameter l . This transition region did not affect the macroscopic response of model. However for the multiphase formulation there is need to drive all the ϕ_i 's to either one or zero because in between values might make irrelevant evolution systems active. Therefore we add a standard nonconvex term $W_{NC}(\phi_1, \phi_2, \phi_3) = \sum_{i=1}^3 \frac{1}{2} \phi_i^2 (1 - \phi_i)^2$ to the energy which drives all phase parameters to 0 or 1.

Now, dissipation is the difference between external work done and the rate of change of stored energy (Kinetic + elastic energy):

$$\begin{aligned}
 \mathcal{D} = \text{External working} - \frac{d}{dt} \left(\int_{\Omega_0} \left[\dot{W}(\mathbf{F}, \phi_1, \phi_2, \phi_3) + W_{NC}(\phi_1, \phi_2, \phi_3) + \frac{1}{2} \epsilon \sum_{I=1}^3 \frac{\partial \phi_I}{\partial x_i} \frac{\partial \phi_I}{\partial x_i} \right] d\Omega_0 \right. \\
 \left. + \frac{1}{2} \int_{\Omega_0} \rho_0 V_{0i} V_{0i} d\Omega_0 \right) \\
 = \int_{\Omega_0} \sum_{I=1}^3 \left(-\frac{\partial \dot{W}}{\partial \phi_I} - \frac{\partial W_{NC}}{\partial \phi_I} + \epsilon \nabla^2 \phi_I \right) \dot{\phi}_I \\
 = \int_{\Omega_0} \sum_{I=1}^3 t_I \dot{\phi}_I
 \end{aligned} \tag{5.2.11}$$

where, $t_I := -\frac{\partial \dot{W}}{\partial \phi_I} - \frac{\partial W_{NC}}{\partial \phi_I} + \epsilon \nabla^2 \phi_I$ for notational convenience.

Linear momentum balance was used in the first step in the above calculation just as it was in the case of dual phase system and we omit the details here. So the dissipation is (5.2.11) along with the condition (5.2.4). To find the work conjugate to interface velocities, we can either use the condition (5.2.4) to eliminate one of the three $\dot{\phi}_I$ in the above expression of dissipation and then substitute the remaining two from the rate laws in (5.2.5), or, since the rate laws (5.2.5) already satisfy the constraint (5.2.4), we can find the work conjugates by substituting all the three $\dot{\phi}_I$ directly in (5.2.11).

Ignoring the nucleation terms for the time being, we have:

$$\begin{aligned} \mathcal{D} = \int_{\Omega_0} & \left(t_1 \{v_{12} |\nabla \phi_1 - \nabla \phi_2| - v_{31} |\nabla \phi_3 - \nabla \phi_1|\} \right. \\ & + t_2 \{v_{23} |\nabla \phi_2 - \nabla \phi_3| - v_{12} |\nabla \phi_1 - \nabla \phi_2|\} \\ & \left. + t_3 \{v_{31} |\nabla \phi_3 - \nabla \phi_1| - v_{23} |\nabla \phi_2 - \nabla \phi_3|\} \right) \end{aligned} \quad (5.2.12)$$

or

$$\mathcal{D} = \int_{\Omega_0} \left(v_{12} |\nabla \phi_1 - \nabla \phi_2| (t_1 - t_2) + v_{23} |\nabla \phi_2 - \nabla \phi_3| (t_2 - t_3) + v_{31} |\nabla \phi_3 - \nabla \phi_1| (t_3 - t_1) \right) \quad (5.2.13)$$

5.2.3 Kinetic constraint

Unlike in the situation for only one type of interface, in the case of multiple types of interface, kinetic laws have another constraint apart from the one due to thermodynamics. Consider a 1-3 interface, the equations we are solving for ϕ_i 's are:

$$\begin{aligned} 3\dot{\phi}_1 &= v_{12} |\nabla \phi_1 - \nabla \phi_2| - v_{31} |\nabla \phi_3 - \nabla \phi_1| + G_{12} - G_{31} \\ 3\dot{\phi}_2 &= v_{23} |\nabla \phi_2 - \nabla \phi_3| - v_{12} |\nabla \phi_1 - \nabla \phi_2| + G_{23} - G_{12} \\ 3\dot{\phi}_3 &= v_{31} |\nabla \phi_3 - \nabla \phi_1| - v_{23} |\nabla \phi_2 - \nabla \phi_3| + G_{31} - G_{23} \end{aligned}$$

Because a 1-3 interface is evolving, ϕ_2 should not change at all, therefore $\dot{\phi}_2$ should be zero however this is not in-built in the formulation. Because of the choice of $f_{ij} = \phi_i - \phi_j$ in the above equation $\nabla(\phi_2 - \phi_3)$ is non-zero even when there is an interface between phase 1 and 3. This term will make $\dot{\phi}_2$ nonzero and might lead to spurious evolution of ϕ_2 .

We avoid this spurious growth by imposing a *kinetic constraint*. We define the kinetic law zero when there is no interface of that kind, i.e., $v_{ij} = 0$ if there is no $i - j$ interface:

$$v_{ij} = 0 \quad \text{if} \quad t_i < tol \text{ or } t_j < tol \quad (5.2.14)$$

In the above constraint we are basically using the driving forces, t_i and t_j , to "ensure" the existence of i - j interface.

Note: One can use $\nabla\phi_i$ instead of driving force but that wasn't working well numerically, reason is not clear. Briefly, isolated 1-2 and 2-3 interface were behaving properly but when a 1-2 interface approached a 2-3 interface, the ϕ fields evolved such that none of them crossed value of 0.5 in a region. This weird region kept increasing as the evolution progressed.

5.3 An example

We perform a calculation to demonstrate that the formulation leads to proper evolution of phase parameters and hence the interfaces. From the calculations it is also clear that when two kinds of interface coalesce, the phase in between the two interfaces disappears without any numerical issues.

The wells are:

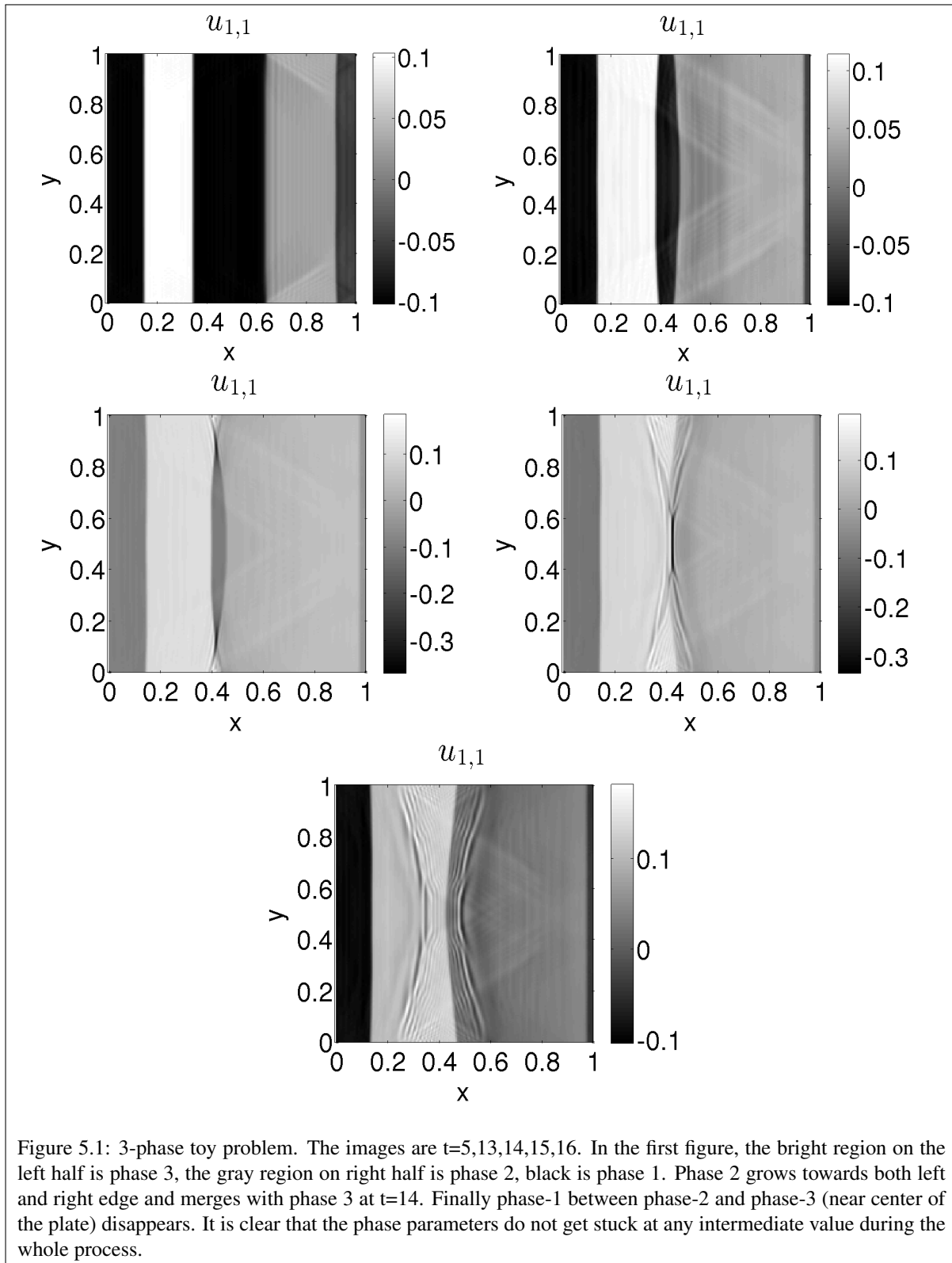
$$\mathbf{U}_1 = \begin{bmatrix} 0.9 & 0 \\ 0 & 1 \end{bmatrix}, \mathbf{U}_2 = \begin{bmatrix} 1 & 0 \\ 0 & 1 \end{bmatrix}, \mathbf{U}_3 = \begin{bmatrix} 1.1 & 0 \\ 0 & 1 \end{bmatrix} \quad (5.3.1)$$

These wells were chosen for simplicity and might not represent a physical material. They represent a square, a square with one side shortened, and a square with one side elongated respectively. They are compatible, which can be verified using Result 5.1 from [Bha03b], with the normal $\mathbf{n} = \pm\mathbf{e}_1$. Note that these are not shear related wells ,i.e., one cannot be obtained by a simple shear of the other, therefore they are not twins.

The specimen is a 2D square plate of unit size. As can be seen in the first image of Fig.5.1, the plate is in phase 1 everywhere except on a rectangular strip near $x = 0.25$ where it is in phase 3 and on a rectangular strip near $x = 0.75$ where it is in phase 2. Left edge is fixed, top and bottom edges are traction free. A constant tensile load is applied on right edge at $t = 0$ which sends an elastic wave travelling towards left. There are total four phase interfaces, starting from left edge we have (1 – 2) then (2 – 1) then (1 – 3) and then finally a (3 – 1) interface. This wave hits all the interfaces as it propagates and drives them. Since the wave is tensile both phase 2 and phase 3 surrounded by phase 1 grow in size, i.e., both the (2 – 1) interface and (1 – 3) move towards each other and eventually coalesce leaving just three interfaces as

shown in the last figure in Fig.5.1.

Linear kinetics was used for these calculations. The tolerance for (5.2.14) was 0.001.



5.4 Discussion

- We have extended our original dual phase model in [AD15a] to model three or more phases. The model retains its features, namely, straightforward prescription of kinetic law and nucleation criteria for each kind of interface.
- Different from standard phase-field method for n -phases because no use of lagrange multipliers in the energy which, though harmless in quasistatic problem, might affect the effective kinetics in the dynamic setting.
- We have not addressed junction kinetics. A triple point or junction with even more kinds of interfaces merging can have a kinetics of its own [SB98]. However we do not impose any such kinetics and the effective kinetics at any junction is the resultant of kinetics of individual interfaces. We lose the information about junction kinetics because throughout the derivation of the balance law we consider only the normal velocity. Tangential or in-plane component of velocity will not play any role in the evolution of interface only if the interface is either infinite or closed surface, however if the interface ends at a material boundary or at another phase interface then the tangential and normal velocity together define kinetics at the junction. This is a theoretical argument, I do not know if physically it is important or not.
- The value tol in the constraint for kinetic law in (5.2.14) is arbitrary and we do not know if it has anything to do with material properties, however it is necessary to avoid the spurious growth of phases. It might be possible to avoid this constraint on kinetic law if there is a function f_{ij} whose gradient is nonzero only when there as in $i - j$ interface. But that function should also be simple so that evolution equations for \dot{f}_{ij} can be simplified to give evolution equations for ϕ_i s. Further, the only other method to control spurious growth we know of is by [LR15] and they use potentials in the energy to penalize existence of three or more non-zero phase at any point, these potentials are also arbitrary.

Chapter 6

Fracture

6.1 Introduction

Solids develop cracks when subjected to high loads or even when subjected to smaller cyclic loads for very long duration. Crack in a solid can be thought of as a plane across which the bonds between the constituting atoms have broken creating two free surfaces. These two surfaces cannot interact elastically as the bulk of the material and can only interact via contact forces, such as one surface pressing upon the other resulting in compressive stress. The region where the two surfaces start separating (or joining) is mathematically sharp, i.e., normal to the surface changes very rapidly. We refer to this as crack tip. Sharp changes like these result in high stresses near crack tip promoting crack growth and causing material failure.

Cracks can be classified into two categories: Brittle fracture and ductile fracture. In the former situation solid is assumed to be either in elastic state or cracked state, i.e., just before failure the material is still elastic, and, if unloaded it would return to its original undeformed state. In the ductile fracture, the region near the tip may undergo plastic deformation. This work is concerned with phase field modelling of brittle fracture only.

The traditional approach to model brittle fracture at the continuum level was started by Griffith and developed by many including Irwin, Rice and Yoffe, see [Gri21, Irw57, RR68]. Essentially, apart from the standard elasticity, another energy \mathcal{G} is introduced which represents the surface energy of the crack. Crack propagates iff the energy release rate, i.e., the total change in elastic energy due to crack propagation is

equal to the surface energy consumed in forming the additional length/surface of the crack.

As the crack propagates new surfaces are generated. Ideally, one should impose boundary conditions on these surfaces (for e.g. traction free boundary). This boundary changes every time a crack grows hence it requires redefining the domain boundary and hence remeshing of the domain. See for e.g. [CO96, BGV09]. Just like as in the case of phase transformations, these evolving surfaces pose severe problems in solving elastodynamics. It requires tracking of the discontinuity surface and re-meshing which increases the computational cost significantly.

Phase-field methods introduce another field ϕ apart from material displacement \mathbf{u} . This scalar parameter, ϕ , can take any value between two values, say 0 and 1. The two values represent two phases of the material, i.e., in this case a cracked phase or an intact phase. Energy is constructed such that it drives ϕ towards one of the energy wells. Another term in the energy penalizes $\nabla\phi$ which resists formation of discontinuities, thus, the resulting fields are smooth. The interface or crack faces are characterized by rapidly varying but continuous $\phi(\mathbf{x})$. Thus this approach eliminates computational issues of tracking discontinuities. Some previous work on cracks using phase-field method are [BFM08, BVS⁺12, BLR11, KKL01]. Briefly, crack is modelled as a two phase material, one phase being the elastic material considered and the other a damaged material. Cracked region is typically modelled as a material of zero or negligible stiffness along with a constant surface energy. Elastodynamic or equilibrium equation is solved for displacement while the phase-field, which represents crack, evolves according to either a variational principle or gradient flow i.e., $\operatorname{argmin}_{\phi} E[\mathbf{u}, \phi]$ or $\dot{\phi} \propto -\frac{\partial U}{\partial \phi}$. The former criterion reflects Griffith's criterion for propagation. While the latter models crack propagation as a dissipative process, i.e., contrary to Griffith's criterion which is energy conserving, there is a decrease in the total energy (sum of elastic energy and surface energy of the crack). As explained earlier in [AD15a], the latter criterion does not reflect all the possible forms of kinetics and nucleation criteria.

We extend our earlier model [AD15a] for phase-transformations to model fracture. The formulation of the model is presented in Section 2. Existing approaches to approximate the response of the cracked region are either a zero-or-negligible stiffness response or a response based on eigen-decomposition of the strain tensor[MHW10]. We discuss the issues with these approaches and present a way to model the response of the cracked region by taking crack-face normal into account in Section 3. In section 4, we implement anisotropic kinetics and characterize its effect in both elastostatic and elastodynamic setting.

Note that anisotropy in crack propagation can also be modelled energetically, we discuss that approach in the beginning of section 4.

6.2 Formulation

Define a scalar field $\phi(\mathbf{x}, t)$. Let $\phi = 0$ represents completely cracked or damaged material and $\phi = 1$ represent undamaged material. Then a crack face can be represented as an interface between cracked ($\phi = 0$) and intact ($\phi = 1$) region. ϕ will transition from 0 to 1 rapidly at such inter-facial regions. The displacement is denoted by \mathbf{u} and small strain is $\boldsymbol{\varepsilon} = \frac{1}{2}(\nabla\mathbf{u} + \nabla\mathbf{u}^T)$.

For detailed motivation and feature of the energy and balance law, we refer to our earlier work [AD15a], [AD15b]. In the original paper $\nabla\phi$ represents an interface between two phases, here it represents interface between cracked and intact material, i.e., crack face. The governing equations of our model are as follows.

The energy density has the form:

$$\dot{W}(\boldsymbol{\varepsilon}, \phi) = (1 - H_l(\phi - 0.5)) \psi_1(\boldsymbol{\varepsilon}) + (H_l(\phi - 0.5)) \psi_2(\boldsymbol{\varepsilon}, \nabla\phi) \quad (6.2.1)$$

where H_l is a smooth function that resembles the Heaviside. The function ψ_1 and ψ_2 represent the elastic response of the undamaged material and cracked material respectively. For our purpose we assume linear elastic response for the undamaged material:

$$\psi_A(\boldsymbol{\varepsilon}) = \frac{1}{2} \boldsymbol{\varepsilon} : \mathbf{C} : \boldsymbol{\varepsilon} \quad (6.2.2)$$

The common approach to model the damage material is a zero or negligible stiffness material with a surface energy, see for e.g.[BFM08, BLR11]. This approach does not model a crack under compression well and an alternate based on eigen-decomposition of strain was suggested by [MWH10]. Later in section 6.5 we discuss this issue in detail but for now we use the negligible stiffness material to model mechanical response of crack. There are issues but for the simple situations of a pure mode-I or mode-II crack, this is a decent approximation.

$$\psi_2(\boldsymbol{\varepsilon}, \nabla\phi) = \eta \frac{1}{2} \boldsymbol{\varepsilon} : \mathbf{C} : \boldsymbol{\varepsilon} + \mathcal{G}_c \quad (6.2.3)$$

where, η is a small number to avoid numerical difficulties associated with elasticity with zero stiffness. \mathcal{G}_c is the surface energy of crack and is a constant.

The total energy is then:

$$\int_{\Omega_0} \left(\dot{W} + \frac{1}{2} \epsilon |\nabla \phi|^2 \right) d\Omega_0 \quad (6.2.4)$$

The displacement field evolves through momentum balance:

$$\text{div}_{\mathbf{x}_0} \left(\frac{\partial \dot{W}(\boldsymbol{\varepsilon}, \phi)}{\partial \boldsymbol{\varepsilon}} \right) = \rho_0 \ddot{\mathbf{x}}(\mathbf{x}_0, t) \quad (6.2.5)$$

In quasistatics, the inertial contribution is set to 0.

The phase field evolution is governed by the conservation law posed in [AD15a]:

$$|\nabla \phi| v_n^\phi + G = \dot{\phi} \quad (6.2.6)$$

G is a constitutively-prescribed nucleation term, and v_n^ϕ is the interface velocity field – completely distinct from the material velocity field – through which the kinetic relation is prescribed.

ϵ is the regularization constant which sets the width of the smeared interface (one face of crack) and \mathcal{G}_c is the surface energy of the crack. Dissipation $D = (\text{Rate of external work done}) - \frac{d}{dt} \int (U + K.E)$

$$D = - \int_{\Omega} \frac{\delta U}{\delta \phi} \dot{\phi} = - \int_{\Omega} \frac{\delta U}{\delta \phi} |\nabla \phi| v_n = \int_{\Omega} |\nabla \phi| f v_n \quad (6.2.7)$$

Where we have defined the driving force f to be :

$$f = - \frac{\delta U}{\delta \phi} \quad (6.2.8)$$

and to ensure non-negative dissipation we prescribe velocity as:

$$v_n(f) = \text{sign}(f) \hat{v}(|f|) \quad \text{where, } \hat{v}(|f|) > 0 \quad (6.2.9)$$

We want to solve linear momentum balance and evolution equation for ϕ .

$$\rho \mathbf{u}_{tt} = \nabla \cdot \{H_a(\phi - 0.5) \mathbf{C} : \boldsymbol{\varepsilon}\} \quad (6.2.10)$$

$$\dot{\phi}_t = |\text{grad } \phi| v_n(f) + G \quad (6.2.11)$$

We also need to impose a condition such that ϕ only decreases (to avoid "crack healing"), therefore we have:

$$\dot{\phi} \leq 0 \quad (6.2.12)$$

The two main differences of our model from other phase-field models is the evolution equation for ϕ and the form of stored energy density.

In the gradient flow approaches of phase field method, both kinetics of existing cracks and nucleation of new cracks is governed by the same term, while the balance law in the current model has two separate terms. One for interface velocity or kinetics, the other for nucleation of new cracks.

The energy of form (6.2.1) was shown, in [AD15a], to decouple nucleation from kinetics. This was a consequence of vanishing partial derivative of energy density w.r.t ϕ at wells as well as outside the transition region. i.e., $\frac{\partial \dot{W}}{\partial \phi} = 0$ for $\phi \in \mathbb{R} \setminus (0, 1)$. Since the kinetic law is always a function of driving force, if the material point corresponds to a well and there is no existing interface nearby then, the kinetic term is always zero hence no nucleation due to the kinetic term.

6.3 Mode-I calculations

We demonstrate mode-I crack propagation, branching and its analysis. Specimen is a 2D square plate of unit dimension with a notch at the bottom edge (see 6.1(a)). The plate is fixed at left end, the top and bottom edges are traction free and a constant load is applied at the right edge. Evolution of crack starts from a prestressed configuration, i.e., the initial displacement corresponds to the stress equilibrium solution of the plate with notch subjected to above boundary conditions. Linear kinetics proportional to driving force is used for the calculation. Elastic response is assumed to be isotropic ($\mathcal{C} = \lambda \mathbf{I} \otimes \mathbf{I} + \mu \mathcal{I}$, $\lambda = 1.0$, $\mu = 0.2$). No viscous damping was added in the material model. Figures 6.1 and 6.2 show the crack evolution, elastic waves emanating due to crack propagation and waves reflected from the domain

boundary.

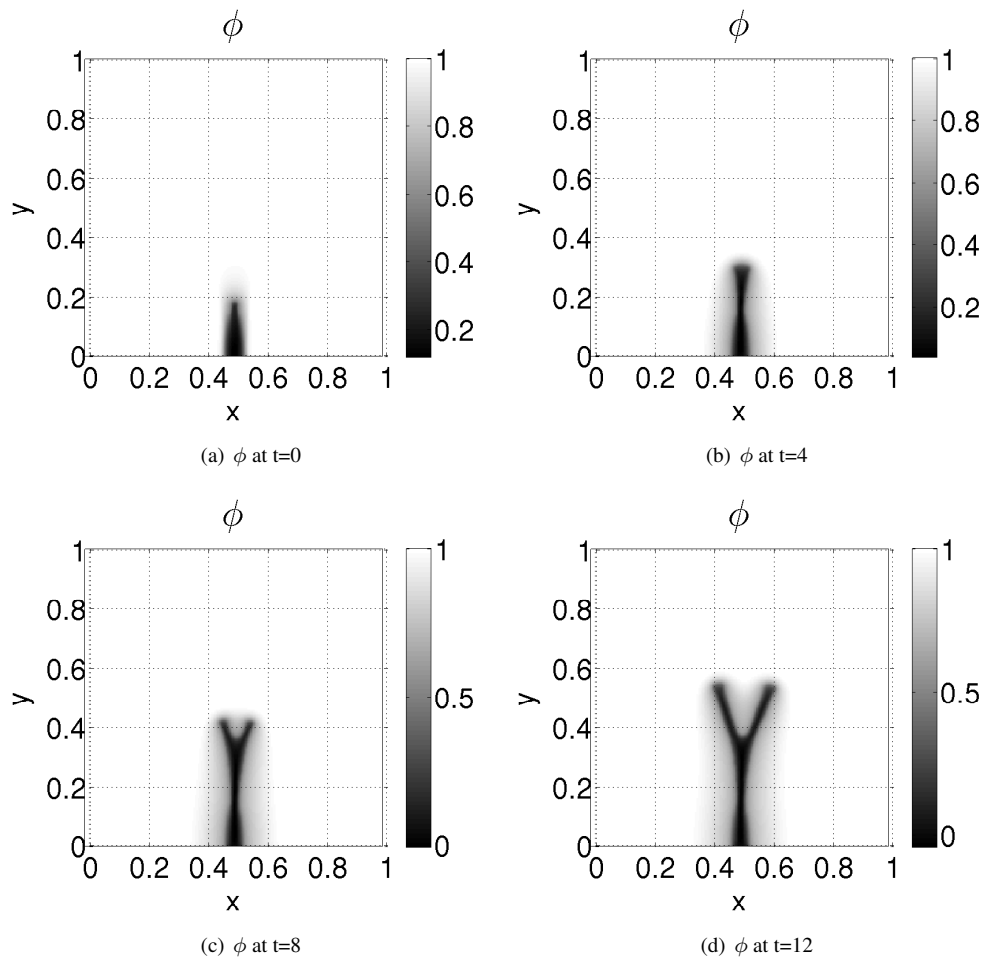


Figure 6.1: Isotropic kinetics: ϕ at different times

The above calculation also highlights an aspect of crack branching in phase-field models. In the phase-field setting, the crack has a length scale i.e., it has finite width which depends upon parameters in the energy such as diffusion coefficient, the small parameter in the smeared out Heaviside function, the elastic response of the material and as will be described later in 6.6, even on the crack speed. A consequence of this is that a stress wave may interact with the different parts of the tip at slightly different times. For e.g. imagine a wave travelling in $-y$ direction towards the crack tip as shown in the Fig.6.3. The wave will hit the head of the tip before the slopes of the crack tip. If the nature of the reflected wave is such that it tends to slow down the crack (for e.g. compressive load) then the sides of the crack tip will grow but the head will not (or grow slower than sides) during that slight time difference. The resulting shape of the tip

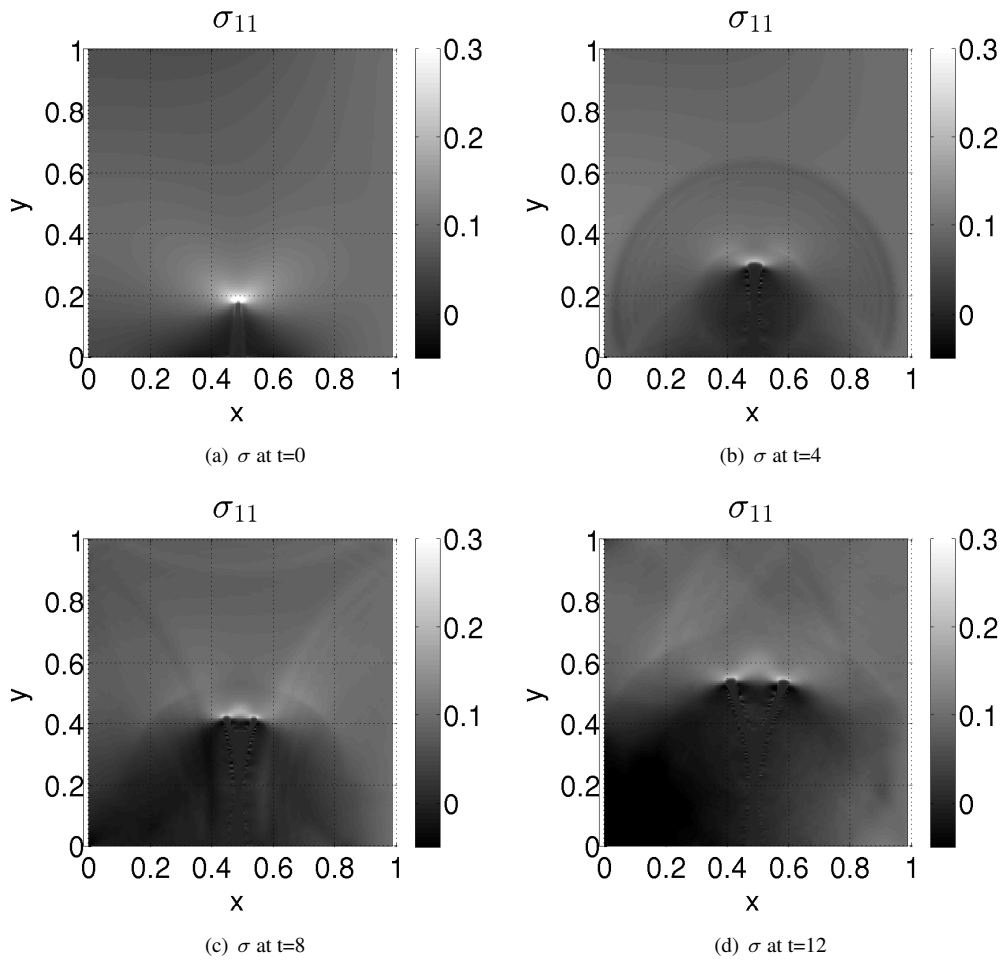


Figure 6.2: Isotropic kinetics: $|\sigma_{11}|$ at different times

will be a Y-shape or a branched crack.

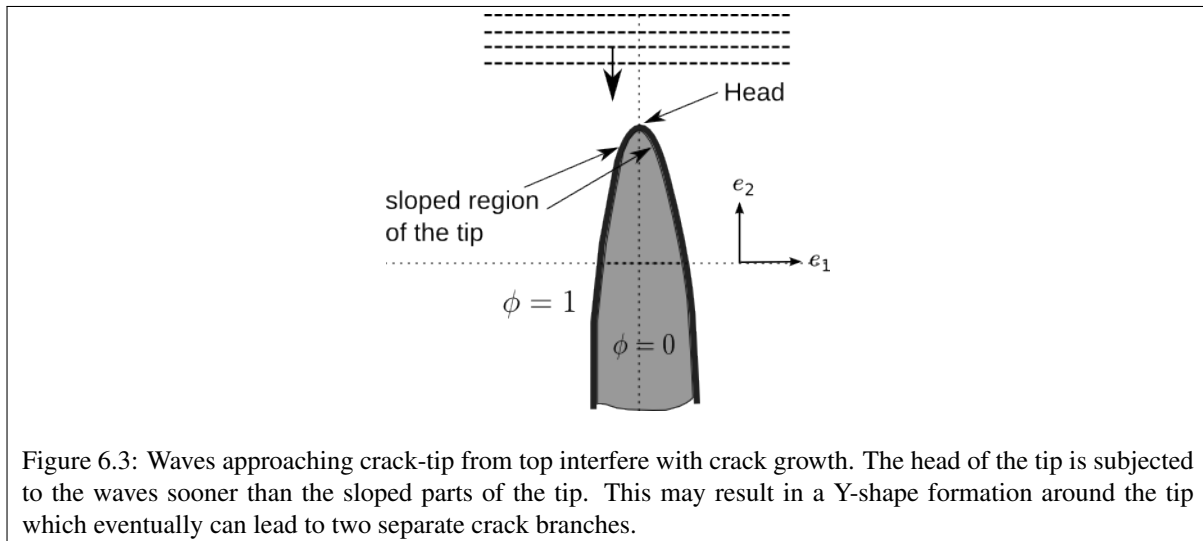


Figure 6.3: Waves approaching crack-tip from top interfere with crack growth. The head of the tip is subjected to the waves sooner than the sloped parts of the tip. This may result in a Y-shape formation around the tip which eventually can lead to two separate crack branches.

This effect can be seen in the above calculation (figure 6.2). Elastic waves emanating due to crack growth get reflected from the domain boundary and interfere with crack growth. The wave reflected from the bottom edge is the first among all the reflected waves to reach the crack tip. Branching seems (visually inspected) to start $t = 5$ which approximately coincides with the time the wave reflected from bottom edge reaches the crack tip (can also be computed using λ and μ).

6.4 Anisotropic Kinetics

Anisotropy in crack growth is important. One way to model is by making the energy anisotropic as in [LPM⁺15]. This approach requires addition of second order derivative of ϕ in the energy and incorporates anisotropy in surface energy via a fourth order tensor. It allows to model strong anisotropy however the possible form of anisotropy is restricted to what can be represented by a fourth order tensor. Further, higher order derivatives require smoother shape functions for numerical implementation. We suggest a simple way to model anisotropy in the crack propagation via kinetic anisotropy rather than energetic one. The approach is more transparent as well as does not require smoother shape functions for numerics. Similar approach has been used in the context of crystal growth (grains) for e.g. see [US03]. Define:

$$\hat{v} = v(f, \hat{\nabla}\phi) \quad (6.4.1)$$

We present calculations to characterize the effect of above form of kinetic anisotropy in both elastostatic and elastodynamic settings.

6.4.1 Anisotropy + Elastostatics

The configuration is 2D plate fixed in y -direction on the left and right edges (traction free in x -direction). The bottom edge is subjected to traction such that $\mathbf{e}_1 \cdot \boldsymbol{\sigma} \cdot \mathbf{e}_2 = -\sigma_0$ if $x < 0.45$ and $\mathbf{e}_1 \cdot \boldsymbol{\sigma} \cdot \mathbf{e}_2 = \sigma_0$ if $x > 0.55$. The top edge and y -degree of freedom (y -dof) on the bottom edge are traction free BCs. Here we solve the evolution law for ϕ and linear momentum balance with material inertia, ρ , set to zero. Initially there is a small nucleus at $(0.5, 0)$. The above boundary conditions which are symmetric w.r.t. y -axis along with isotropic kinetics will result in crack growth parallel to y -axis (mode-I). In this section

we use an anisotropic kinetic law which is symmetric about y -axis:

$$\hat{v} = \kappa |f| \left(\sin(2\theta) + 0.001 \right) \quad (6.4.2)$$

where, $\theta = \cos^{-1}(\hat{\nabla}\phi \cdot \mathbf{e}_2)$.

Since the two preferred directions ($\mathbf{e}_1 \pm \mathbf{e}_2$) and loading are both symmetric w.r.t y -axis, the initial nucleus splits into two crack branches and they grow in the two directions symmetrically.

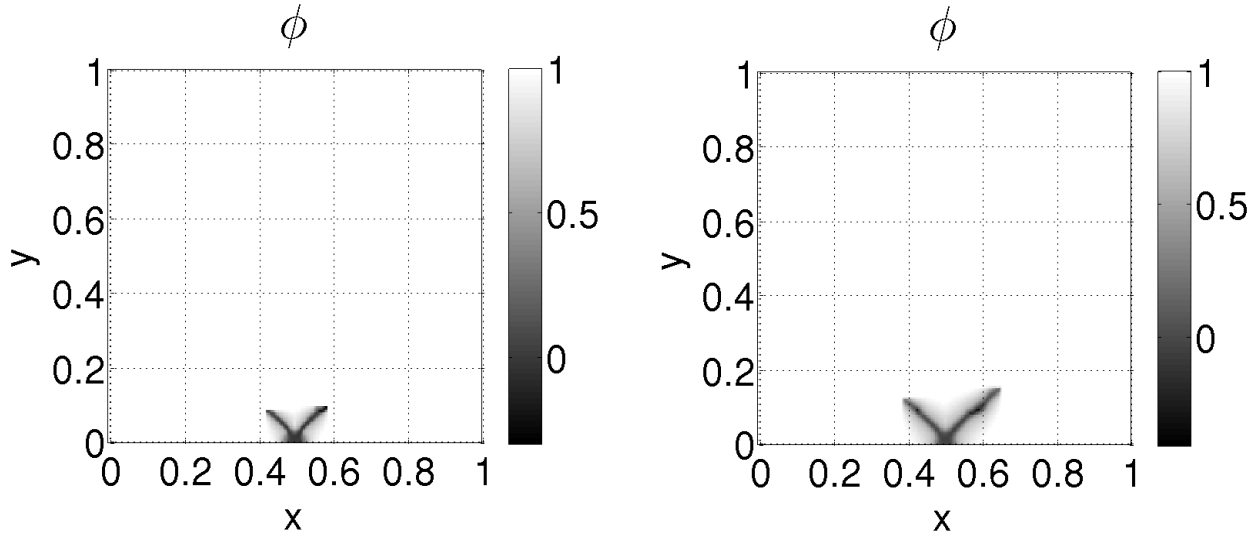


Figure 6.4: Elastostatics. Crack evolution at $t = 7$ and $t = 19$

6.4.2 Anisotropy + Elastodynamics

The configuration is 2D plate fixed in y -direction on the left and right edges (traction free in x -direction). The top edge is traction free and bottom edge is subjected to displacement boundary condition: $u(x) = -u_0$ if $x < 0.45$ and $u(x) = u_0$ if $x > 0.55$. This loading is symmetric w.r.t. y -axis or the initial axis of the crack and in the condition of isotropic kinetics will result in crack growth parallel to y -axis (mode-I). We solve linear momentum balance and evolution equation. The material is considered to be linear elastic and isotropic elastically. The kinetic law has the form:

$$\hat{v} = \kappa |f| \left(\underbrace{|\cos(2\theta - \pi/2)|}_{v_{aniso}} + \underbrace{0.001}_{v_{iso}} \right) \quad (6.4.3)$$

where, $\theta = \text{Cos}^{-1}(\nabla\hat{\phi} \cdot \mathbf{a})$ and \mathbf{a} = a unit vector at an angle of $\pi/12$ (clockwise) from y -axis. \mathbf{a} was not chosen to be y -axis so that we have anisotropy which is not symmetric w.r.t. y -axis. The function makes $\theta = \pi/4$ and $\theta = 3\pi/4$ the most preferred directions. The term, $v_{iso} = 0.001$ is a small constant term corresponding to isotropic component of kinetics. Since crack has rounded tip and the v_{aniso} will be zero for certain directions, the crack shape may become rough. So we keep this term to keep crack tip smooth and rounded however it might not be necessary.

A small amount of viscous damping was introduced in the linear momentum balance to reduce the effect of waves reflecting off the domain boundaries.

Initially there is a small nucleus at $(0.5, 0)$, the plots below (Fig. 6.6) show crack evolution at two different times. The crack branches soon after starting to evolve, the two branches point towards the direction which has faster kinetics. It can be seen that the branch towards left is thicker which has many smaller branches emanating from it towards the other preferred direction. Note that the left branch is more aligned towards y -axis than the right branch because of the choice of \mathbf{a} . Since the loading is such that driving force is highest for a crack parallel to y -axis, the left branch grows faster than the branches pointing towards right. As will be explained later in the section 6.6, the faster the crack the thicker it becomes in the dynamic setting. Hence, the left branch is thicker than the right branches.

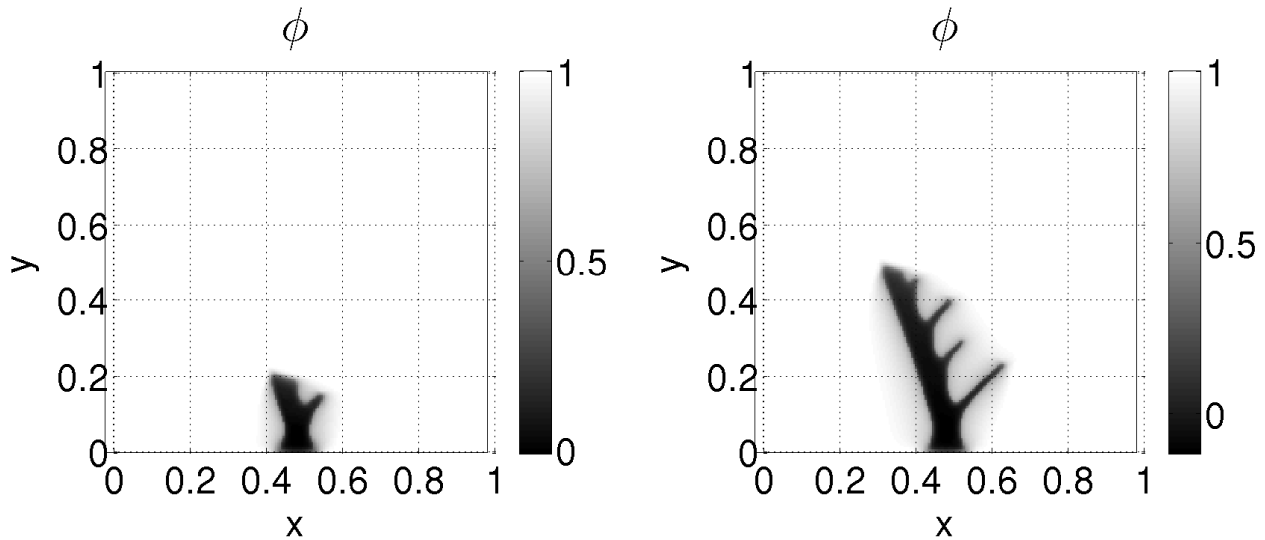


Figure 6.5: Damped elastodynamics. Crack evolution at $t = 15$ and $t = 35$

From the above two calculations it is clear that we can prescribe anisotropy via kinetics without any

difficulty and it results in desired response.

6.5 Modifying energy to account for crack-face compression

Energy density (6.2.3) and many of the existing phase-field models for cracks model cracked region as a material of zero or negligible stiffness. It is a reasonable approximation if only antiplane deformation is considered, i.e., mode-III crack for e.g. see [BLR11]. The model results in correct (w.r.t Griffith's theory) stress fields when the crack is subjected to tensile mode-I loading conditions. However, when the loading is compressive the model predicts stress fields just negative of the tensile loading conditions. While physically the crack should behave as an intact material under compression (mode-I compression) because of crack closure. Zero or negligible stiffness is like modelling the region as a void rather than broken/disconnected material which can come in contact under compression. Apart from the unphysical stress response, this effect can also cause crack growth under compression which is spurious.

There have been attempts, see [MHW10], to fix this by resolving the stored energy density of intact material into energy due to tensile strain and the remaining part of the strain. Then the elastic response of the cracked region is modelled as only the latter component rather than zero-stiffness response.

The decomposition is based on spectral decomposition of strain. Briefly, the symmetric small strain tensor is written as $\boldsymbol{\varepsilon} = \varepsilon_i \mathbf{e}_i \otimes \mathbf{e}_i = \langle \varepsilon_i \rangle_+ \mathbf{e}_i \otimes \mathbf{e}_i + \langle \varepsilon_i \rangle_- \mathbf{e}_i \otimes \mathbf{e}_i = \boldsymbol{\varepsilon}_+ + \boldsymbol{\varepsilon}_-$, where $\langle x \rangle_{\pm} = (x \pm |x|)/2$. The stored energy density of undamaged elastic material is written as $\psi(\boldsymbol{\varepsilon}) = \psi_+(\boldsymbol{\varepsilon}) + \psi_-(\boldsymbol{\varepsilon})$ where, $\psi^{\pm}(\boldsymbol{\varepsilon}) := \frac{1}{2} \lambda \langle \text{tr } \boldsymbol{\varepsilon} \rangle_{\pm}^2 + \mu \boldsymbol{\varepsilon}_{\pm} : \boldsymbol{\varepsilon}_{\pm}$. The damaged region has elastic energy density $\psi_-(\boldsymbol{\varepsilon})$ which means it penalizes certain types of strain such as uniaxial compression or hydrostatic compression but it is indifferent to strains such as uniaxial stretching or volumetric expansion. This modification is better than zero-stiffness response because a compressive mode-I loading of crack will result in a response as if there is no crack, which is physically reasonable and will not result in crack propagation. However, this is not a complete fix. The function $\psi_-(\boldsymbol{\varepsilon})$ modifies the response of intact material based on information about the local strain state (making use of just $\langle \boldsymbol{\varepsilon} \rangle_-$). It reproduces desired response under compression but not under every loading condition. For an example,

Consider a strain state corresponding to simple shear and lets analyse how a zero stiffness material and the modified material responds:

$$\boldsymbol{\varepsilon} = \begin{bmatrix} 0 & \gamma \\ \gamma & 0 \end{bmatrix}$$

The zero-stiffness material energetically does not penalize this strain, which means such a material will not resist simple shear which is a good approximation of a physical crack.

For the modified material's response $\psi_-(\boldsymbol{\varepsilon})$ we decompose the strain tensor based on spectral decomposition. The eigenvalues are γ and $-\gamma$, eigenvectors are $\frac{e_1+e_2}{\sqrt{2}}$ and $\frac{e_1-e_2}{\sqrt{2}}$ respectively.

Let, $\Lambda = \begin{bmatrix} \gamma & 0 \\ 0 & -\gamma \end{bmatrix}$ be the diagonal matrix formed by eigenvalues.

Also, let P be the matrix formed by eigenvectors (as columns), i.e., $P = \frac{1}{\sqrt{2}} \begin{bmatrix} 1 & 1 \\ 1 & -1 \end{bmatrix}$.

Now, $\boldsymbol{\varepsilon} = P\Lambda P^T$.

The "negative" strain tensor was defined to be $\boldsymbol{\varepsilon}_- := P\Lambda_-P^T$. Where, Λ_- is obtained from Λ by zeroing out the positive eigenvalues. Therefore, $\Lambda_- = \begin{bmatrix} 0 & 0 \\ 0 & -\gamma \end{bmatrix}$.

which gives $\boldsymbol{\varepsilon}_- = P\Lambda_-P^T = \frac{1}{2} \begin{bmatrix} -\gamma & \gamma \\ \gamma & -\gamma \end{bmatrix}$

Now, the modified material's response for simple shear strain state is : $\psi_- = \lambda \langle \text{tr } \boldsymbol{\varepsilon} \rangle_-^2 + 2\mu(\boldsymbol{\varepsilon}_- : \boldsymbol{\varepsilon}_-) = 0 + 2\mu\gamma^2$. Which means the modified material resists simple shear, which is physically counter intuitive.

Using $\boldsymbol{\varepsilon}_-$ to model the cracked material's response solves the problem of crack growth under compression (uniaxial or hydrostatic) but introduces newer problems such as the example shown above.

These examples and reasoning highlight the importance of taking crack orientation into account for modelling the elastic response of the cracked region.

6.5.1 Modifying energy by resolving strain into normal and shear components

Consider a crack in a 2D sample and let \mathbf{n} be the normal to the crack face. We expect the crack to close under compression and resist the stress on the crack face, however under tension we want the elastic response of cracked region as a zero-stiffness material. That is, we want to it to resist $\mathbf{n} \cdot \boldsymbol{\sigma} \cdot \mathbf{n}$ if it is negative but not if it is positive. For tension in any other direction damaged region should behave just as

intact material. Also, we want the cracked material to not resist any stress of the form $\mathbf{t} \cdot \boldsymbol{\sigma} \cdot \mathbf{n}$, i.e., shear on the crack faces.

Note that we are trying to emulate the fields in the surroundings of two surfaces (created by broken bonds, i.e., crack faces) due to their interaction by a material volume instead of two surfaces. Hence, the above expected behaviour is an approximation of the interaction of two surfaces.

Let $\mathbf{n} := \frac{\nabla\phi}{|\nabla\phi|}$, it represents normal to crack face and let \mathbf{t} be the unit vector normal to \mathbf{n} , it represents tangent to the crack face. In 2D there is only one unique \mathbf{t} (up to the $\pm\mathbf{t}$) however in 3D there is whole plane perpendicular to \mathbf{n} . For now we consider only 2D setting. We write the energy as:

$$U = W(\boldsymbol{\varepsilon})H_l(\phi - 0.5) + \left(1 - H_l(\phi - 0.5)\right) \left\{W_{crack}(\boldsymbol{\varepsilon}, \mathbf{n})\right\} \quad (6.5.1)$$

Elastic response of cracked region should be same as intact material except for the positive strain components normal to the crack face and shear components on the crack face. This can be achieved by defining:

$$W_{crack}(\boldsymbol{\varepsilon}, \mathbf{n}) := \mathcal{G}_c + W(\boldsymbol{\varepsilon} - \varepsilon_{tensile}\mathbf{n} \otimes \mathbf{n} - \varepsilon_{shear}\mathbf{t} \otimes \mathbf{n}) \quad (6.5.2)$$

Note that $\nabla\phi$ will be zero away from crack phase or away from interface between cracked and intact region. This can happen at any point in the intact material and on a thin strip within the crack (where the two crack faces meet). In this situation, we cannot define \mathbf{n} as $\frac{\nabla\phi}{|\nabla\phi|}$. So we define $\mathbf{n} := \mathbf{0}$ and $\mathbf{t} := \mathbf{0}$ when $|\nabla\phi| \rightarrow 0$. Which essentially means $W_{crack}(\boldsymbol{\varepsilon}, \mathbf{n})$ is same as $W(\boldsymbol{\varepsilon})$ when normal to crack face is not defined. Because \mathbf{n} is defined everywhere on the interface, this intact material is completely isolated from the intact material outside the interface. Hence, we expect that it will not resist any stress, resulting in the desired elastic behaviour of the cracked material.

There is one remaining problem in the above formulation: $\nabla\phi$ will not represent crack face orientation near crack tip. So we need to make some modification to take care of crack tip. Because finding crack face normal is not possible at the crack tip, we model tip as a zero stiffness material. So first we need to detect if the material is a crack tip or not.

The tip of the crack is the region of the interface where it bends or curves a lot, in other words the region

where the normal to the interface varies rapidly. $\mathbf{n} = \hat{\nabla}\phi$ is the normal to the interface and therefore its gradient contains the information about the curvature but since it is a second order tensor we cannot use it directly. We need a scalar out of $\nabla\mathbf{n}$ which tells us the curvature. Intuitively the invariants or determinant can be used as a measure of curvature. Also there are many other choices possible because we demand very little, i.e., an expression which becomes high when there is a rapid change in \mathbf{n} . Here we use $|\nabla\mathbf{n}^T \cdot \mathbf{t}|$ as the measure. The reason for which is that for an arbitrary vector \mathbf{r} , $\nabla\mathbf{n}^T \cdot \mathbf{r}$ represents change in \mathbf{n} if we move along \mathbf{r} . An example of this is if $\mathbf{r} = \mathbf{n}$:

$$\begin{aligned}\mathbf{n} \cdot \mathbf{n} &= n_i n_i = 1 \\ \Rightarrow \nabla(\mathbf{n} \cdot \mathbf{n}) &= 2n_{i,j}n_i = \nabla\mathbf{n}^T \cdot \mathbf{n} = \mathbf{0}\end{aligned}$$

Which makes sense because \mathbf{n} does not change if we move along \mathbf{n} (only the magnitude of $\nabla\phi$ changes not the direction).

Now we use this measure to detect crack tip in the energy and write the energy density for the damaged region to be:

$$W_{crack}(\boldsymbol{\varepsilon}, \phi) = \mathcal{G}_c + \left\{ 1 - H_l(|\nabla\mathbf{n} \cdot \mathbf{t}| - \alpha_0) \right\} W(\boldsymbol{\varepsilon} - \varepsilon_{tensile}\mathbf{n} \otimes \mathbf{n} - \varepsilon_{shear}\mathbf{t} \otimes \mathbf{n}) \quad (6.5.3)$$

The above equation (6.5.3) is only for the damaged region. It says energy is \mathcal{G}_c if $|\nabla\mathbf{n}^T \cdot \mathbf{t}| > \alpha_0$ where α_0 is the threshold value for curvature. Otherwise energy is $\mathcal{G}_c + (\text{energy due to modified strain})$. α_0 needs to be found out empirically by doing calculations. One issue with this approach is that from section 6.6 we know that crack width (and hence the tip radius) depends upon crack speed in dynamic setting. Therefore, the value of α_0 might not work for crack moving at arbitrary speeds. However, for quasistatic setting, where crack width depends only upon the parameters in the model, we do not have to worry about this issue.

Now we calculate stress and driving force for this formulation. Let, $\boldsymbol{\varepsilon}' := \varepsilon_{tensile}\mathbf{n} \otimes \mathbf{n} + \varepsilon_{shear}\mathbf{t} \otimes \mathbf{n}$

$$\frac{\partial W_{crack}}{\partial \varepsilon_{ij}} = \left\{ 1 - H_l(|\nabla \mathbf{n}^T \cdot \mathbf{t}| - \alpha_0) \right\} \frac{\partial W}{\partial \varepsilon_{ab}} \Big|_{\varepsilon=(\varepsilon-\varepsilon')} (\delta_{ai}\delta_{bj} - n_a n_b n_i n_j - t_i n_j t_a n_b) \quad (6.5.4)$$

Define, $\boldsymbol{\sigma}' = \frac{\partial W}{\partial \varepsilon_{ab}} \Big|_{\varepsilon=(\varepsilon-\varepsilon')}$ then the expression for stress can be simplified to:

$$\frac{\partial W_{crack}}{\partial \varepsilon_{ij}} = \left\{ 1 - H_l(|\nabla \mathbf{n}^T \cdot \mathbf{t}| - \alpha_0) \right\} \left(\boldsymbol{\sigma}' - (\mathbf{n} \cdot \boldsymbol{\sigma}' \mathbf{n}) \mathbf{n} \otimes \mathbf{n} - (\mathbf{t} \cdot \boldsymbol{\sigma}' \mathbf{n}) \mathbf{t} \otimes \mathbf{n} \right) \quad (6.5.5)$$

Note that $\boldsymbol{\sigma}'$ is stress response of intact material at modified strain. Since strain is modified only according to crack face shear and crack face tension, the rest of the components of stress are not affected.

It also means that tensile and shear stress on crack face turn out to be zero which can be clearly seen from the above expression, i.e., by dotting the (6.5.5) with \mathbf{n} and \mathbf{t} appropriately.

Now we want to take the variation of energy functional w.r.t. ϕ to get the driving force.

$$E[\mathbf{u}, \phi] = \int_{\Omega} U = \int_{\Omega} \left(W(\boldsymbol{\varepsilon}) H_l(\phi - 0.5) + (1 - H_l(\phi - 0.5)) \left\{ W_{crack}(\boldsymbol{\varepsilon}, \mathbf{n}) \right\} \right) \quad (6.5.6)$$

$$\frac{\delta E}{\delta \phi} = \lim_{\epsilon \rightarrow 0} \frac{d}{d\epsilon} E[\mathbf{u}, \phi + \epsilon \psi] \quad (6.5.7)$$

Note that $\mathbf{n} = \frac{\nabla \phi}{|\nabla \phi|}$ is valid only if $|\nabla \phi| > 0$, for $|\nabla \phi| = 0$ we need to define \mathbf{n} to be \mathbf{o} . So define,

$$\mathbf{n} := \frac{\nabla \phi}{|\nabla \phi|} g_a(|\nabla \phi| - \theta_0) \quad (6.5.8)$$

Where $g_a(x)$ is a smeared out Heaviside type of function but its derivative has compact support unlike tanh or erf. The width of transition region = $2a$.

$$g_a(x) = \begin{cases} 0 & \text{if } x \leq -a \\ \frac{1}{1 + \exp\left(\frac{4xa}{x^2 - a^2}\right)} & \text{if } |x| < a \\ 1 & \text{if } x \geq a \end{cases} \quad (6.5.9)$$

Now,

$$\frac{\delta E}{\delta \phi} = \int_{\Omega} \delta_l(\phi - 0.5) W(\boldsymbol{\varepsilon}) - \delta_l(\phi - 0.5) W_{crack}(\boldsymbol{\varepsilon}, \mathbf{n}) + (1 - H_l(\phi - 0.5)) \frac{dW_{crack}}{d\epsilon} \quad (6.5.10)$$

Recall from (6.5.3), that W_{crack} is:

$$W_{crack}(\boldsymbol{\varepsilon}, \phi) = \mathcal{G}_c + \left\{ 1 - H_l(|\nabla \mathbf{n} \cdot \mathbf{t}| - \alpha_0) \right\} W(\boldsymbol{\varepsilon} - \varepsilon_{tensile} \mathbf{n} \otimes \mathbf{n} - \varepsilon_{shear} \mathbf{t} \otimes \mathbf{n}) \quad (6.5.11)$$

where $\varepsilon_{tensile} := (\mathbf{n} \cdot \boldsymbol{\varepsilon} \cdot \mathbf{n}) g_b$.

To compute the derivative of $W_{crack}(\boldsymbol{\varepsilon}, \phi + \epsilon\psi)$ w.r.t. ϵ we use chain rule for each term. The last term in the variational derivative of E can written as:

$$\begin{aligned} & - \int_{\Omega} (1 - H_l(\phi - 0.5)) W(\boldsymbol{\varepsilon})|_{\varepsilon=\bar{\varepsilon}} \delta_l(|\nabla \mathbf{n}^T \cdot \mathbf{t}| - tol) \left(\frac{\nabla \mathbf{n}^T \cdot \mathbf{t}}{|\nabla \mathbf{n}^T \cdot \mathbf{t}|} \right)_i \frac{d(\nabla \mathbf{n} \cdot \mathbf{t})_i}{d\epsilon} \\ & + \int_{\Omega} (1 - H_l(\phi - 0.5)) (1 - H_l(|\nabla \mathbf{n}^T \cdot \mathbf{t}| - tol)) \frac{\partial W}{\partial \varepsilon_{ij}} \Big|_{\varepsilon=\bar{\varepsilon}} \frac{\partial \tilde{\varepsilon}_{ij}}{\partial n_p} \\ & \left\{ \left(\frac{\psi_{,p}}{|\nabla \phi|} - \frac{\phi_{,p} \phi_{,k} \psi_{,k}}{|\nabla \phi|^3} \right) g_a(|\nabla \phi| - \theta_0) + g'_a(|\nabla \phi| - \theta_0) \frac{\phi_{,p} \phi_{,k} \psi_{,k}}{|\nabla \phi|^2} \right\} \end{aligned} \quad (6.5.12)$$

The expression for $\frac{d(\nabla \mathbf{n} \cdot \mathbf{t})_i}{d\epsilon}$ is:

$$\begin{aligned} & \left\{ g'_a(|\nabla \phi| - \theta_0) \frac{\phi_{,k} \psi_{,k}}{|\nabla \phi|^2} \left(\phi_{,ji} + \frac{\phi_{,j} \phi_{,k} \phi_{,ki}}{|\nabla \phi|^2} \right) \right. \\ & + g_a(|\nabla \phi| - \theta_0) \left(\frac{\psi_{,ji}}{|\nabla \phi|} - \frac{\phi_{,ji} \phi_{,\lambda} \psi_{,\lambda}}{|\nabla \phi|^3} - \frac{3\phi_{,p} \psi_{,p} \phi_{,j} \phi_{,k} \phi_{,ki}}{|\nabla \phi|^5} + \frac{\psi_{,j} \phi_{,k} \phi_{,ki} + \phi_{,j} \psi_{,k} \phi_{,ki} + \phi_{,j} \phi_{,k} \psi_{,ki}}{|\nabla \phi|^3} \right) \\ & + \left(\frac{\psi_{,j}}{|\nabla \phi|} - \frac{\phi_{,j} \phi_{,\alpha} \psi_{,\alpha}}{|\nabla \phi|^3} \right) g'_a(|\nabla \phi| - \theta_0) \frac{\phi_{,m} \phi_{,mi}}{|\nabla \phi|} + \frac{\phi_{,j}}{|\nabla \phi|} g''_a(|\nabla \phi| - \theta_0) \frac{\phi_{,\mu} \psi_{,\mu} \phi_{,m} \phi_{,mi}}{|\nabla \phi|^2} \\ & + \left. \frac{\phi_{,j}}{|\nabla \phi|} g'_a(|\nabla \phi| - \theta_0) \left(\frac{\psi_{,m} \phi_{,mi} + \phi_{,m} \psi_{,mi}}{|\nabla \phi|} - \frac{\phi_{,m} \phi_{,mi} \phi_{,r} \psi_{,r}}{|\nabla \phi|^3} \right) \right\} R_{j\alpha} \frac{\phi_{,\alpha}}{|\nabla \phi|} g_a(|\nabla \phi| - \theta_0) \\ & + \left\{ \left(g_a(|\nabla \phi| - \theta_0) \left(\frac{\phi_{,ji}}{|\nabla \phi|} + \frac{\phi_{,j} \phi_{,k} \phi_{,ki}}{|\nabla \phi|^3} \right) + \frac{\phi_{,j} \phi_{,m} \phi_{,mi}}{|\nabla \phi|^2} \right) \right. \\ & \left. R_{j\alpha} \left(\left(\frac{\psi_{,\alpha}}{|\nabla \phi|} - \frac{\phi_{,\alpha} \phi_{,r} \psi_{,r}}{|\nabla \phi|^3} \right) g_a(|\nabla \phi| - \theta_0) + \frac{\phi_{,\alpha} \phi_{,s} \psi_{,s}}{|\nabla \phi|^2} g'_a(|\nabla \phi| - \theta_0) \right) \right\} \end{aligned} \quad (6.5.13)$$

The expression for $\frac{\partial \varepsilon_{ij}}{\partial n_p}$ is :

$$\begin{aligned}
& - \{ (\varepsilon_{pb}n_b + \varepsilon_{ap}n_a)g_b(\varepsilon_{mnn_mn_n})n_in_j + \varepsilon_{ab}n_an_b(\delta_{ip}n_j + \delta_{jp}n_i)g_b(\varepsilon_{mnn_mn_n}) \\
& \quad + \varepsilon_{ab}n_an_bn_in_jg'_b(\varepsilon_{mnn_mn_n})(\varepsilon_{pn}n_n + \varepsilon_{mp}n_p) \} \\
& - \{ \varepsilon_{rs}R_{rp}n_sR_{i\beta}n_\beta n_j + \varepsilon_{rp}R_{r\alpha}n_\alpha R_{i\beta}n_\beta n_j \\
& \quad + \varepsilon_{rs}R_{r\alpha}n_\alpha n_s R_{ip}n_j + \varepsilon_{rs}R_{r\alpha}n_\alpha n_s R_{i\beta}n_\beta \delta_{jp} \}
\end{aligned} \tag{6.5.14}$$

where, \mathbf{R} is a rotation such that $\mathbf{t} = \mathbf{R} \cdot \mathbf{n}$.

Below are the calculations demonstrating the above formulation. The domain is a 2D plate with a crack at center. Left and right edges impose either tensile or compressive boundary conditions. Every other boundary condition is traction free.

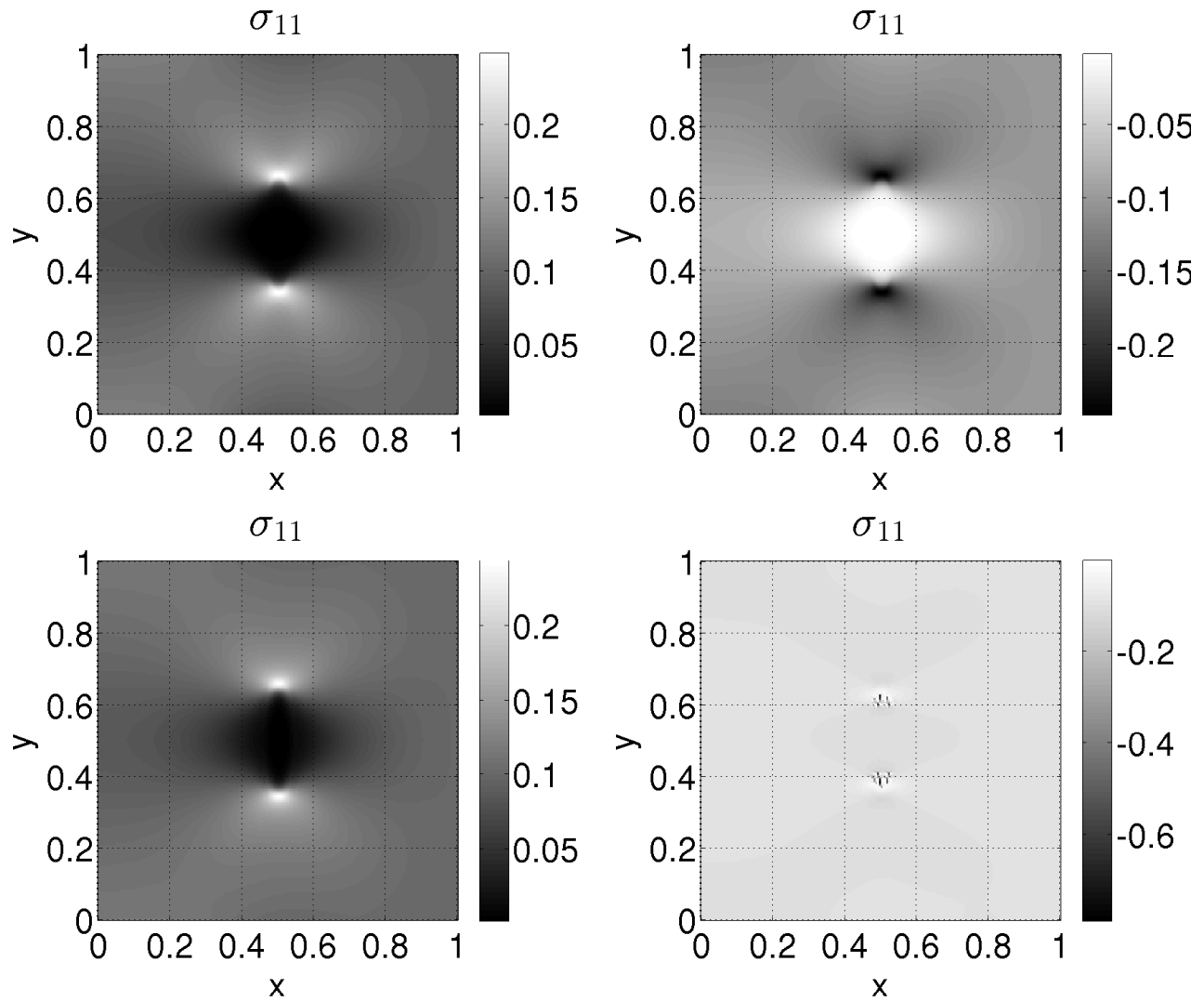


Figure 6.6: The first row of figures is corresponding to a 0-stiffness material. The second row is the response of model described above. Both the figures on the left correspond to tensile boundary conditions and the figures on right correspond to compressive boundary conditions.

In the tensile situation both the models give similar results, as desired. The bottom-right figure shows crack under compression from our model. The plate takes uniform stress everywhere except in small regions at the crack tip because we are modelling them as zero-stiffness material. While the zero-stiffness material models this scenario as a complete void and cracked region has zero stress as can be seen in the figure on top-right.

The above calculations only show the elastic response. We did not perform crack evolution calculations with this energy. Even though this is a better approximation than any of the existing ones, we were unable to capture the correct response at the tip region. Most of the interesting phenomena takes place near the tip, for e.g. crack branching, anisotropy, determination of crack speed, etc. Therefore any crack propagation calculations would have still been untrustworthy for any quantitative prediction or analysis as it is the case when we approximate the response by either negligible stiffness or based on eigen-strain decomposition.

6.6 Width of the phase-field crack

Crack width in the dynamic phase field model depends upon the crack speed. The faster the crack, the thicker it is. By thicker or wider crack I do not mean thicker interface between damaged and intact material which is governed solely by the small parameter l and the diffusion coefficient ϵ , but I mean the bulk of the crack itself will become thicker. This widening only happens when material inertia is considered and not in the quasistatic or stress-equilibrium situation. The model developed in this paper suffers from this issue and according to our understanding of the problem all the existing dynamic phase-field models ([BVS⁺12, BLR11, KKL01]) should have this problem. We use one of the existing models [BLR11] to explain and demonstrate the issue.

$$E[\mathbf{u}, \phi] = \int_{\Omega} (\phi^2 + \eta_\epsilon) W(\boldsymbol{\varepsilon}) + \mathcal{G}_c \int_{\Omega} \left[\frac{(1 - \phi)^2}{4\epsilon} + \epsilon |\nabla \phi|^2 \right] d\Omega \quad (6.6.1)$$

For the antiplane deformations or mode-III crack $W(\boldsymbol{\varepsilon})$ reduces to $|\nabla u|^2$. However, we will be performing in-plane calculations. As mentioned earlier in 6.5, negligible stiffness approximation has some important issues but for simple mode-I calculations it should not cause any problem. Also, for the mode-I crack propagation problem there is no difference between modelling cracked region as a negligible stiffness response or eigen-strain based decomposition or as the response we constructed in 6.5.1.

$$\rho \mathbf{u}_{tt} = Div \left(\frac{\partial W}{\partial \boldsymbol{\varepsilon}} \right) \quad (6.6.2)$$

$$\phi = \arg \min_{\phi} E[\mathbf{u}, \phi] \quad (6.6.3)$$

The evolution of \mathbf{u} is governed by linear momentum balance and ϕ evolves according to the minimum principle as described in [BLR11] along with the irreversibility condition for the phase field. We also add small amount of viscosity to minimize the effect of waves reflected from domain boundaries.

6.6.1 Approximation of surface energy as a volume integral

In the classical theory of Griffith the crack surface energy is proportional to its surface area (and crack length in 2D) [Gri21], while in phase field formulation it is a volume integral over the cracked region:

$$\mathcal{G}_c \int_{\Omega} \left[\frac{(1 - \phi)^2}{4\epsilon} + \epsilon |\nabla \phi|^2 \right] d\Omega \quad (6.6.4)$$

The first term contributes to the integral wherever $\phi = 0$, hence its contribution scales with the volume of the cracked ($\phi = 0$) region. The second term contributes only at crack faces because everywhere else $\nabla \phi = 0$. Thus its contribution depends only on the "sharpness" of the crack faces and their surface area (length in 2D). Thus the overall energy of the cracked region (6.6.4) depends upon the volume of the cracked region.

First consider the quasistatic loading conditions. Points within the cracked region (i.e., \mathbf{x} s.t. $\phi = 0$ and $\nabla \phi = 0$) have an energy \mathcal{G}_c . The intact region outside the crack face (away from tip) cannot take tension and therefore has zero stress and zero elastic energy. In quasistatics, energy is minimized with respect to both \mathbf{u} and ϕ , therefore the energy cost of the cracked region (proportional to \mathcal{G}_c times the volume of the cracked region) keeps it from growing wider.

For e.g. consider a crack oriented parallel to y-axis (or an ellipse with high aspect ratio parallel to y-axis) in a 2D plate. If we subject the crack to mode-I loading conditions, i.e., far-field tensile loading parallel to x-axis quasistatically, stress concentration will develop near the tips while stress right outside of crack anywhere away from tip will be zero. This is a consequence of stress equilibrium, or physically, because the damaged material cannot transmit any stress. Hence the phase-field driving force (i.e., $\frac{\delta E}{\delta \phi}$), which is proportional to difference between the stored energy in the intact and in the damaged region turns out to be zero, thus resulting in no evolution of phase field. This vanishing of driving force at the crack-face (away from crack-tip) is crucial to keep the crack from widening and becoming a void.

In the elastodynamic setting, the evolution is not governed by minimization. Cracks under mode-I loading conditions will keep getting wider until the region outside it has zero stresses. This duration depends upon the elastic wave speed. Hence the crack width is governed by competition between crack speed and elastic wave speed. The argument holds irrespective of whether the cracked region $(\psi_2(\varepsilon, \nabla\phi))$ is modelled as a negligible stiffness material, or as proposed in [MWH10] using spectral decomposition, or as constructed in section 6.5.1, because at any point within the crack the energy density, under the mode-I loading conditions, is \mathcal{G}_c according to all the approaches. This implies that the width of the crack depends upon the crack speed and thus upon loading conditions.

Since, the energy of the crack in the phase-field context depends upon the volume and hence on the speed of the crack rather than just the surface area as in the classical theory of crack by Griffith, the dynamic model is not expected to match all the results of classical theory.

If the phase field crack width remains fixed irrespective of the conditions under which crack formed then the above energy proportional to volume can be seen as essentially proportional to just the surface area of the crack. But this happens only in the quasistatic situation and not in the dynamic setting.

6.6.2 Calculations

The specimen is a 2D square plate with traction boundary conditions on the left and right edge (corresponding to mode-I tensile loading conditions). Top and bottom edges are tractions free. The results from solving (6.6.2) for two different values of applied loads are shown in Fig. 6.7. Higher applied load makes the crack grow faster leading to thicker crack.

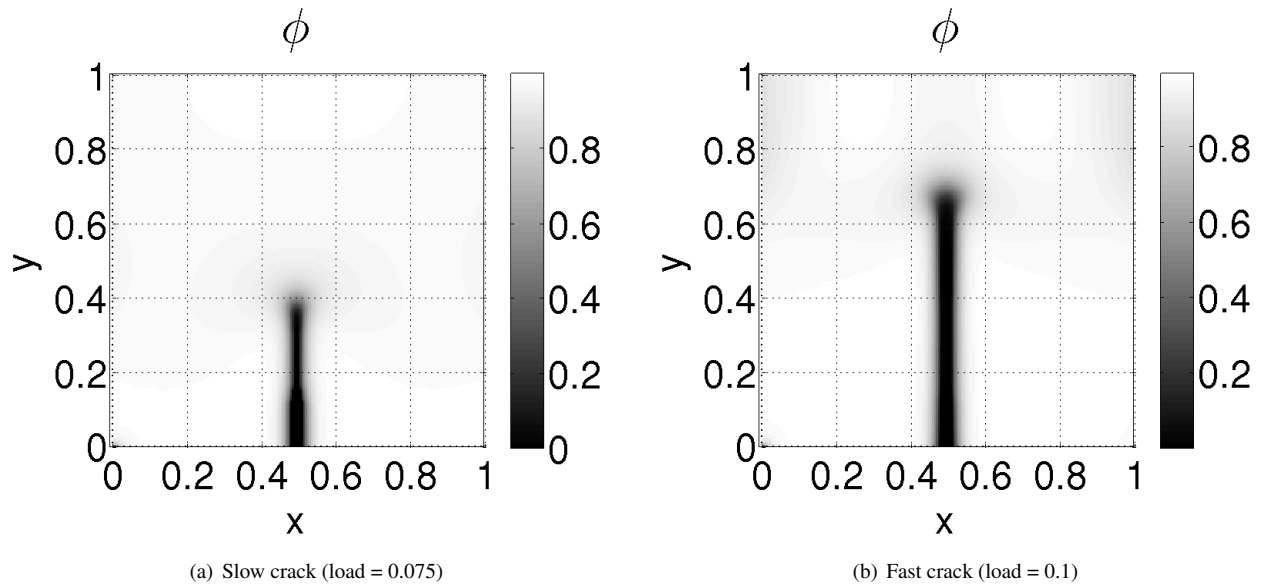


Figure 6.7: Results from solving (6.6.2). Every parameter is same for the two calculations except magnitude of tensile load applied on the left and right edges. Crack width is higher for the second case in which applied load is higher.

6.7 Crack nucleation on a bi-material interface

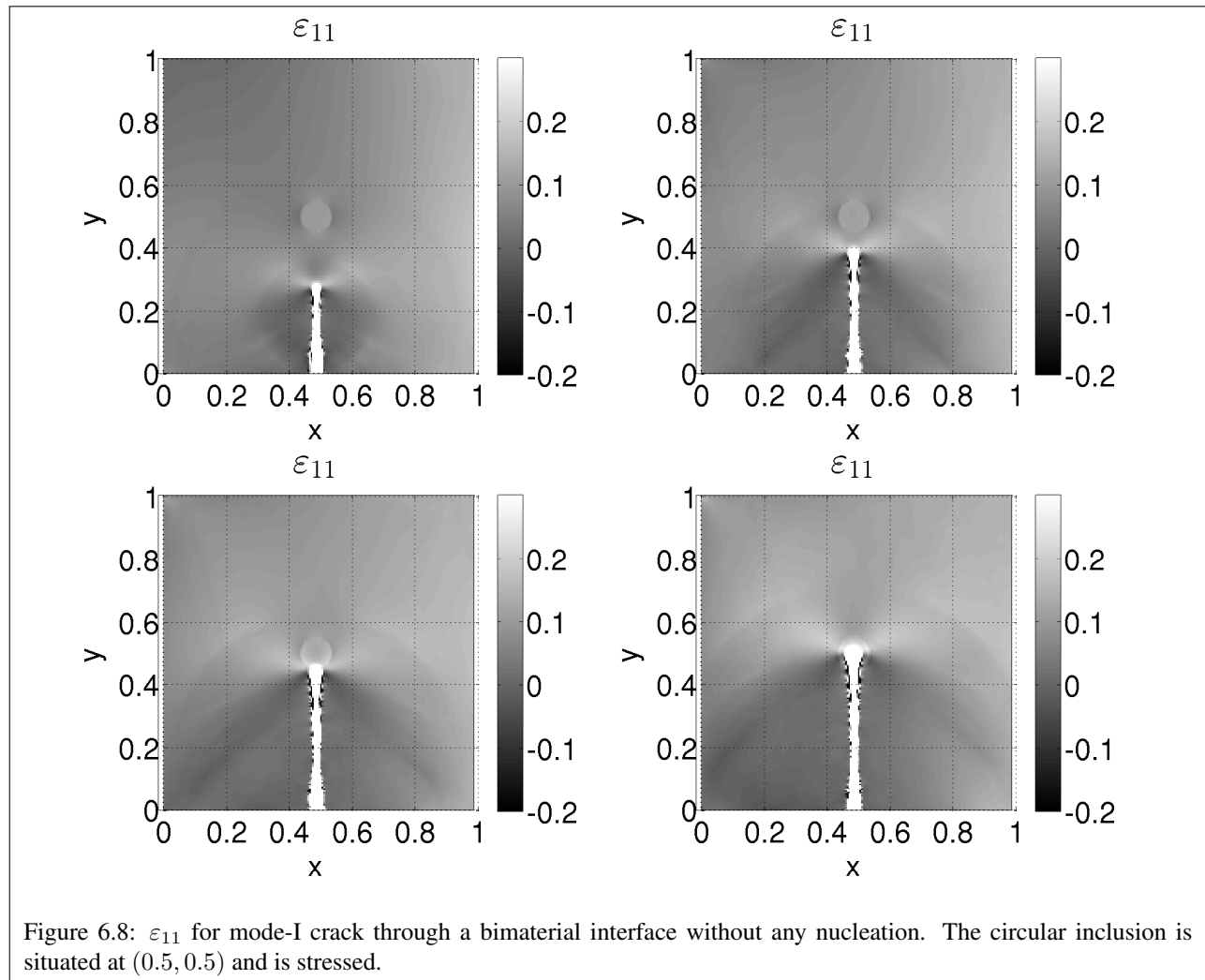
The configuration is a 2D square plate with unit dimensions. The plate is fixed at left edge, top and bottom edges are traction free. A constant tensile load is applied at the right edge. A notch exists near $x = 0.5$ (see figure). A circular inclusion at $(0.5, 0.5)$ of radius $r_0 = 0.05$ is situated. This inclusion is non-transforming and has different elastic properties than the surrounding matrix. The initial displacement corresponds to equilibrium solution ($div \sigma = 0$) for the plate, therefore the plate and notch are prestressed. We study crack propagation through the bimaterial interface between the inclusion and the matrix.

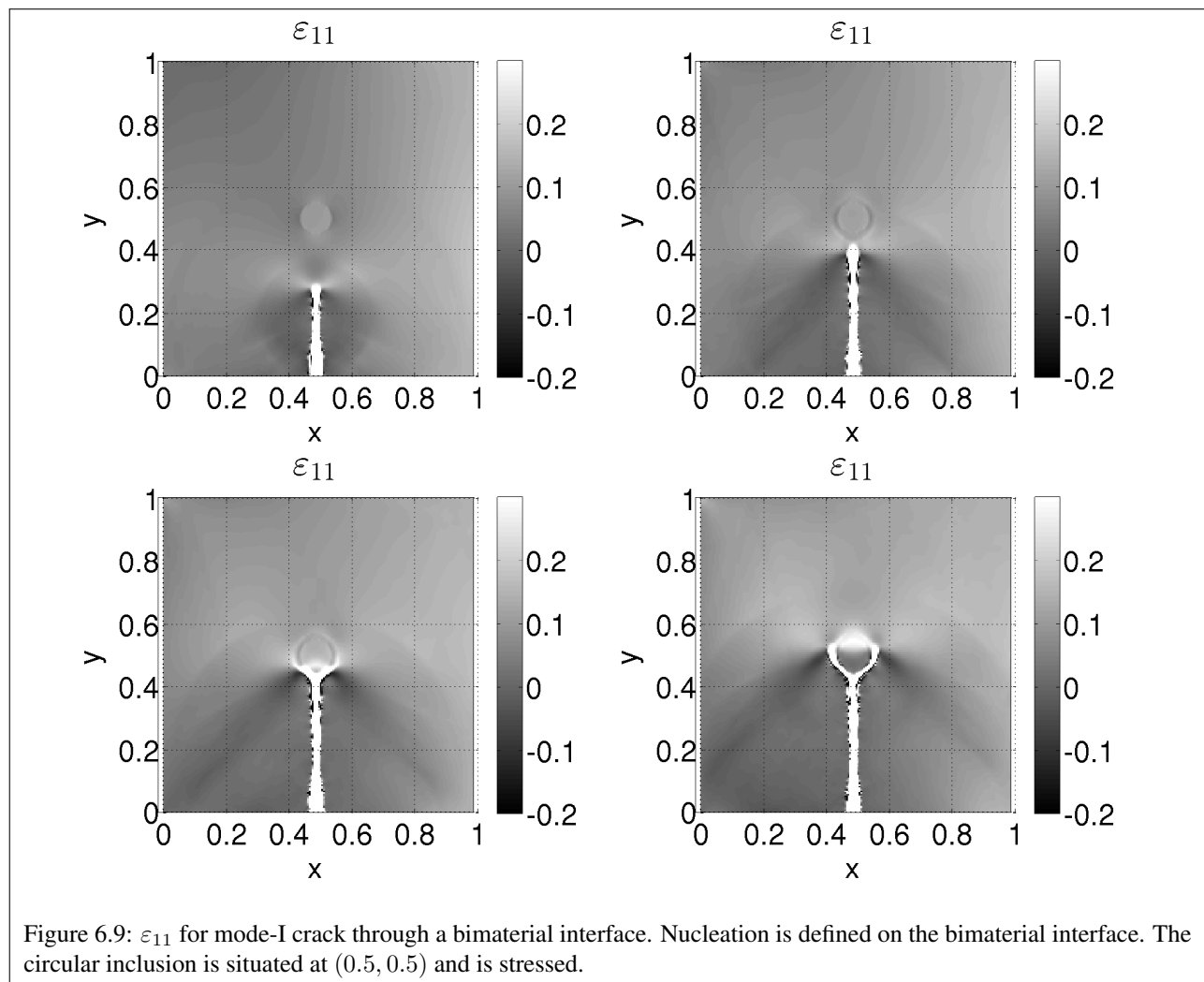
We model the matrix as linear elastic material with quadratic energy $\frac{1}{2} \varepsilon : \mathbf{C} : \varepsilon$ and the inclusion as material with same stiffness but non-zero eigenstrain: $\frac{1}{2} (\varepsilon - \varepsilon_0) : \mathbf{C} : (\varepsilon - \varepsilon_0)$. Inclusion can be made to have different stiffness or completely different elastic response than the matrix such as anisotropy, etc. In such case, as the crack propagates the emanating elastic waves will interact with the inclusion and the waves reflected back may or may not affect the crack growth by curving it or branching it. However, the purpose of this calculation is to show that it is straightforward to prescribe nucleation at the interface. So to avoid any complexities of crack path due to interaction with inclusion, we use the simplest possible form of energy for the inclusion. The eigenstrain for inclusion is $\varepsilon_0 = 0.05 \mathbf{I}$.

We perform two calculations, one with the nucleation active at the interface and without any nucleation which serves as a control. The nucleation function is:

$$G = \begin{cases} H_l(\phi - 0.5)(H_l(r - 0.05) - H_l(r - 0.1)) & \text{if } \sigma_{11} > \sigma_0 \\ 0 & \text{otherwise} \end{cases} \quad (6.7.1)$$

where H_l is the smeared out step function defined earlier. The first $H_l(\phi - 0.5)$ imposes the condition that crack nucleation only happens when the material is intact. The $(H_l(r - 0.05) - H_l(r - 0.1))$ specify the region where nucleation is active.





In the first case (Fig. 6.8) when nucleation is not active, crack grows and passes through the bimaterial interface into the inclusion. While in the second situation (Fig 6.9) as the crack approaches the interface, the nucleation gets active because of the stress concentration at the crack tip and forms new cracks along the interface. Note that the interface was stressed before the crack reached, but the stress was not high enough to cause nucleation.

It may also be possible to achieve similar macroscopic response by modifying the fracture toughness or surface energy \mathcal{G}_c along the interface. However, the approaches represent different underlying mechanism. Reducing fracture toughness is an energetic criteria based on how much energy does the new surface cost, while the nucleation approach can be related to instability at the atomic level.

6.8 A comment on mass density for cracked phase

In all the works we know, the mass density ρ required for the elastodynamics is assumed to be same for the cracked region as it is for intact material. This is necessary to ensure that mass is conserved during crack propagation. However modelling damaged region with mass has its own set of issues. Because the damaged region has negligible stiffness (at least w.r.t tensile mode-I loading conditions), the displacement and material velocity in the damaged region can be arbitrary (or very large) but do not mean anything physically. Now since mass density is not zero, these velocities have an associated kinetic energy. Therefore, the system lost some of its mechanical energy as kinetic energy of the cracked region which cannot be recovered. While crack propagation is a dissipative process and losing some energy this way is not a big concern, it may cause problems if the results are to be compared with some other models such as atomistic level models. For e.g. one may want to compare the dissipation in the two models to calibrate kinetic law or confirm Griffith's criteria of crack propagation, in such a situation it is not clear whether to account kinetic energy associated with cracked region as dissipation or not.

6.9 Supersonic mode-II crack

The theoretical upper limit of remotely loaded mode-I crack speed is Rayleigh wave speed, c_R . The energy flux to the crack tip vanishes for cracks propagating faster than c_R . From similar energy considerations, a remotely loaded mode-II crack can propagate at speeds less than Rayleigh wave speed or between shear wave speed and longitudinal wave speed, but not between Rayleigh and shear wave speed. See [Fre98, Bro96] for detailed analysis. We attempt simulating mode-II cracks using our model and explore if we can make the crack propagate faster than theoretical limits by applying higher loads.

The configuration is a 2D square plate. Left edge edge is fixed, top and bottom edges are traction free. Shearing traction is applied on the right edge. Mode-II cracks in experiments (see for e.g. [SHR02] and the references therein) have been shown to curve and bend at about 45° angle w.r.t to shear loading direction to maintain the opening mode unless there is a weak plane. We first do calculations with isotropic kinetics and without any weak plane to see if the crack curves and bends. Then we make an attempt to keep the crack evolve straight using anisotropic kinetics. In all the calculations below, cracks

are pre-stressed which means initially there is a crack stressed due to boundary shear load, i.e., initial conditions correspond to equilibrium solution for a fixed crack.

Linear momentum balance ($\rho \ddot{\mathbf{u}} = \text{div}(\boldsymbol{\sigma})$) and balance law are solved. Linear kinetics is used (i.e., $\hat{v} = \kappa \text{sign}(f)|f|$). Stress response function is isotropic ($\lambda = 1.0, \mu = 0.2$)

6.9.1 Isotropic kinetics

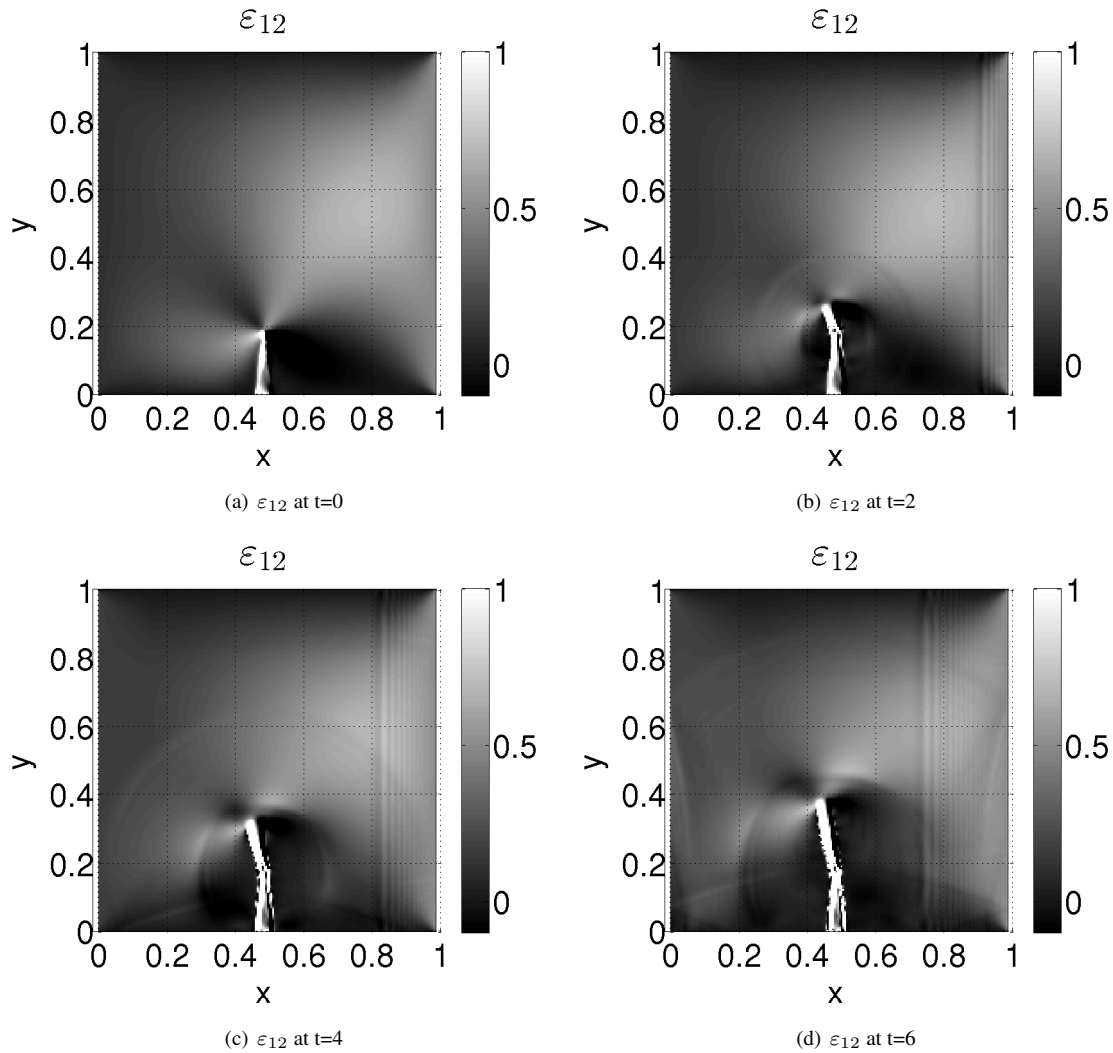


Figure 6.10: ε_{12} for a mode-II crack at different times (for $t = 0$ to $t = 6$). Shear loading is applied on the right edge, left edge is fixed. As expected, the crack curves.

6.9.2 Anisotropic kinetics: subsonic crack growth

Now we use anisotropic kinetics in the same configuration to see if it can keep the crack evolving in a straight path.

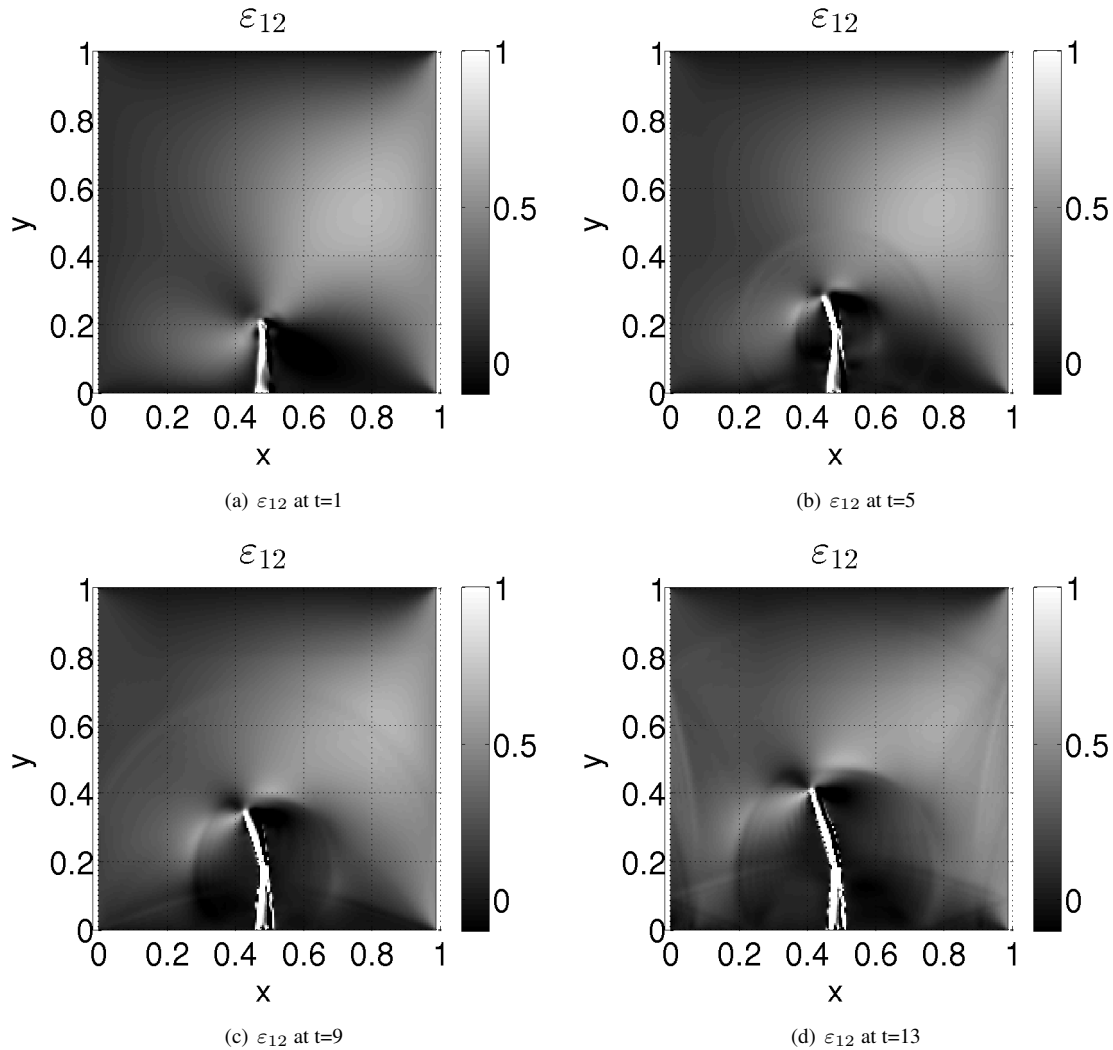


Figure 6.11: ε_{12} for a mode-II crack with anisotropic kinetics at different times (for $t = 1$ to $t = 14$). Shear loading ($\tau = 0.1$) is applied on the right edge, left edge is fixed. Crack evolution is subsonic w.r.t shear waves speed and crack still curves. The plots look very similar to [6.10](#)

Crack evolution is subsonic w.r.t shear waves speed and crack still curves. Next we try to increase the prestress load to see if that makes the crack grow faster.

6.9.3 Anisotropic kinetics: supersonic crack growth

We report supersonically growing cracks with anisotropic kinetics when they are sufficiently pre-stressed.

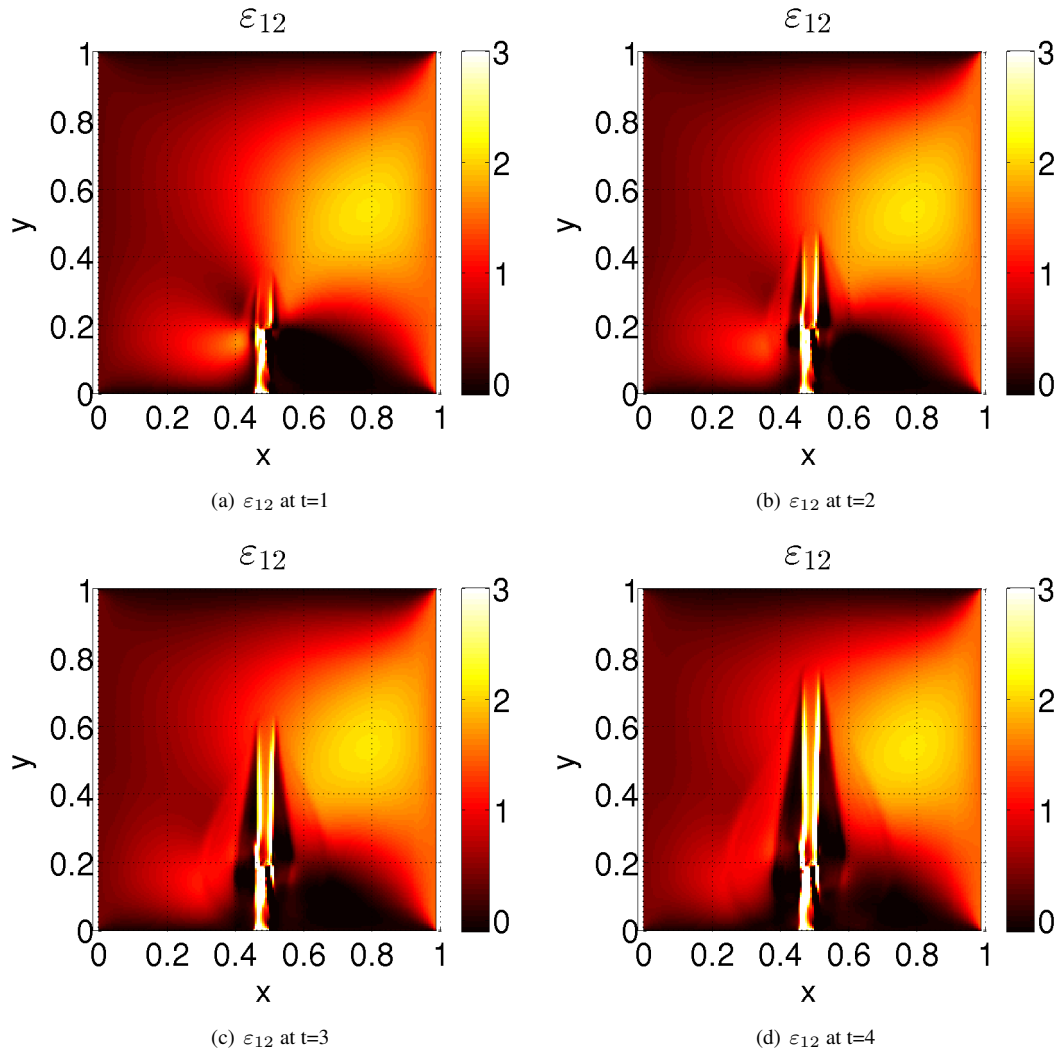


Figure 6.12: ε_{12} for a mode-II crack at different times (for $t = 0$ to $t = 4$). Shear loading ($\tau = 0.1$) is applied on the right edge, left edge is fixed. Linear kinetics ($\hat{v} = \kappa \cdot (\nabla \phi \cdot e_2) \text{sign}(f) |f|$). Mach cones formed by shear waves can be seen. Unlike calculation in Fig.6.11 for mode-II cracks, in this calculation the crack did not bend. Also, the crack was slightly thicker than earlier cases

For lower prestressed loads the crack grows at subsonic speed and curves even when kinetics is anisotropic. However at high loads we see that mode-II cracks grow at supersonic speed and do not curve. Figure 6.13 shows Poynting vector ($\mathbf{p} = \boldsymbol{\sigma}^T \cdot \mathbf{v}$) plots for sub-sonically and supersonically propagating cracks. For the subsonic, the energy seems to be flowing to the crack tip from surroundings. For the supersonic crack, energy seems to be flowing towards the crack-face from the right side (just below the crack tip) and away from the crack-face on the left hand side of the crack face. At first, the supersonic plot may seem counter-intuitive because no energy is flowing to the crack tip but crack propagation consumes energy. But we see supersonic cracks only for very highly pre-stressed specimens. Therefore, the energy required

to propagate the crack (both the amount needed for surface energy and dissipation) can be inferred to be coming from the elastically stored energy ahead of the tip due to pre-stress.

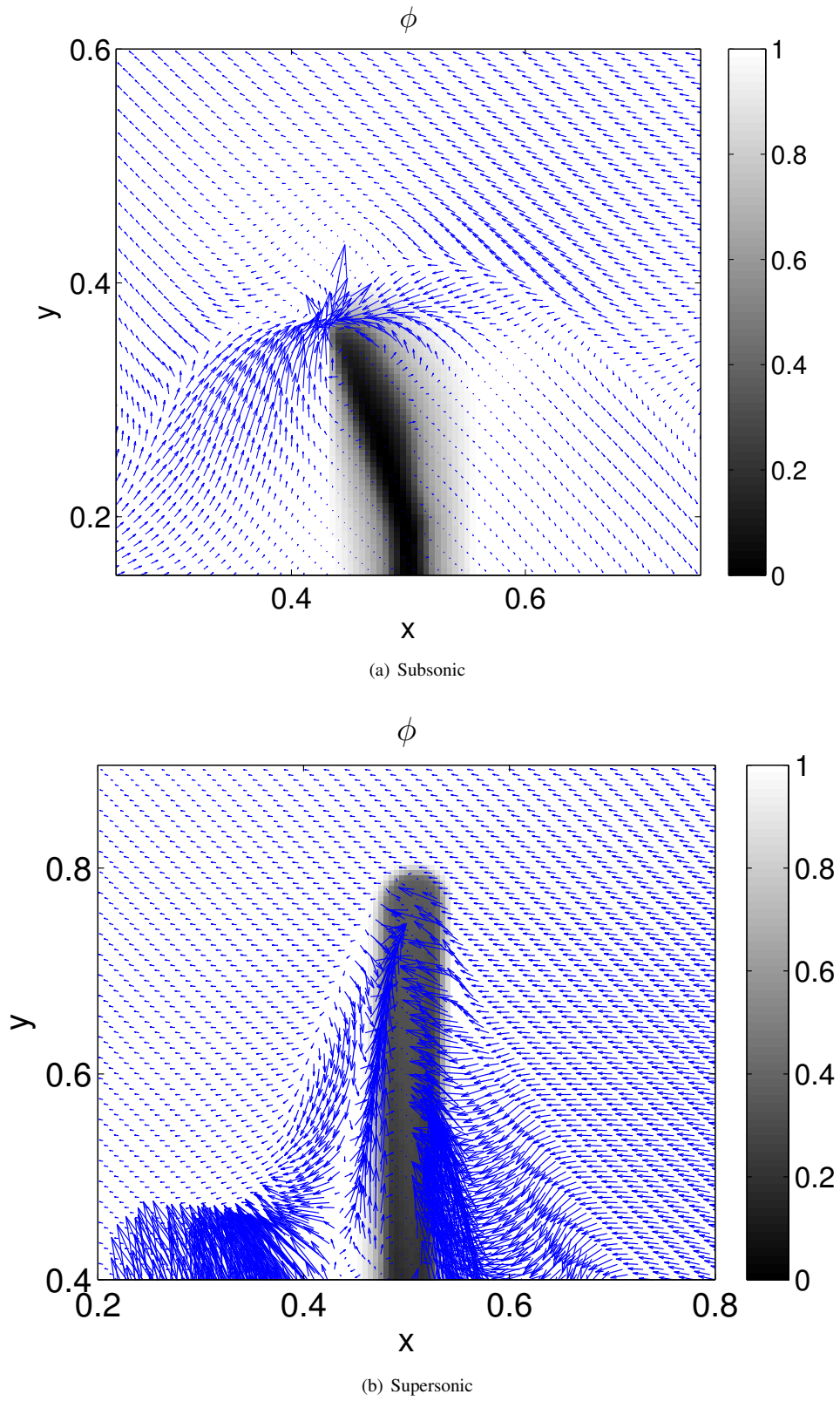


Figure 6.13: Poynting vector for supersonic and subsonic mode-II crack

Chapter 7

Conclusions

- The phase field model for phase interfaces developed in this thesis has advantages for both the sharp interface model and diffuse interface models, i.e., one can do easy computation with prescribable kinetics and nucleation. However, this comes at a cost. All the phase field models re-parametrize the original non-convex energy to make it a function of the phase field ϕ . This increases the size of the solution space. To see this consider a trilinear material. According to the original non-convex energy, the low strain phase cannot exist beyond a certain strain level and the high strain phase cannot exist below a certain strain level. For a given stress, there exist two values of strain corresponding to the two phases, but there is no value of strain which corresponds to both phases. However, in the phase-field models the energy is defined for each pair of strain and phase field. Therefore, given a value of strain, I can choose ϕ to be either 0 or 1 which means both phases can exist at this strain level. This is one of the points where phase-field models differ from sharp interface approaches in a fundamental way.
- It is known, see [AK91b], that in a trilinear material with different stiffness, a supersonic(w.r.t. softer phase) phase interface can exist. However, our model does not capture this behaviour nor do any of the other phase field models. One reason might be the fact that supersonic interfaces do not require a kinetic relation, they get uniquely determined just by the elastodynamics. However, in the phase-field context, the kinetic relation is always playing a role and it does not become redundant automatically when the situation(elastic fields and material properties) corresponds to a supersonic interface. This should ideally over-determine the system and no solution should exist but we do see

some solution in our numerical simulations. Recalling the above reasoning about larger solution space, it seems like because the solution space is bigger and we are imposing a kinetic law on the problem, the model picks up a different solution which does not exist in the sharp interface model's solution space. If this is actually what the model is doing, then it might be possible to resolve both of the above issues by using the nucleation function which transforms the material immediately if the strain at the material point changes to a value corresponding to the different phase.

- Some of the early work on phase-field models for crack ([[KKL01](#)]) have used gradient flow of energy for crack evolution which leads to dissipative kinetics. The recent existing phase-field models for crack both for quasistatic elasticity and elastodynamics, minimize energy w.r.t. phase-field for crack evolution. This captures the essence of Griffith's theory that energy release rate or the total loss in elastic energy per unit crack advance should be equal to energy consumed to generate the crack and this energy goes to the crack as surface energy. So the total energy of the system, i.e. sum of elastic strain energy and crack surface energy remains constant as crack propagates, which means the crack kinetics is non-dissipative in nature. While this is a reasonable assumption to start studying the subject, we think evolution of all kinds of defects are dissipative in nature. Dissipation is a macroscopic concept. In a molecular dynamics simulation, energy of the system is always conserved (unless hypothetical thermostats are used). The large wavelength oscillations at that scale appear as elastic deformation in macroscopic or a continuum model. The short wave length oscillations of atoms also constitute some energy and they appear as dissipation in continuum level model. Therefore, using molecular dynamics calculation for a propagating crack and calculating energy of short and long wavelength oscillations might be able to confirm the hypothesis. Such studies already exist for twinning, for e.g. see [[DWWR14](#)].
- Crack in phase-field context is modelled as a material region. Note that this perspective is counter-intuitive to the physical description of an ideal crack. Physically, if there is a single crack in material, there is no region which is cracked, there are just two free surfaces. With the phase-field models we hope that it approximates the behaviour of the crack or the way crack faces interact. This assumption, although allows one to develop a phase-field model, it raises certain fundamental issues which reduce the confidence in model for quantitative prediction. The issues are:
 1. Because there is a cracked region, either it can be modelled as having a mass density or as

massless. The former is what we have used and has been used in the existing literature. Those particles are defined to have negligible stiffness (at least under tensile loading) however they have velocity therefore they have an associated kinetic energy. As the crack propagates some energy gets converted into kinetic energy of the cracked material particles – i.e., it disappears. It is not associated with actual particles and if the exact same problem is done using an atomistic model such as molecular dynamics simulation, the respective components of energy may not match. If we model the cracked region as massless, then as crack propagates the specimen loses mass which also is a severe problem because it cannot be associated with atomistics.

2. Stiffness of the cracked region. We have discussed the issues with negligible-stiffness approximation and stiffness penalizing only the "positive" part of strain. We suggested an approach which resolves strain based on crack face orientation. However, it is not clear how to model the crack tip where the normal, $\frac{\nabla\phi}{|\nabla\phi|}$, does not represent crack face orientation. Most of the important phenomena, i.e., crack speed, anisotropy and branching, crucially depend upon how the tip interacts with the surrounding intact material.
 3. Difficult to model large deformation. We have not attempted to extend the model to large deformations or finite strains and to the best of my knowledge, no literature exists on large deformation phase-field models for cracks. The problem seems difficult if we work with the current (Eulerian) configuration. We can't think of a way to model just the opening of crack, i.e., crack is not propagating but the whole specimen is deforming which leads to crack faces moving apart. If we choose to define crack as a material region then this crack opening will cost some surface energy which is not a reasonable approximation of the physical situation. Further, unlike crack propagation, crack opening is reversible.
- One possible way to address the above issues might be to use peridynamics. Although, it has its own limitations regarding possible choice of kinetics and nucleation it does not treat crack as material region but as broken bonds. So, the above three issues never come up in peridynamic formulation. Typically, there is a force function (or spring) which models both the elastic properties of the material and the point where material breaks. This function can be made to depend on another phase-field type of field. Controlling the force function by another field will open up the possibility to impose kinetics and nucleation. And then the additional field can be evolved from some other

equation such as the balance law developed in this thesis. However, this is just an insight and will require more thought and effort before we can call it a consistent theory.

Also, a class of models for fracture are cohesive zone models. Crack surface energy is modelled as a function of distance between the crack faces or crack opening displacement. This results in crack faces exerting a cohesive force. One of the recent efforts in implementing the cohesive zone effect in phase-field models is [VB13]. They introduce another auxiliary field, apart from displacement and the phase-field, to quantify the jump in displacement across the crack faces. It might be possible to implement such an effect in our phase-field model also, however we have not addressed that issue. For phase transformations we believe that phase-field models are in good shape in the sense they do not have severe shortcomings but for dynamic fracture there are issues that need to be resolved before they are used for quantitative predictions.

Bibliography

- [AA12] Amir Abdollahi and Irene Arias, *Phase-field modeling of crack propagation in piezoelectric and ferroelectric materials with different electromechanical crack conditions*, Journal of the Mechanics and Physics of Solids **60** (2012), no. 12, 2100–2126.
- [Ach01] Amit Acharya, *A model of crystal plasticity based on the theory of continuously distributed dislocations*, Journal of the Mechanics and Physics of Solids **49** (2001), no. 4, 761–784.
- [AD14] Amit Acharya and Kaushik Dayal, *Continuum mechanics of line defects in liquid crystals and liquid crystal elastomers*, Quarterly of Applied Mathematics **72** (2014), no. 1, 33–64.
- [AD15a] Vaibhav Agrawal and Kaushik Dayal, *A dynamic phase-field model for structural transformations and twinning: Regularized interfaces with transparent prescription of complex kinetics and nucleation. part i: Formulation and one-dimensional characterization*, Journal of the Mechanics and Physics of Solids (2015), –.
- [AD15b] ———, *A dynamic phase-field model for structural transformations and twinning: Regularized interfaces with transparent prescription of complex kinetics and nucleation. part ii: Two-dimensional characterization and boundary kinetics*, Journal of the Mechanics and Physics of Solids (2015), –.
- [AK90] Rohan Abeyaratne and James K Knowles, *On the driving traction acting on a surface of strain discontinuity in a continuum*, Journal of the Mechanics and Physics of Solids **38** (1990), no. 3, 345–360.
- [AK91a] ———, *Implications of viscosity and strain-gradient effects for the kinetics of propagating phase boundaries in solids*, SIAM Journal on Applied Mathematics **51** (1991), no. 5, 1205–1221.
- [AK91b] ———, *Kinetic relations and the propagation of phase boundaries in solids*, Archive for rational mechanics and analysis **114** (1991), no. 2, 119–154.
- [AK06] ———, *Evolution of phase transitions: a continuum theory*, Cambridge University Press, 2006.

- [Ant05] Stuart S Antman, *Nonlinear problems of elasticity*, vol. 107, Springer, 2005.
- [AV03] Rohan Abeyaratne and Srikanth Vedantam, *A lattice-based model of the kinetics of twin boundary motion*, *Journal of the Mechanics and Physics of Solids* **51** (2003), no. 9, 1675–1700.
- [BCR10] Nathalie Bozzolo, Lisa Chan, and Anthony D Rollett, *Misorientations induced by deformation twinning in titanium*, *Journal of Applied Crystallography* **43** (2010), no. 3, 596–602.
- [BEKT12] CD Barrett, Haitham El Kadiri, and MA Tschopp, *Breakdown of the schmid law in homogeneous and heterogeneous nucleation events of slip and twinning in magnesium*, *Journal of the Mechanics and Physics of Solids* **60** (2012), no. 12, 2084–2099.
- [BFM08] Blaise Bourdin, Gilles A Francfort, and Jean-Jacques Marigo, *The variational approach to fracture*, *Journal of elasticity* **91** (2008), no. 1-3, 5–148.
- [BGV09] Ted Belytschko, Robert Gracie, and Giulio Ventura, *A review of extended/generalized finite element methods for material modeling*, *Modelling and Simulation in Materials Science and Engineering* **17** (2009), no. 4, 043001.
- [Bha03a] Kaushik Bhattacharya, *Microstructure of martensite: why it forms and how it gives rise to the shape-memory effect*, vol. 2, Oxford University Press, 2003.
- [Bha03b] ———, *Microstructure of martensite: why it forms and how it gives rise to the shape-memory effect*, vol. 2, Oxford University Press, 2003.
- [BJ87] JM Ball and RD James, *Fine phase mixtures as minimizers of energy*, *Archive for Rational Mechanics and Analysis* **100** (1987), no. 1, 13–52.
- [BJ92] John M Ball and Richard D James, *Proposed experimental tests of a theory of fine microstructure and the two-well problem*, *Philosophical Transactions of the Royal Society of London. Series A: Physical and Engineering Sciences* **338** (1992), no. 1650, 389–450.
- [BJM12] P.C. Bollada, P.K. Jimack, and A.M. Mullis, *A new approach to multi-phase formulation for the solidification of alloys*, *Physica D: Nonlinear Phenomena* **241** (2012), no. 8, 816 – 829.

- [BLR11] Blaise Bourdin, Christopher J Larsen, and Casey L Richardson, *A time-discrete model for dynamic fracture based on crack regularization*, International journal of fracture **168** (2011), no. 2, 133–143.
- [Bro96] KB Broberg, *How fast can a crack go?*, Materials Science **32** (1996), no. 1, 80–86.
- [BT10] IJ Beyerlein and CN Tomé, *A probabilistic twin nucleation model for hcp polycrystalline metals*, Proceedings of the Royal Society A: Mathematical, Physical and Engineering Science **466** (2010), no. 2121, 2517–2544.
- [BVS⁺12] Michael J Borden, Clemens V Verhoosel, Michael A Scott, Thomas JR Hughes, and Chad M Landis, *A phase-field description of dynamic brittle fracture*, Computer Methods in Applied Mechanics and Engineering **217** (2012), 77–95.
- [Che02] Long-Qing Chen, *Phase-field models for microstructure evolution*, Annual review of materials research **32** (2002), no. 1, 113–140.
- [Cia88] Philippe G Ciarlet, *Mathematical elasticity: Three dimensional elasticity, vol. 1*, Studies in Mathematics and its Applications, Elsevier Science Publishers BV, Amsterdam (1988).
- [CK11] John D Clayton and Jarek Knap, *A phase field model of deformation twinning: nonlinear theory and numerical simulations*, Physica D: Nonlinear Phenomena **240** (2011), no. 9, 841–858.
- [Cla10] John D Clayton, *Nonlinear mechanics of crystals*, vol. 177, Springer Science & Business Media, 2010.
- [CMZ⁺06] W Cai, XL Meng, YF Zheng, JX Zhang, and LC Zhao, *Interface structure and mobility in martensitic shape memory alloys*, Materials Science and Engineering: A **438** (2006), 900–904.
- [CO96] Godofredo T Camacho and M Ortiz, *Computational modelling of impact damage in brittle materials*, International Journal of solids and structures **33** (1996), no. 20, 2899–2938.
- [CSWRS09] J Cai, S Shekhar, J Wang, and M Ravi Shankar, *Nanotwinned microstructures from low stacking fault energy brass by high-rate severe plastic deformation*, Scripta Materialia **60** (2009), no. 8, 599–602.

- [DB06] Kaushik Dayal and Kaushik Bhattacharya, *Kinetics of phase transformations in the peridynamic formulation of continuum mechanics*, Journal of the Mechanics and Physics of Solids **54** (2006), no. 9, 1811–1842.
- [DWWR14] NP Daphalapurkar, JW Wilkerson, TW Wright, and KT Ramesh, *Kinetics of a fast moving twin boundary in nickel*, Acta Materialia **68** (2014), 82–92.
- [EC93] JC Escobar and RJ Clifton, *On pressure-shear plate impact for studying the kinetics of stress-induced phase transformations*, Materials Science and Engineering: A **170** (1993), no. 1, 125–142.
- [Eri75] JL Ericksen, *Equilibrium of bars*, Journal of elasticity **5** (1975), no. 3, 191–201.
- [FG94] Eliot Fried and Morton E Gurtin, *Dynamic solid-solid transitions with phase characterized by an order parameter*, Physica D: Nonlinear Phenomena **72** (1994), no. 4, 287–308.
- [FM06] Cristian Făciu and Alain Molinari, *On the longitudinal impact of two phase transforming bars. elastic versus a rate-type approach. part ii: The rate-type case*, International journal of solids and structures **43** (2006), no. 3, 523–550.
- [Fre98] L Benjamin Freund, *Dynamic fracture mechanics*, Cambridge university press, 1998.
- [FS11] Eilon Faran and Doron Shilo, *The kinetic relation for twin wall motion in nimga*, Journal of the Mechanics and Physics of Solids **59** (2011), no. 5, 975–987.
- [GBV08] R Gröger, AG Bailey, and V Vitek, *Multiscale modeling of plastic deformation of molybdenum and tungsten: I. atomistic studies of the core structure and glide of $1/2\langle 111 \rangle$ screw dislocations at $0k$* , Acta Materialia **56** (2008), no. 19, 5401–5411.
- [GF97] German Grach and Eliot Fried, *An order-parameter-based theory as a regularization of a sharp-interface theory for solid-solid phase transitions*, Archive for Rational Mechanics and Analysis **138** (1997), no. 4, 355–404.
- [GRBV08] R Gröger, V Racherla, JL Bassani, and V Vitek, *Multiscale modeling of plastic deformation of molybdenum and tungsten: II. yield criterion for single crystals based on atomistic studies of glide of $1/2\langle 111 \rangle$ screw dislocations*, Acta Materialia **56** (2008), no. 19, 5412–5425.

- [Gri21] Alan A Griffith, *The phenomena of rupture and flow in solids*, Philosophical transactions of the royal society of london. Series A, containing papers of a mathematical or physical character **221** (1921), 163–198.
- [HB14] A Hunter and IJ Beyerlein, *Predictions of an alternative pathway for grain-boundary driven twinning*, Applied Physics Letters **104** (2014), no. 23, 233112.
- [HM12] Martina Hofacker and Christian Miehe, *Continuum phase field modeling of dynamic fracture: variational principles and staggered fe implementation*, International journal of fracture **178** (2012), no. 1-2, 113–129.
- [HRL99] Thomas Y Hou, Phoebus Rosakis, and Philippe LeFloch, *A level-set approach to the computation of twinning and phase-transition dynamics*, Journal of Computational Physics **150** (1999), no. 2, 302 – 331.
- [Irw57] George R Irwin, *Analysis of stresses and strains near the end of a crack traversing a plate*, J. App. Mech. **24** (1957), 361–364.
- [KAF09] Yashashree Kulkarni, Robert J Asaro, and Diana Farkas, *Are nanotwinned structures in fcc metals optimal for strength, ductility and grain stability?*, Scripta Materialia **60** (2009), no. 7, 532–535.
- [Kal98] Surya R Kalidindi, *Incorporation of deformation twinning in crystal plasticity models*, Journal of the Mechanics and Physics of Solids **46** (1998), no. 2, 267–290.
- [KKL01] Alain Karma, David A Kessler, and Herbert Levine, *Phase-field model of mode iii dynamic fracture*, Physical Review Letters **87** (2001), no. 4, 045501.
- [KS72] James K Knowles and Eli Sternberg, *On a class of conservation laws in linearized and finite elastostatics*, Archive for Rational Mechanics and Analysis **44** (1972), no. 3, 187–211.
- [Lev14] Valery I Levitas, *Phase field approach to martensitic phase transformations with large strains and interface stresses*, Journal of the Mechanics and Physics of Solids (2014).
- [LL07] Valery I Levitas and Dong-Wook Lee, *Athermal resistance to interface motion in the phase-field theory of microstructure evolution*, Physical review letters **99** (2007), no. 24, 245701.

- [LLP10] Valery I Levitas, Dong-Wook Lee, and Dean L Preston, *Interface propagation and microstructure evolution in phase field models of stress-induced martensitic phase transformations*, International Journal of Plasticity **26** (2010), no. 3, 395–422.
- [LLSL10] CH Lei, LJ Li, YC Shu, and JY Li, *Austenite–martensite interface in shape memory alloys*, Applied Physics Letters **96** (2010), no. 14, 141910.
- [LPM⁺15] Bin Li, Christian Peco, Daniel Millán, Irene Arias, and Marino Arroyo, *Phase-field modeling and simulation of fracture in brittle materials with strongly anisotropic surface energy*, International Journal for Numerical Methods in Engineering **102** (2015), no. 3-4, 711–727.
- [LR15] Valery I Levitas and Arunabha M Roy, *Multiphase phase field theory for temperature- and stress-induced phase transformations*, Physical Review B **91** (2015), no. 17, 174109.
- [MH94] Jerrold E. Marsden and Thomas JR Hughes, *Mathematical foundations of elasticity*, Courier Dover Publications, 1994.
- [MHW10] Christian Miehe, Martina Hofacker, and Fabian Welschinger, *A phase field model for rate-independent crack propagation: Robust algorithmic implementation based on operator splits*, Computer Methods in Applied Mechanics and Engineering **199** (2010), no. 45–48, 2765 – 2778.
- [MWH10] C Miehe, F Welschinger, and M Hofacker, *Thermodynamically consistent phase-field models of fracture: Variational principles and multi-field fe implementations*, International Journal for Numerical Methods in Engineering **83** (2010), no. 10, 1273–1311.
- [NRC06] J Niemczura and K Ravi-Chandar, *Dynamics of propagating phase boundaries in niti*, Journal of the Mechanics and Physics of Solids **54** (2006), no. 10, 2136–2161.
- [OSPM14] A Ojha, H Sehitoglu, L Patriarca, and HJ Maier, *Twin nucleation in fe-based bcc alloys? modeling and experiments*, Modelling and Simulation in Materials Science and Engineering **22** (2014), no. 7, 075010.
- [PAD14] Hossein Pourmatin, Amit Acharya, and Kaushik Dayal, *A fundamental improvement to ericksen-leslie kinematics.*, to appear in Quarterly of Applied Mathematics (2014).

- [PB03] Prashant K Purohit and Kaushik Bhattacharya, *Dynamics of strings made of phase-transforming materials*, Journal of the Mechanics and Physics of Solids **51** (2003), no. 3, 393–424.
- [PL13] Marcel Porta and Turab Lookman, *Heterogeneity and phase transformation in materials: Energy minimization, iterative methods and geometric nonlinearity*, Acta Materialia **61** (2013), no. 14, 5311–5340.
- [RK97] Phoebus Rosakis and James K Knowles, *Unstable kinetic relations and the dynamics of solid-solid phase transitions*, Journal of the Mechanics and Physics of Solids **45** (1997), no. 11, 2055–2081.
- [Ros95] Phoebus Rosakis, *An equal area rule for dissipative kinetics of propagating strain discontinuities*, SIAM Journal on Applied Mathematics **55** (1995), no. 1, 100–123.
- [RR68] JRa Rice and GI F Rosengren, *Plane strain deformation near a crack tip in a power-law hardening material*, Journal of the Mechanics and Physics of Solids **16** (1968), no. 1, 1–12.
- [SB98] NK Simha and K Bhattacharya, *Kinetics of phase boundaries with edges and junctions*, Journal of the Mechanics and Physics of Solids **46** (1998), no. 12, 2323–2359.
- [SB99] ———, *Edge effects on the propagation of phase boundaries*, Materials Science and Engineering: A **273** (1999), 241–244.
- [SB00] ———, *Kinetics of phase boundaries with edges and junctions in a three-dimensional multi-phase body*, Journal of the Mechanics and Physics of Solids **48** (2000), no. 12, 2619–2641.
- [SHR02] O Samudrala, Y Huang, and AJ Rosakis, *Subsonic and intersonic mode ii crack propagation with a rate-dependent cohesive zone*, Journal of the Mechanics and Physics of Solids **50** (2002), no. 6, 1231–1268.
- [SL07] Yu Su and Chad M Landis, *Continuum thermodynamics of ferroelectric domain evolution: Theory, finite element implementation, and application to domain wall pinning*, Journal of the Mechanics and Physics of Solids **55** (2007), no. 2, 280–305.

- [SP99] I Steinbach and F Pezzolla, *A generalized field method for multiphase transformations using interface fields*, *Physica D: Nonlinear Phenomena* **134** (1999), no. 4, 385–393.
- [SP03] N Sukumar and J-H Prévost, *Modeling quasi-static crack growth with the extended finite element method part i: Computer implementation*, *International journal of solids and structures* **40** (2003), no. 26, 7513–7537.
- [SPN⁺96] I Steinbach, F Pezzolla, B Nestler, M Seeßelberg, R Prieler, GJ Schmitz, and JLL Rezende, *A phase field concept for multiphase systems*, *Physica D: Nonlinear Phenomena* **94** (1996), no. 3, 135–147.
- [SY08] YC Shu and JH Yen, *Multivariant model of martensitic microstructure in thin films*, *Acta Materialia* **56** (2008), no. 15, 3969–3981.
- [TR94] Hungyu Tsai and Phoebus Rosakis, *On anisotropic compressible materials that can sustain elastodynamic anti-plane shear*, *Journal of Elasticity* **35** (1994), no. 1, 213–222.
- [TR01] Hungyu Tsai and Phoebus Rosakis, *Quasi-steady growth of twins under stress*, *Journal of the Mechanics and Physics of Solids* **49** (2001), no. 2, 289 – 312.
- [Tra09] John A Trangenstein, *Numerical solution of hyperbolic partial differential equations*, Cambridge University Press, 2009.
- [Tru82] LM Truskinovskii, *Equilibrium phase interfaces*, *Sov. Phys. Dokl*, vol. 27, 1982, pp. 551–552.
- [Tru93] L Truskinovsky, *Kinks versus shocks*, *Shock induced transitions and phase structures in general media*, Springer, 1993, pp. 185–229.
- [Tur97] Sergio Turteltaub, *Viscosity of strain gradient effects on the kinetics of propagating phase boundaries in solids*, *Journal of Elasticity* **46** (1997), no. 1, 53–90.
- [US03] Takuya Uehara and Robert F Sekerka, *Phase field simulations of faceted growth for strong anisotropy of kinetic coefficient*, *Journal of crystal growth* **254** (2003), no. 1, 251–261.
- [VB13] Clemens V Verhoosel and René Borst, *A phase-field model for cohesive fracture*, *International Journal for numerical methods in Engineering* **96** (2013), no. 1, 43–62.

- [WBT10] J Wang, IJ Beyerlein, and CN Tomé, *An atomic and probabilistic perspective on twin nucleation in mg*, *Scripta Materialia* **63** (2010), no. 7, 741–746.
- [Whi65] GB Whitham, *A general approach to linear and non-linear dispersive waves using a lagrangian*, *Journal of Fluid Mechanics* **22** (1965), no. 02, 273–283.
- [WTAF09] T Waitz, K Tsuchiya, T Antretter, and FD Fischer, *Phase transformations of nanocrystalline martensitic materials*, *MRS bulletin* **34** (2009), no. 11, 814–821.
- [XB08] Yu Xiao and Kaushik Bhattacharya, *A continuum theory of deformable, semiconducting ferroelectrics*, *Archive for Rational Mechanics and Analysis* **189** (2008), no. 1, 59–95.
- [YD10] Lun Yang and Kaushik Dayal, *Formulation of phase-field energies for microstructure in complex crystal structures*, *Applied Physics Letters* **96** (2010), no. 8, 081916.
- [YD12] ———, *Influence of strain on space-charge distribution at ferroelectric thin-film free surfaces*, *Acta Materialia* **60** (2012), no. 19, 6457–6463.
- [YEC09] S-Y Yang, J Escobar, and RJ Clifton, *Computational modeling of stress-wave-induced martensitic phase transformations in niti*, *Mathematics and Mechanics of Solids* **14** (2009), no. 1-2, 220–257.
- [ZB05] W Zhang and K Bhattacharya, *A computational model of ferroelectric domains. part i: model formulation and domain switching*, *Acta materialia* **53** (2005), no. 1, 185–198.